NAVAL POSTGRADUATE SCHOOL
Monterey, California

THESIS

R8143

MONTEREY BAY ACOUSTIC TOMOGRAPHY:
RAY TRACING AND
ENVIRONMENTAL ASSESSMENT

by

Theresa M. Rowan

September 1988

Thesis Advisor James H. Miller

Approved for public release; distribution is unlimited.

T242312

REPORT DOCUMENTATION PAGE

a Report Security Classification Unclassified		1b Restrictive Markings
a Security Classification Authority		3 Distribution Availability of Report Approved for public release; distribution is unlimited.
b Declassification Downgrading Schedule		
Performing Organization Report Number(s)		5 Monitoring Organization Report Number(s)
a Name of Performing Organization Naval Postgraduate School	6b Office Symbol *(if applicable)* 3A	7a Name of Monitoring Organization Naval Postgraduate School
c Address *(city, state, and ZIP code)* Monterey, CA 93943-5000		7b Address *(city, state, and ZIP code)* Monterey, CA 93943-5000
a Name of Funding Sponsoring Organization	8b Office Symbol *(if applicable)*	9 Procurement Instrument Identification Number
c Address *(city, state, and ZIP code)*		10 Source of Funding Numbers Program Element No / Project No / Task No / Work Unit Accession No

Title *(include security classification)* MONTEREY BAY ACOUSTIC TOMOGRAPHY: RAY TRACING AND ENVIONMENTAL ASSESSMENT

Personal Author(s) Theresa M. Rowan

a Type of Report	13b Time Covered	14 Date of Report *(year, month, day)*	15 Page Count
Master's Thesis	From To	September 1988	92

Supplementary Notation The views expressed in this thesis are those of the author and do not reflect the official policy or position of the Department of Defense or the U.S. Government.

Cosati Codes			18 Subject Terms *(continue on reverse if necessary and identify by block number)*
eld	Group	Subgroup	acoustic tomography, eigenrays, arrival times, bathymetry

Abstract *(continue on reverse if necessary and identify by block number)*

This thesis recommends the locations for placement of five sonobuoys which are to be used in the 12-16 December 1988 oustic tomography experiment in Monterey Bay. The experiment will test a low-cost tomographic system for studying ternal waves and surface waves. The five sites were determined to be the most optimal locations for acoustic signal acquiion, based on predicted eigenray simulation and oceanic environment assessment. The Multiple Profile Ray-Tracing Proam (MPP) simulated the probable ray paths from the specified source location to receiver positions throughout Monterey ay, predicted eigenrays for the various sites, and determined the arrival time, transmission loss, and ray path for each genray.

Distribution Availability of Abstract unclassified unlimited ☐ same as report ☐ DTIC users	21 Abstract Security Classification Unclassified	
Name of Responsible Individual nes H. Miller	22b Telephone *(include Area code)* (408) 646-2384	22c Office Symbol 62Mr

FORM 1473,84 MAR 83 APR edition may be used until exhausted
All other editions are obsolete

Approved for public release; distribution is unlimited.

Monterey Bay Acoustic Tomography: Ray Tracing and Environmental Assessment

by

Theresa M. Rowan
Electronics Engineer, Naval Training Systems Center
B.S., Florida Technological University, 1971
B.S.E., University of Central Florida, 1980

Submitted in partial fulfillment of the
requirements for the degree of

MASTER OF SCIENCE IN SYSTEMS TECHNOLOGY (ANTISUBMARINE WARFARE)

from the

NAVAL POSTGRADUATE SCHOOL
September 1988

ABSTRACT

This thesis recommends the locations for placement of five sonobuoys which are to be used in the 12-16 December 1988 acoustic tomography experiment in Monterey Bay. The experiment will test a low-cost tomographic system for studying internal waves and surface waves. The five sites were determined to be the most optimal locations for acoustic signal acquisition, based on predicted eigenray simulation and oceanic environment assessment. The Multiple Profile Ray-Tracing Program (MPP) simulated the probable ray paths from the specified source location to receiver positions throughout Monterey Bay, predicted eigenrays for the various sites, and determined the arrival time, transmission loss, and ray path for each eigenray.

TABLE OF CONTENTS

I. INTRODUCTION 1

II. BACKGROUND 2
A. RAY THEORY 2
B. OCEAN ACOUSTIC TOMOGRAPHY 5
C. MONTEREY BAY TOMOGRAPHY PROJECT 6
D. THESIS OBJECTIVES 8

III. OCEANIC ENVIRONMENT 9
A. LOCATION AND DESCRIPTION 9
1. Monterey Bay 9
2. Seamount 10
B. BATHYMETRY 10
1. Continental Shelf and Slope 10
2. Submarine Canyons 10
C. GEOLOGY AND SEDIMENTS 12
D. CURRENTS 15
1. California Current System 15
2. Monterey Bay Current Flow 17
E. TEMPERATURE AND SALINITY VARIATIONS 19
F. TIDES 21
G. SURFACE WAVES 21
H. INTERNAL WAVES AND CANYON CURRENTS 25

IV. THE MULTIPLE PROFILE RAY-TRACING PROGRAM (MPP) 28
A. DESCRIPTION 28
B. PROGRAM FLOW 28
1. MPP1 30
2. MPP2COUT (1st pass) 31
3. MPP2COUT (2nd pass) 32
4. NRAYFIL2 33

V. MPP INPUT/OUTPUT 34
A. SIMULATED RECEIVER LOCATIONS 34
B. INPUT 37
C. OUTPUT 40
1. Receiver Location 1. 42
2. Receiver Location 2. 42
3. Receiver Location 4. 43
4. Receiver Location 5. 43
5. Receiver Location 7. 44
6. Receiver Location 8. 45
7. Receiver Location 13. 45
8. Receiver Location 17. 46

VI. CONCLUSIONS 51
A. TOMOGRAPHY EXPERIMENT REQUIREMENTS 51
B. SIMULATION VS REAL WORLD 51
C. RECEIVER LOCATION RECOMMENDATIONS 53

APPENDIX A. BATHYMETRY DATA FOR RECEIVER LOCATIONS 56

APPENDIX B. RAY TRACES AND STICK PLOTS 62

LIST OF REFERENCES 78

INITIAL DISTRIBUTION LIST 82

LIST OF TABLES

Table 1. UP- AND DOWN-CANYON REVERSAL CYCLE DATA FOR MONTEREY CANYON. 26
Table 2. UP- AND DOWN-CANYON REVERSAL CYCLE DATA FOR CARMEL CANYON. 27
Table 3. SIMULATION RECEIVER POSITIONS, RANGE AND DEPTH. . . . 36
Table 4. DECEMBER SOUND SPEED PROFILE VALUES FOR MONTEREY BAY REGION. 40
Table 5. EIGENRAY INFORMATION FOR SITE 16 BASED ON CHANGE OF SOURCE PLACEMENT. 42
Table 6. EIGENRAY INFORMATION FOR SITES 1, 2, 4, 5, 7, 8 AND 13. . . 49
Table 7. EIGENRAY INFORMATION FOR SITE 17. 50
Table 8. BATHYMETRY DATA FOR RECEIVER LOCATIONS 1, 2 AND 3. 56
Table 9. BATHYMETRY DATA FOR RECEIVER LOCATIONS 4, 5 AND 6. 57
Table 10. BATHYMETRY DATA FOR RECEIVER LOCATIONS 7, 8 AND 9. 58
Table 11. BATHYMETRY DATA FOR RECEIVER LOCATIONS 10, 11 AND 12. 59
Table 12. BATHYMETRY DATA FOR RECEIVER LOCATIONS 13, 14 AND 15. 60
Table 13. BATHYMETRY DATA FOR RECEIVER LOCATIONS 16 AND 17. 61

LIST OF FIGURES

Figure 1. Ray diagram for typical Atlantic Ocean sound channel. 3
Figure 2. Ray path in a stratified ocean medium. 4
Figure 3. Monterey Bay tomography source and receiver locations. 7
Figure 4. Monterey Submarine Canyon with Tributaries. 11
Figure 5. Distribution of sediment types in Monterey Bay. 14
Figure 6. Offshore surficial geologic map of experimental region. 16
Figure 7. Monterey Bay Seasonal Current Patterns. 18
Figure 8. Mean temperature and salinity variation at mouth of Monterey Bay (station 3) and CalCOFI station during 1950-1962. 20
Figure 9. Monterey Bay tidal pattern. 22
Figure 10. North Monterey Bay buoy, December 1987, wave energy data. 23
Figure 11. North Monterey Bay buoy, December 1987, wave energy spectra graph. 24
Figure 12. Temperature distribution (°C) at (a) high, and (b) low internal tide, Monterey Canyon axis, 13-14 September 1979. 27
Figure 13. MPP block diagram with input and output files. 29
Figure 14. Possible receiver hydrophone locations for tomography experiment. . . . 35
Figure 15. Typical December sound speed profile for Monterey Bay. 39
Figure 16. Recommended receiver positions. 54

ACKNOWLEDGMENT

I would like to thank my thesis advisor, Dr. James H. Miller, for providing such an interesting thesis topic and for his enthusiasm, encouragement and confidence that I would get the job done in the short time allotted. Arthur Newhall, Woods Hole Oceanographic Institution, provided much needed information and help during a period when the simulation program was not predicting any eigenrays.

I am very grateful for the total support from my three superiors at the Naval Training Systems Center: Hank Okraski, Director of Research, Bill Harris, Code 74 Division Head, and Frank Jamison, my supervisor. From the beginning when I first requested their approval for Long Term Training at the Naval Postgraduate School, they provided immeasurable help in the long and tedious procedures and paperwork leading to Long Term Training approval.

Finally, I dedicate this thesis to my husband, Bill, for without his total support, love, concern and understanding, I would not have been able to acquire this education that I long desired.

I. INTRODUCTION

This thesis is the end-product of a front-end eigenray simulation analysis and oceanic environment assessment for an acoustic tomography project designed to measure internal waves and surface waves in Monterey Bay. The project is a two year effort to develop and test a low-cost tomographic system for studying both internal and surface waves, with the results possibly contributing to the study and knowledge of underwater acoustics. The goal of this thesis is to determine the optimum placement of five receiver hydrophones for a mid-December 1988 field test of the newly developed tomographic system. The receiver locations will be selected on the basis of eigenray and travel time predictions from an existing ray tracing program, as well as an educated appraisal of the effects of the environment on the tomography experiment.

A computer program that has been used by Scripps Institute and the Woods Hole Oceanographic Institution was the determinator for the eigenray information. The Multiple Profile Ray-Tracing Program (MPP) routines calculate the eigenray arrivals with associated travel times, and determine the ray path for a specified source and receiver location, using two-dimensional ray tracing logic based on inputted range-dependent sound speed profiles and bathymetry.

The information contained in this thesis includes:

1. background information on ray theory, acoustic tomography, the Monterey Bay tomography project and the scope of the thesis;
2. environmental data for the experimental region regarding bathymetry, currents, sediment, temperature, salinity, tides, surface waves and internal waves;
3. a description of the MPP routines that are used in the eigenray and ray path determination;
4. a statement of the MPP input values used and an explanation of the output data; and
5. conclusions and recommendations for receiver placements for the December experiment.

In recommending receiver hydrophone positions and supplying important information on probable eigenray characteristics and expected environmental conditions, this thesis meets its intended objectives.

II. BACKGROUND

This thesis is a report on one aspect of a tomography experiment that is scheduled to be performed during December 1988, in the vicinity of Monterey Bay. Prior to describing the computer simulation and front-end analysis that was done as a requirement of the thesis for the upcoming field trial, an overview of ray theory, ocean acoustic tomography, the December experiment, and the thesis objectives will be provided.

A. RAY THEORY

The propagation of sound in fluids, such as the ocean, can be described mathematically by the linearized, lossless wave equation [Ref. 1]

$$\nabla^2 p = \frac{1}{c^2}\frac{\partial^2 p}{\partial t^2} \qquad \{1\}$$

where p is the acoustic pressure, c is the sound speed and t is time. One theoretical approach to solving the wave equation is called *ray theory*. Urick [Ref. 2] states, "The essence of ray theory is (1) the postulate of wavefronts, along which the phase or time function of the solution is constant, and (2) the existence of rays that describe where in space the sound emanating from the source is being sent." By using ray theory, one can trace the path of a ray as it propagates through the ocean. Figure 1 on page 3 illustrates the path of a ray in a ray diagram. This method, however, is not valid for very low frequencies, where the wavelength is on the order of the water depth or the source-to-receiver range [Ref. 3].

If the ocean is modeled as horizontally stratified, sound speed $c(z)$ is only a function of depth. For a grazing angle θ_i at initial depth z_i, one can find θ at depth z by using Snell's Law:

$$\frac{\cos\theta}{c(z)} = \frac{\cos\theta_i}{c(z_i)} = a \qquad \{2\}$$

where a is the Snell's Law constant of the ray. To calculate travel times of rays, integrate the sound slowness $\frac{1}{c(z)}$ along the ray path as follows:

$$d\tau = \frac{ds}{c(z)} \qquad \{3\}$$

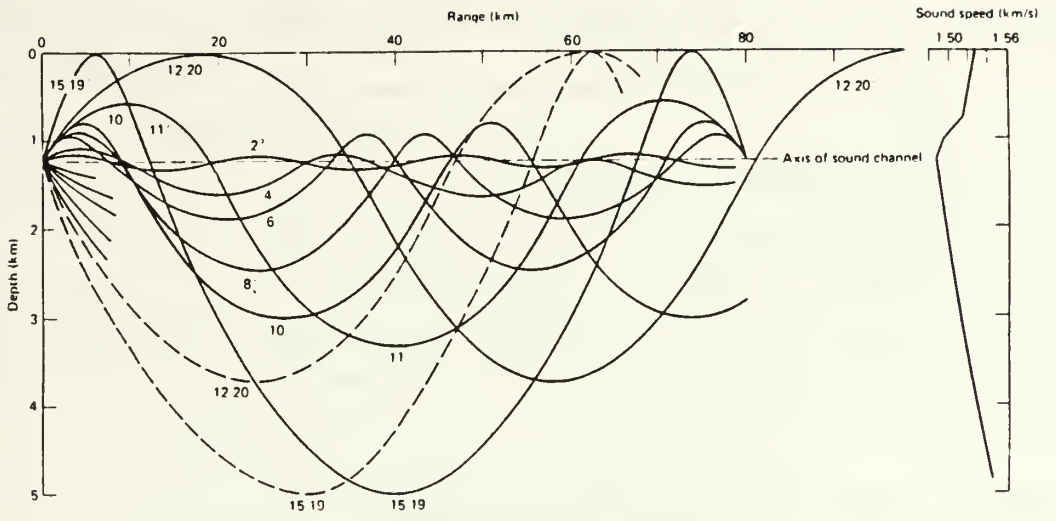

Figure 1. Ray diagram for typical Atlantic Ocean sound channel. [Ref. 3]

$$\tau_i = \int_{S_i} \frac{ds}{c(z)} \qquad \{4\}$$

where τ_i is the travel time associated with the ray path S_i and s is the arc length.

Of importance to ocean acoustic tomography is an eigenray. Eigenrays are those rays which propagate from the source and intercept the receiver location. Ray theory can be used to determine eigenray travel times. A simplified eigenray path between a source and receiver is shown in Figure 2 on page 4, where S_i is the ray path, ds is a differential distance along that path, r is the range and z is the depth.

The total travel time for an eigenray in a three-dimensional ocean, τ_i , is given by

$$\tau_i = \int_{S_i} \frac{ds}{c(x,y,z)} \qquad \{5\}$$

where

$$c(x,y,z) = c_o(x,y,z) + \delta c(x,y,z), \qquad \{6\}$$

c_o is known as the initial (background) sound speed, while δc is the perturbation (incremental change). The total travel time can now be stated as

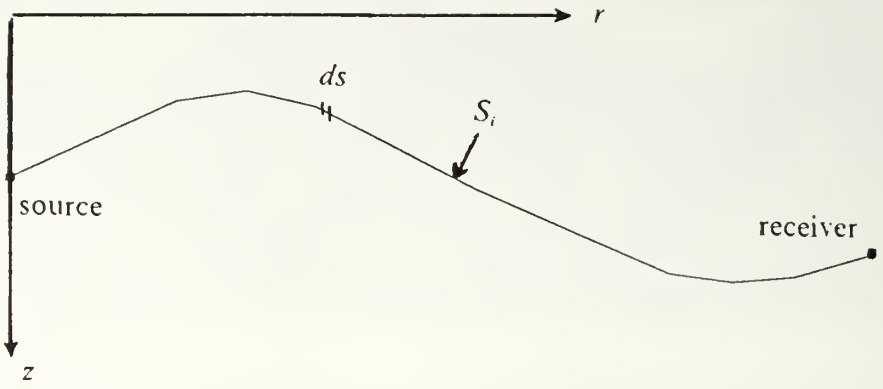

Figure 2. Ray path in a stratified ocean medium.

$$\tau_l = \int_{S_i} \frac{ds}{c_o + \delta c} = \int_{S_i} \frac{ds}{c_o} \left(\frac{1}{1 + \frac{\delta c}{c_o}} \right) \qquad \{7\}$$

By using the binomial expansion, where $\frac{1}{1+x} \simeq 1 - x$ for $x \ll 1$,

$$\tau_l \cong \int_{S_i} \frac{ds}{c_o} \left(1 - \frac{\delta c}{c_o} \right) \cong \int_{S_i} \frac{ds}{c_o} - \int_{S_i} \frac{ds\, \delta c}{c_o^2} \qquad \{8\}$$

This can be simplified to

$$\tau_l = \tau_{lo} + \delta \tau_l \qquad \{9\}$$

where the eigenray's measured travel time is equal to the initial guess for the travel time and some difference between the guess and measured times. This measured difference can be stated as

$$\delta \tau_l = - \int_{S_i} \frac{ds\, \delta c(x,y,z)}{c_o^2(x,y,z)} \qquad \{10\}$$

where $\delta c(x,y,z)$ is inferred using linear inverse theory. However, for the inversions to be valid, it must be known which ray arrival τ_l corresponds to which ray path S_i. This

is sometimes not an easy task. Numerical ray tracing programs provide the ray paths and ray arrival pattern.

B. OCEAN ACOUSTIC TOMOGRAPHY

The technique of *ocean acoustic tomography* was first formulated by Walter Munk and Carl Wunsch [Refs. 4,5] in 1977 as a way to observe mesoscale fluctuations in the ocean basins by measuring perturbations in the travel time of acoustic transmissions (pulses) between widely separated sources and receivers. Using acoustic inverse techniques to invert the travel time fluctuations, interior variability in the sound speed structure and current fields can be inferred. This method is similar to the medical x-ray procedure called CAT-scan (for computer-assisted tomography).

The amount of information obtained using tomography is the product of the number of sources, receivers and ray multipaths that can be resolved for each source-receiver pair. Very few sources and receivers are needed to provide a wealth of information. Another virtue with this technique is that the observations are integrating, resulting in long space and time observations [Ref. 5].

Mesoscale oceanic features, such as eddies, currents and fronts, contain most of the ocean circulation's kinetic energy, but they have been difficult to measure. Since the ocean is transparent to sound, acoustic transmissions can be used as a probe to measure the mesoscale variations which disturb the mean oceanic sound speed field. Density (one-way) tomography provides information on the sound speed field, while reciprocal (near-simultaneous two-way) tomography may be used for measuring the ocean basin heat content, vorticity and upwelling. [Refs. 5,6]

The transmitted signals are continuous or multi-period bursts of constant amplitude, phase modulated waveforms [Ref. 7]. The values for the source level and center frequency of the signal are equipment and locale specific. The success of an acoustic tomography experiment depends on [Ref. 6]:

1. a stable eigenray arrival pattern to allow for long periods of unambiguous tracking of ray arrivals;
2. eigenray arrivals that are identifiable, i.e., correspond to a ray trace;
3. large enough arrival time separation between eigenrays to resolve individual rays; and
4. signals that are strong enough to be received above the background noise.

There have been a few major experiments conducted to test out Munk and Wunsch's theory. In 1981 a tomography experiment was conducted southwest of

Bermuda [Ref. 8] in a 300 km square using four acoustic sources and five receivers. The measured results were within experimental error of predicted arrival patterns, thus indicating that tomography can be used to map the ocean with mesoscale resolution. A 1983 reciprocal experiment [Ref. 6] used higher frequency transmitting transceivers to test reciprocal transmission tomography. Even though one of the instruments failed to function correctly, the experiment still allowed for the determination of the average current profile along one transceiver-transceiver path. The MIZEX '84 expedition [Ref. 9] addressed issues of stability, resolvability, identifiability, attenuation due to scattering, and coherence of ray and/or mode arrivals in the Marginal Ice Zone. Fast fluctuations in acoustic ray arrival times were observed which were ascribed to surface waves. Slow fluctuations were ascribed to internal waves, but without corroborative oceanographic measurements. The overall conclusion was that shallow-water tomography is more difficult than deep-water tomography but not impossible to achieve.

C. MONTEREY BAY TOMOGRAPHY PROJECT

Dr. James H. Miller [Ref. 7] is in the process of developing and testing a low-cost tomographic system to analyze surface waves and internal waves. Tomography can be used to determine the time and space characteristics of the frequency-direction spectrum of the waves. The time scale is short since a surface wave period is normally under 30 seconds. Internal waves will alter the sound speed profile in their vicinity, which will then disturb rays traveling through the wave field. However, the time scale of internal waves is on the order of 20 or more minutes. Since the time scales differ between surface and internal waves, both can be studied with the same signal. [Refs. 7,10]

The project's first tomography field experiment is scheduled to be conducted during the week of 12 December 1988, using one acoustic source moored on the top of a seamount in the Pacific Ocean west of Point Sur at a depth of approximately 830 meters. This position is at latitude 36° 22′ N and longitude 122° 19′ W. The bottom-mounted receivers will be scattered throughout Monterey Bay at approximately the 100 meter depth. Possible locations for these receivers are shown in Figure 3 on page 7 and are detailed in CHAPTER V.

Eleven omnidirectional US Navy AN/SSQ-57A sonobuoys have been modified for the experiment. The modifications for these receivers include new long-life batteries, new hydrophones, and the removal of the scuttling device mechanism. The sonobuoys will transmit to a shore-based van that has equipment to record both the sonobuoy acoustic signals and internal ocean temperature data from ancillary ocean equipment.

Figure 3. Monterey Bay tomography source and receiver locations.

Since the December experiment's acoustic observations must be corroborated by other measurements, the additional information needed will be obtained from:

1. a frequency directional spectra buoy, which is maintained by the National Data Buoy Center (NDBC) in Bay St. Louis, Mississippi, and
2. NDBC modified ARGOS RC/WASID drifting buoys that measure the internal ocean temperature.

Woods Hole Oceanographic Institution will design and manufacture a mooring system for the sonobuoys, and refurbish the tomographic source. The source will continuously transmit a pseudo-random phase-encoded signal of 1.9375 s duration, with a center frequency of 224 Hz and a source level of 183 dB.

D. THESIS OBJECTIVES

The purpose of this thesis is to determine the optimal placement of the receiver hydrophones for the December tomography experiment, and to indicate probable eigenray characteristics for each location. The receiver locations will be selected on the basis of the eigenray and associated travel time results from an existing wave propagation simulation program, as well as an assessment of the Monterey Bay ocean environment. The goal is to select locations in the bay in which a manageable number of resolvable eigenrays have been identified for each position. A manageable number would be less than eight distinct ray arrivals.

Monterey Bay is a very challenging area to conduct a tomography study since there are rapid changes in bathymetric data as one approaches the submarine canyons, and the receivers will be in shallow water where surface and bottom bounces of the rays will be a major factor. The bay experiences variations in temperature and salinity, both vertically with depth and laterally between nearshore areas and the area over the canyons. Factors that add to the sound speed variable conditions include river runoff, surface heating, convergence and divergence of internal currents within the canyons, surface current flow and pollutant outflow. There is a wide sediment diversification in the experimental region, from mud, fine sand and coarse sand to granite and sedimentary rock. Three different oceanic periods in the area change the current flow within the bay. There are many oceanic environmental parameters which will influence the outcome of the tomography experiment.

An existing simulation program for determining multipath ray tracing in a medium with range-dependent sound speed profile, variable bottom depth and bottom reflectivity has been used as a tool to acoustically analyze the Monterey Bay situation. The program determines the eigenrays for a specified source and receiver location, as well as the travel time and transmission loss for each ray. A majority of this thesis will be dedicated to a description of the simulation program, the input data used and the results obtained.

III. OCEANIC ENVIRONMENT

The December tomography experiment encompasses an area that extends from an unnamed seamount on the continental slope--approximately 19.5 nm (36 km) west of Point Sur--north to Santa Cruz and including Monterey Bay. This is a region of great divergence in bathymetry and sedimentation. There are three seasonal oceanographic periods associated with the California Current system that affect the water movement in the area and the plankton population. Daily and seasonal fluctuations occur in the temperature and salinity of Monterey Bay in both lateral and vertical directions. All of these variations may have an impact on the generation and movement of surface and internal waves.

The purpose of the December tomography experiment is to study both surface and internal waves. Since oceanic variations not only affect these waves but also influence the sound speed profile(s) and acoustic ray paths of the tomography experiment, this chapter will detail the main oceanic environmental parameters of this region.

A. LOCATION AND DESCRIPTION

1. Monterey Bay

Monterey Bay is a semi-enclosed elliptical embayment along the Central Coast of California between latitudes 36°36.05′N and 36°58.70′N. Moss Landing is located at the easternmost point of the bay at longitude 121°47.30′W. Since the bay is open to the Pacific Ocean along its western side, in this thesis the western boundary will be an artificial line between Point Piños to the south (121°56.20′W) and Point Santa Cruz along the north shore (122°01.60′W). Based on these positions, the bay is 22.65 nm (42 km) long and 9.50 nm (17.6 km) wide from Moss Landing due west to the open bay boundary. The surface area of the bay is approximately 534 km^2, of which 81% is above the continental shelf while the rest overlies the submarine canyons [Ref. 11].

Fresh water enters the bay via the San Lorenzo River, Soquel Creek, Aptos Creek, Pajaro River and Salinas River. These streams have a combined mean annual discharge of 1.85×10^6 m^3/day with the Salinas River having the greatest contribution at 55% [Ref. 12]. Precipitation and river runoff are normally greatest during the winter rainy season. During the dry months of May through October, a sand bar blocks the Salinas River, forcing its water to flow north and discharge through Elkhorn Slough [Ref. 11].

2. Seamount

The seamount on which the acoustic source will be mounted rises to the 2700 ft (824 m) depth along a line at longitude 122°19′W and between latitudes 36°18′N and 36°24′N. The southernmost point of this unnamed seamount is approximately 19.2 nm (35.6 km) due west of Point Sur. The continental shelf along the central California coast is generally very narrow; as a result, this seamount rests on the continental slope.

B. BATHYMETRY

1. Continental Shelf and Slope

The continental shelf is fairly narrow south of Monterey Bay, ranging in width from less than 1 mile at Cypress Point on the Monterey Peninsula to about 8 miles at Point Sur and then decreasing in width to less than 1 mile at Partington Point. North of the bay the shelf is wider, ranging from about a 5 nm (9.3 km) to 20 nm (37 km) width south of San Francisco. The shelf in Monterey Bay is cut by submarine canyons and the shelf bottom slopes toward the edge of the canyons. The northern bay shelf is approximately 238 km^2 in area and is at a maximum depth of 90 m at the canyon rim, as compared to the shelf in the south bay that is 195 km^2 and deepens to 180 m [Refs. 11,13]. The maximum slope near Seaside is 2%, while offshore of the Salinas River it is 1-1.5% [Ref. 14].

Between the continental shelf and the deep ocean floor lies the continental slope with its steeper gradient. According to Shepard [Ref. 15], the slope in the greater Monterey Bay region is not consistent. Just south of Monterey Bay the outer part of the slope is set toward the northeast for 20 or more miles. Further south, the slope spreads over a wide area. North of the bay, the continental slope is narrower, has an average grade of 10%, and is marked by a number of submarine canyons.

2. Submarine Canyons

The most prominent feature of Monterey Bay is the Monterey Submarine Canyon (MSC), depicted in Figure 4 on page 11, which bisects the fairly symmetrical bay at Moss Landing. With a volume of 450 km^3, MSC has the distinction of being the largest submarine canyon to cut the California continental slope [Ref. 16]. Shepard, Emery and Dill [Refs. 15,17] have described the Monterey Submarine Canyon system in considerable detail, so the canyon system specification given in this thesis is based on their work.

Monterey Canyon has an axis length of about 51 nm (94.5 km) and ranges in depth from about 60 ft (18 m) to 9600 ft (2925 m) where the true canyon ends and the

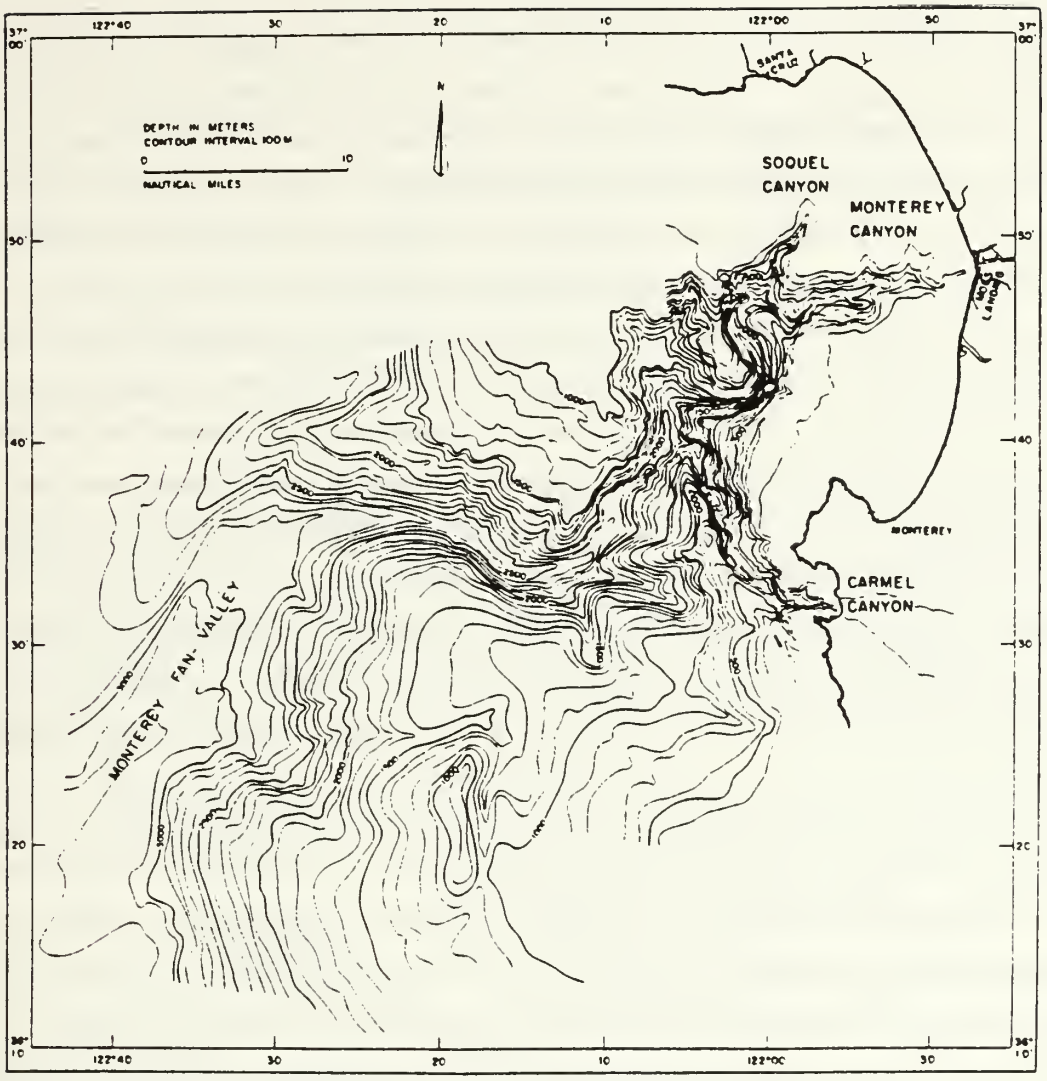

Figure 4. Monterey Submarine Canyon with Tributaries.

Monterey Fan-valley begins. The two largest tributaries entering MSC are the Soquel Submarine Canyon from the north and the Carmel Submarine Canyon from the south. After the Carmel Canyon juncture, only small tributaries enter both sides of MSC.

The Soquel Canyon joins the Monterey Canyon at the 3000 ft (915 m) depth after dropping at a rate of 7.4% along its 7 mile length, giving the appearance of a hanging valley. The axis of MSC winds and meanders beyond the Soquel Canyon juncture, especially off of the Monterey Peninsula where the floor is granite. At the beginning of this granite ridge, at the 5000 ft (1525 m) mark, the axis gradient increases to over 10% or 100 m/km. The Monterey Canyon is V-shaped from its head to past the granite rock, until at an axial depth of 6300 ft (1920 m) the canyon floor becomes more

irregular and broader. This is the point where a northern trough-like valley enters the MSC.

The trough-shaped valley section of the canyon runs southwest for about 20 miles. The walls increase in height along the canyon with the northwest wall reaching up to 1200 ft (370 m). The southeast wall is the continental slope and has a number of valleys entering it with heads as deep as 5000 ft (1520 m).

The Carmel Submarine Canyon connects with the Monterey Canyon at a depth of 6600 ft (2010 m). Carmel Canyon is about 16 nm (29.7 km) long with an average axial slope of 73 m/km. At its 30 ft (9 m) head in Carmel Bay, which may be considered a drowned river valley, are several tributaries cut into granite walls along the shore with no intervening shelf. The head has some portions with gradients as large as 30%, but the base is smooth, probably due to recent erosion. After large storms, there are considerable changes in the nature and thickness of the fill in the head of the canyon.

The V-shaped submarine canyon of Carmel first runs west, then winds northwest and parallels the coast. It appears to run along a fault in soft rock that lies between two hard rock masses. The inner portion of the canyon has an axial slope of 10% with a drop of 1800 ft (550 m) and a floor width about 250 ft (75 m). It ends as a hanging valley at the Monterey Canyon with no fan-valley.

Beyond the tomography experiment area at approximately 122°40′W, the high northwest wall of the MSC drops down to a low ridge where the southeast wall leaves the continental slope and a levee forms on top of the wall. The channel then takes a large 13 nm (24 km) meander before returning to its general course only 2 miles downstream from the point where the meander began. A little farther down the channel, the trough-like portion of MSC opens up into a modified fan-valley with convex-upward levees bordering an eroded valley. This fan-valley is approximately 172.5 nm (320 km) long and 151 nm (280 km) wide with an axial gradient of 4.8 m/km, its apex at a depth of 10,000 ft (3050 m) and base at 15,100 ft (4600 m) [Ref. 18]. The fan-valley eventually opens up into the deep ocean basin.

C. GEOLOGY AND SEDIMENTS

The coastline depression of Monterey Bay was probably carved out by wave attack on the relatively soft sedimentary rocks in the center of the Salinas River Valley trough [Ref. 19]. The promontories at Soquel Point and Point Piños are rocks that were better able to resist the erosional action.

The rivers that empty into Monterey Bay deposit igneous, sedimentary and metamorphic rocks of the central and southern Coast Ranges. The igneous rocks are Mesozoic granite, while the metamorphic rocks are of the Sur Series. Monterey, Pancho Rico, Paso Robles and Aromas Formations contribute to the Tertiary sedimentary rocks. [Ref. 19]

The sediment within Monterey Bay is composed of gravel, various sizes of sand, silt and clay. The following excerpt from a report by Engineering-Science, Inc., for the Monterey Peninsula Water Pollution Control Agency [Ref. 14] provides a succinct description of the Monterey Bay sediment.

> The bottom sediments vary in size and composition according to depth contour, as shown in Figure 5 on page 14. The nearshore bottom and beach consist of coarse and medium sand. The bottom gradates to fine sand down to a depth of 36 m. The sides and bottom of the submarine canyon nearshore are characterized by silt and clay which gradate into gravel and coarse sediments in the deeper parts. The lower portion of the south bay is semiprotected from wave action by the protruding headlands at Point Pinos. This topographical feature, which refracts and dimishes wave energy, produces a pronounced sorting of coarse and medium sand particles in the south bay below the Salinas River.

Monterey Canyon with its Soquel and Carmel tributaries is the predominant feature of the tomography experimental region. MSC's axial path appears to meander and wind in relationship to hard and soft rock zones. The tributaries enter the main canyon as hanging valleys with trellis drainage pattern [Ref. 15]. There are many large-scale slumps along the walls of the Monterey Submarine Canyon, indicating a history of undercutting and erosion [Ref. 14].

At the head of MSC, directly off Elkhorn Slough, there is only unconsolidated sediment. The inner canyon cuts into unconsolidated sediment for about 8 miles, and along the walls and floor of the canyon for this stretch is silt and clay. Based on information from Shepard and Dill, the first rock to appear is Upper Pliocene mudrock at an axial depth of 2100 ft (640 m). The north wall of MSC beyond this point is Pliocene sedimentary rock which also comprises the west wall of Soquel Canyon. A box core sample taken in Soquel Canyon yielded surface mud above rounded pebbles with shells and fragment of siltstone. [Ref. 17]

The first granite to appear in Monterey Canyon is an extension of the Monterey Peninsula formation, and is found only along the south wall where MSC axis makes a large bend to the south. The opposite wall is still sedimentary rock. Beyond the Carmel Canyon junction, the MSC north wall sedimentary rocks include limestone, sandstone,

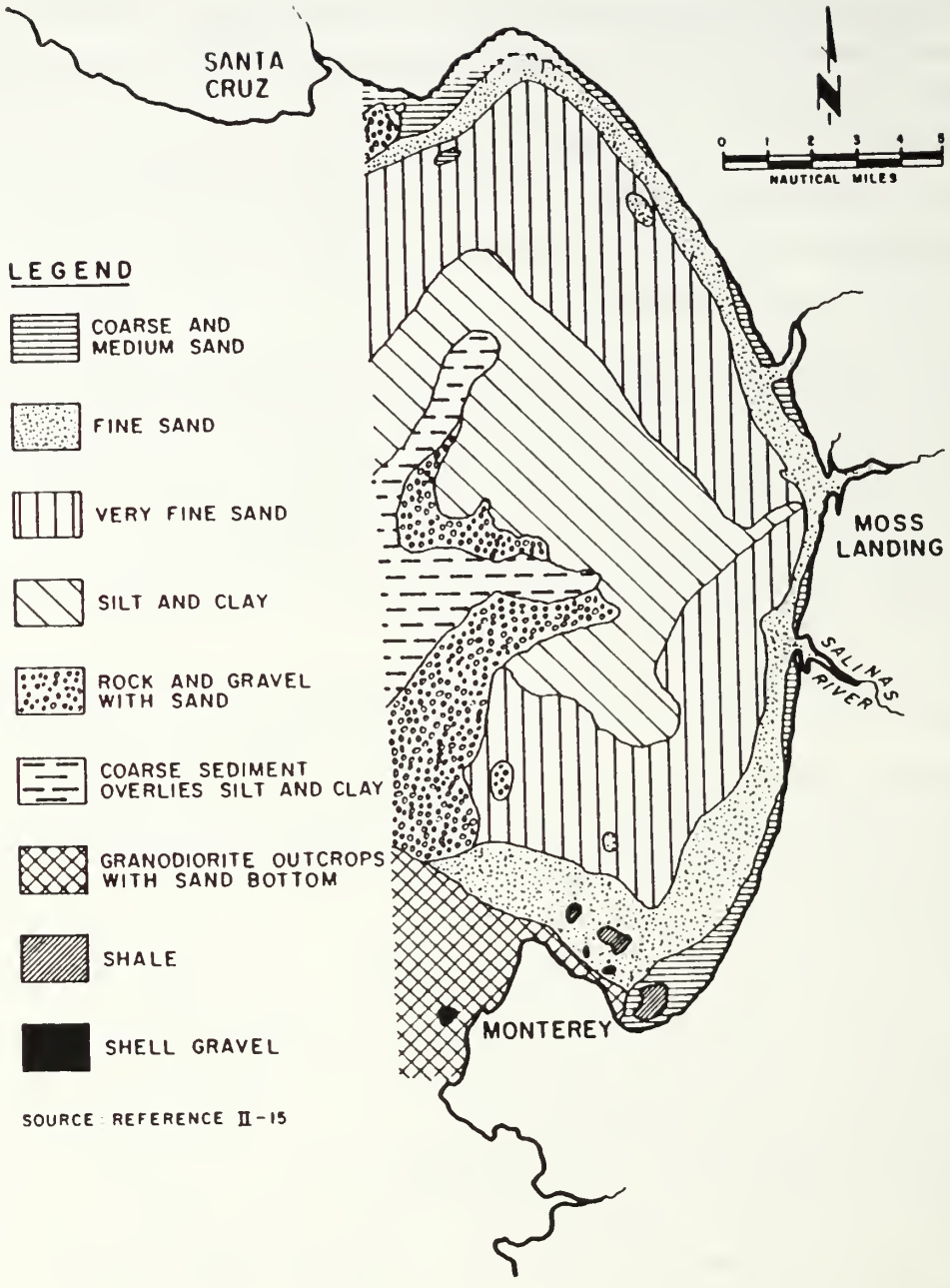

Figure 5. Distribution of sediment types in Monterey Bay. [Ref. 14]

mudstone and Lower Miocene foraminifora and coccoliths (organic calcareous ooze). The south wall is just mud. [Ref. 17]

Based on the Offshore Surficial Geologic Map (Figure 6 on page 16), the Monterey Canyon beyond Monterey Bay is sandy mud (sand < mud) until it becomes mud (silt and clay) after the granite outcroppings. The map does not provide information on the seamount where the source will be placed, but the area northeast and east of the mount is mud. For most of the proposed receiver locations, the rays from the acoustic source will initially bounce off of mud, and then a sandymud bottom, before reaching the canyon(s).

Carmel Submarine Canyon appears to be a seaward extension of the land canyon, with no continental shelf between the canyon heads and the beach. The main head begins directly off the mouth of San Jose creek. As expected, the head fills rapidly with sediment from the creek and is then cleaned out. This fill appears to undergo continuous change in nature and thickness, but changes are especially noticeable after a large storm. [Refs. 17,21]

The Carmel Canyon is narrow, V-shaped and cut in granite. The steep rock walls are mostly granite with a smooth base. The floor is sandy or rocky. Near the juncture to the Monterey Canyon, Carmel Canyon's east wall is composed of weathered granite, while the west wall has Mid-Miocene sedimentary rock. [Refs. 17,21]

D. CURRENTS

1. California Current System

Flowing along western North America in a south to southeasterly direction is the eastern boundary current called the California Current. This current brings Subarctic water to California, which is low in both temperature and salinity but high in nutrients. The California Current is wide, shallow and slow, extending maybe 375-540 nm (700-1000 km) off the coast, down to a depth less than 1650 ft (500 m), and flows at a speed that is less than 25 cm/sec. [Refs. 11,14]

A subsurface current, the California Countercurrent, moves warm and highly saline Equatorial Pacific water north along the coast from Baja California to Cape Mendocino (41°N latitude). The core of this current is at about the 650 ft (200 m) depth, extending 25-55 nm (50-100 km) offshore, with a velocity of less than 22 cm/sec north of 30°N latitude. In the fall or early winter, the California Countercurrent surfaces and becomes the Davidson Current. This surfacing of the current, which occurs somewhere between British Columbia and Point Conception, now provides for another

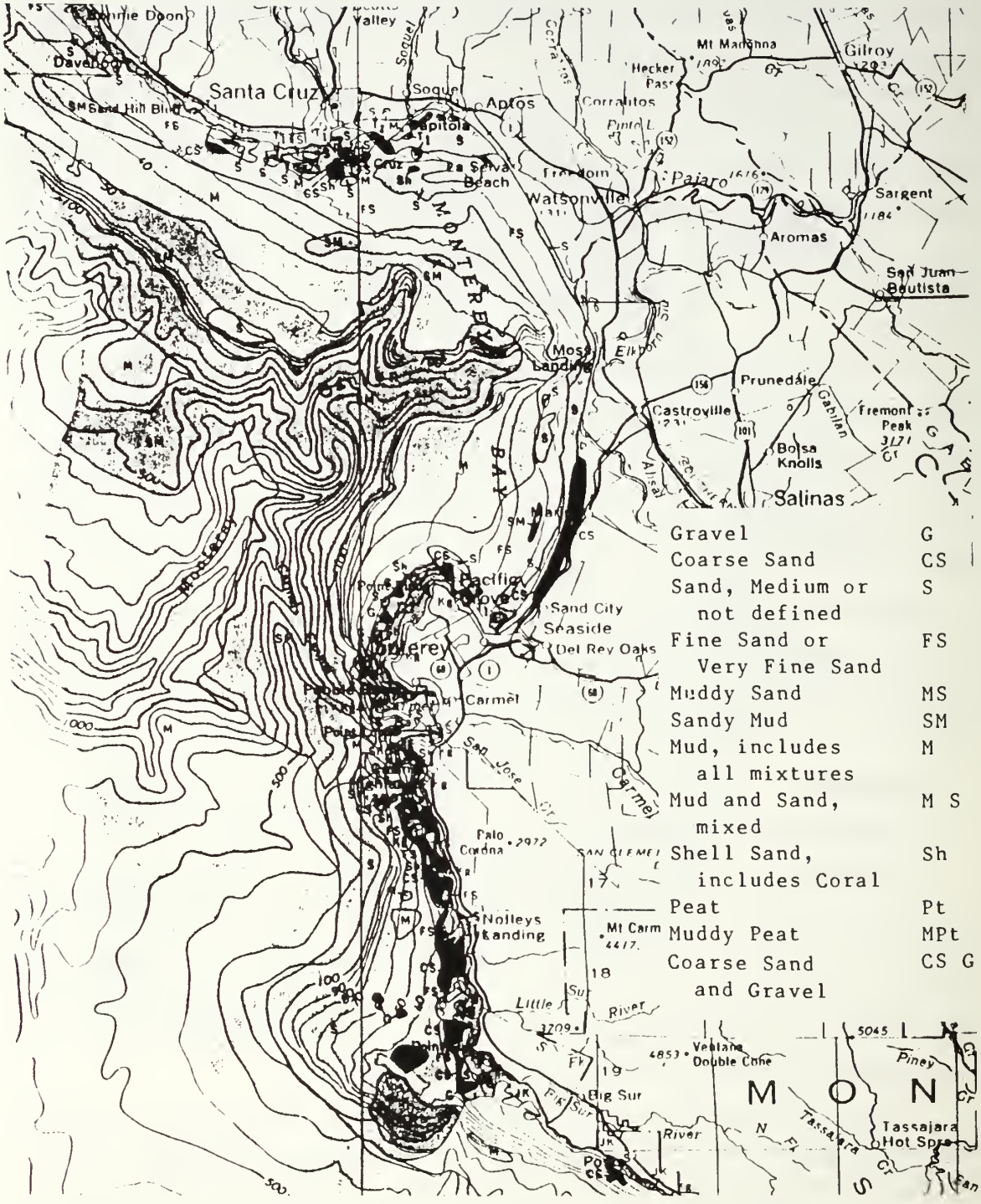

Figure 6. Offshore surficial geologic map of experimental region. [Ref. 20]

surface current to move along the coast inward of the California Current. The Davidson Current, flowing between 16 and 47 cm/sec, is found as far as 43 nm (80 km) offshore. [Refs. 11,14]

Associated with the California Current system are three oceanic seasons, designated the Davidson period, the upwelling period and the oceanic period. These periods appear to be directly affected by wind speed and direction.

The Davidson period generally occurs between November and February, when a semi-permanent Pacific high pressure cell weakens, moves southward, and is replaced by an intermittent low pressure cell. The winds are very light in the fall, and from the west or southwest in the winter. The Davidson Current surfaces and is pushed toward the coast, due to the wind direction and Coriolis force. This water converges along the western North America coast and then sinks, resulting in nutrient-poor water along the coast. [Ref. 11]

From about February to July, the winds are strong and blow out of the north or northwest. The surface water along the shore is carried away from the coast by the Coriolis force, based on the wind direction. Upwelling occurs as subsurface water rises to replace the vacated surface water. The water level is generally a little higher away from the shore, where the surface water has been pushed, rather than close to shore, where the subsurface water has risen. The upwelled water is cooler but high in salinity and nutrients. Upwelling occurs at a rate of 0.7-2.7 m/day and is found as far as 27 nm (50 km) offshore. [Refs. 11,14]

At the end of the upwelling period, the regular current pattern collapses into irregular eddies in connection with the wind abatement. Smethie [Ref. 11] indicated that during this oceanic period "... the sea surface slopes downward, isotherms slope upward toward the coast, and the geostrophic current flows southward." With the irregular eddies, the currents are usually weak and variable.

2. Monterey Bay Current Flow

The surface water in Monterey Bay appears to originate from three water types [Ref. 12]:

1. recently upwelled water;
2. freshwater from the rivers and streams; and
3. warmer, low-nutrient water which has been warmed at the surface.

The bay currents appear to be regulated by the oceanic seasons. Figure 7 on page 18 illustrates the seasonal surface current flow within Monterey Bay.

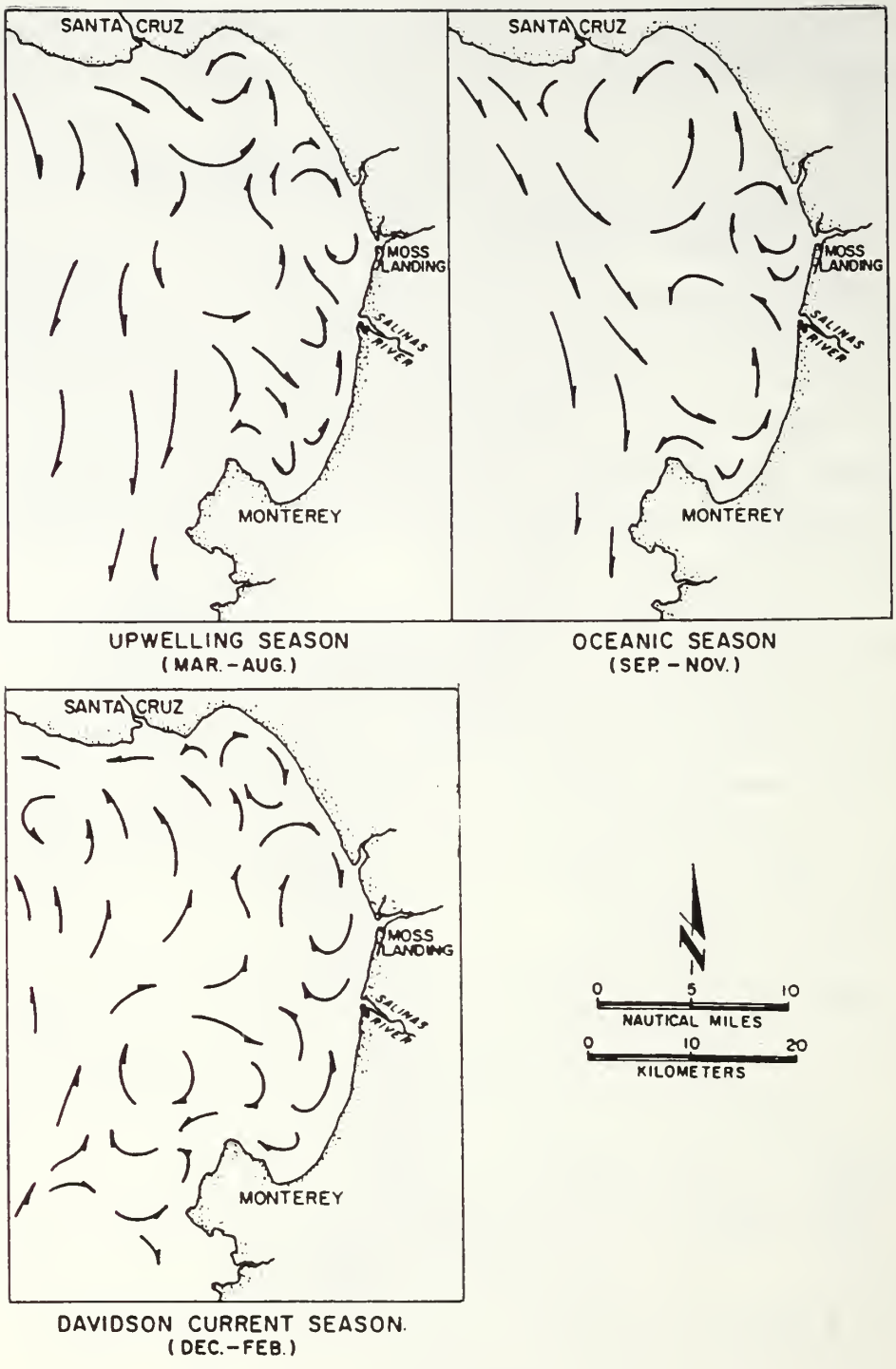

Figure 7. Monterey Bay Seasonal Current Patterns. [Ref. 14]

Engineering-Science, Inc., in their report to the Monterey Peninsula Water Pollution Control Agency [Ref. 14], indicated that during the upwelling period, the bay flow is dominated by the southward flowing offshore current. They cited Broenkow and Smethie's [Ref. 12] conclusion that the offshore waters enter mostly from the southwest up the Monterey Canyon, separate, and then flow over the northern and southern continental shelves in the bay. Clockwise and counterclockwise gyres over the shelves result, with speeds anywhere from 2.5 to 26 cm/sec, but the predominent flow is north and northeast. Even though in the oceanic period the currents become irregular and the wind is light, the bay current pattern continues the pattern established in the upwelling period, except that irregular eddies form over the north shelf. The nearshore ocean currents shift from southerly to northerly, and pass through Monterey Bay as a large, open eddy. However, the bay currents circulate irregularly and slowly.

Broenkow and Smethie [Ref. 12] studied and reported on the Monterey Bay surface circulation and water replenishment during a 27 month period in the mid 1970's. As stated earlier, offshore water predominantly enters up the the canyon into the bay, but sometimes flows directly from the west. The replacement time for the north and south bay waters is between 2 and 14 days, during which time their characteristics can be modified by air temperature at the surface, photosynthesis, sewage outflow and freshwater river discharge. The water parcels had longer paths near the shoreline, and therefore, had longer replenishment times than the water over the canyon. During the period of October 1972 through March 1973, the largest volume of bay freshwater replenishment occurred in February with an estimate of $86 \times 10^6 m^3$. October had the smallest volume at $2 \times 10^6 m^3$. During most of the year the freshwater lens is above the 10 m depth mark, except for January and February when about ⅛ of the freshwater falls to a depth between 10 and 30 m.

E. TEMPERATURE AND SALINITY VARIATIONS

The temperature and salinity within Monterey Bay appear to coincide with seasonal oceanic periods associated with the California Current system, amount of river runoff and with variations in the wind. Figure 8 on page 20 shows the mean variation of temperature and salinity at the mouth of Monterey Bay, and at a point 21.5 nm (40 km) south of the bay, during the years 1950-1962. On any given day the temperature throughout the bay is not uniform, varying from 1 to 3°C for a particular layer, while the salinity is laterally consistent [Refs. 12,14]. The surface waters in the north and

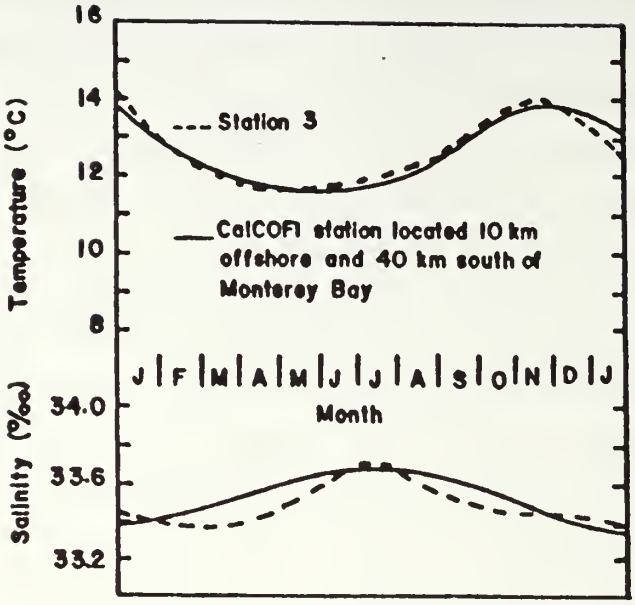

Figure 8. Mean temperature and salinity variation at mouth of Monterey Bay (station 3) and CalCOFI station during 1950-1962. [Ref. 11]

south bight areas are generally warmer in the spring and summer than the mid-bay waters. Also, the maximum temperatures often occur after days of southerly winds. The lowest salinity readings generally occur with the highest temperatures for the year, or during the period of maximum freshwater runoff. The late upwelling period yields the highest salinity levels.

Each seasonal oceanic period greatly affects the temperature and salinity of the Monterey Bay water. In the late fall and early winter, the sinking of nearshore waters during the Davidson period results in a fairly deep layer where the temperature is uniform, with little variance in surface water temperature over the entire bay. The 8°C isotherm deepens and all the isotherms slope deeper towards the coast. Seasonal rainfall, together with large river runoff, combine to dilute the surface water to measurable depths, which brings the salinity in this diluted layer down to around 33.4‰ and variable. Late in the winter the southerly winds die out, and strong northeasterly winds arise. This is the onset of the upwelling period. [Ref. 14]

During early upwelling the cool subsurface water replaces the vacated surface water, bringing the surface temperature down to its lowest yearly value of around 10-11°C. The south and north bights are warmer than the middle of the bay, which lead to a

variation of surface temperature by greater than 3°C. The isotherms rise, so the 8°C isotherm is usually above the 100 m mark during this period. Even with intermittent upwelling in the summer, the water temperature remains cool; however, the maximum salinity level occurs near the end of upwelling in the July timeframe. During the entire upwelling period, the salinity is high because the rising subsurface water has a high salinity value. [Ref. 14]

The oceanic period generally takes place from July to November. The surface temperatures ascend to their warmest yearly values of 13-16°C, but the temperature varies horizontally throughout the bay by 2-3°C. The 8°C isotherm drops, and all of the isotherms slope upward toward the coast. There is usually a sharp thermocline within the first 165 ft (50 m). Since the upwelling has ceased during this period, the salinity level first declines and then levels off, due to the ingress of offshore water that is lower in salinity. [Ref. 14].

F. TIDES

The tidal pattern along the west coast of the United States is classified as a *mixed semidiurnal* tide. As shown by the tidal curve of Figure 9 on page 22, two high tides and two low tides occur each day; however, the high tides are of different heights with respect to each other. The same is true for the two daily low tides. In Monterey Bay, the tidal range between the lower low tide and the higher high tide is on the order of 2 m [Ref. 21], with the tides arriving in the order of lower low tide, lower high tide, higher low tide and higher high tide in a 24-hour day cycle.

G. SURFACE WAVES

The waves that arrive in Monterey Bay hit all points of the shoreline, due to refraction and defraction of the waves as they wrap around the bay. The bay experiences two general types of waves. Winter waves occur usually from November to March and have a short period of 8-10 seconds. These swells come out of the northwest and are the product of local storms or may originate from as far away as the Gulf of Alaska. Winter waves severely erode beaches because the short wave action keeps the beach face saturated with water and the swash cannot permeate the sand. Instead, this type of wave returns as a backwash, carrying much of the beach sand with it and depositing the sand on a sand bar at a typical depth of 30 ft (9 m).

Summer waves have a longer period of 14-16 seconds, arrive at Monterey Bay from the southwest, originate in the Antarctic region, and have flattened out due to the long travel time. These waves move the sand bar deposit back to the shore, so the beach

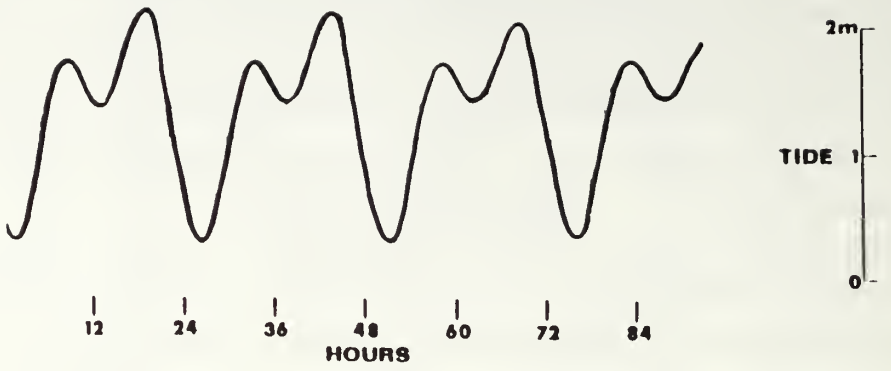

Figure 9. Monterey Bay tidal pattern.

widens. The longer wave action allows the beach face to dry out a little between waves, so the swash permeates the sand and there is no backwash to carry the beach away.

Monthly and annual reports on the surface wave and current conditions along the California coast are distributed through the Coastal Data Information Program (CDIP), a cooperative program by the U.S. Army Corps of Engineers and the California Department of Boating and Waterways [Refs. 22,23]. The data for these reports are gathered by four types of ocean measuring equipment:

1. four gage slope array for nearshore direction and energy measurement;
2. surface following buoy for deepwater wave energy measurement;
3. single point gage for nearshore wave energy measurement; and
4. single point gage for deep ocean wave energy measurement.

A station of particular interest in connection with the upcoming tomography experiment is Station 8, North Monterey Bay buoy, at latitude 36°56.9'N, longitude 122°25.1'W and depth of 320 m. Figure 10 on page 23 and Figure 11 on page 24 are two pages taken out of the December 1987 report [Ref. 22]. The data page for a period of time from 9 December to 19 December 1987, exactly one year prior to the December 1988 tomography experiment, provides numerical information on significant wave height, total amount of wave energy and the percent of energy per band period. Note the high wave energy level on 16 December 1987, with the greatest energy occurring in the period between 8-14 seconds. The wave energy spectra of Figure 11 on page 24 visually illustrates this surge. In all likelihood, a storm passed through the area on this date, kicking up the waves.

NORTH MONTEREY BAY BUOY
DEC 1987

PST DAY/TIME	SIG HT (CM.)	TOT EN (CM SQ)	PERCENT ENERGY IN BAND (TOTAL ENERGY INCLUDES RANGE 2048-4 SECS) BAND PERIOD LIMITS (SECS) 22+	22-18	18-16	16-14	14-12	12-10	10-8	8-6	6-4
9 1501	324.4	6577.5	0.3	0.5	9.1	23.8	25.3	11.4	18.4	7.7	4.1
9 2100	357.4	7983.0	0.2	0.3	1.5	25.1	38.3	14.9	10.7	6.3	3.1
10 0300	338.7	7170.8	0.1	0.1	1.9	11.6	30.2	25.0	20.1	7.9	3.5
10 0906	309.3	5979.7	0.4	0.4	1.4	19.0	30.9	22.2	13.8	8.4	4.0
10 1523	363.2	8246.5	9.2	5.4	3.0	14.9	27.7	20.6	9.9	7.4	2.4
10 2101	490.2	15016.1	2.1	16.3	13.2	20.1	15.5	13.2	6.8	7.3	6.0
11 0300	461.5	13308.6	0.8	7.0	19.2	11.9	12.8	11.3	17.1	13.9	6.5
11 0900	461.7	13322.3	0.4	4.3	14.3	14.5	16.7	21.3	16.8	8.2	4.1
11 1503	470.4	13829.8	1.1	2.3	8.3	11.9	20.6	24.8	15.7	9.8	6.0
11 2102	455.9	12990.1	0.3	1.7	8.3	16.4	20.0	20.4	18.9	9.9	4.5
12 0302	449.5	12626.9	0.2	0.3	2.1	10.5	36.9	22.5	15.1	7.9	5.0
12 0902	414.0	10714.6	0.3	0.3	1.7	3.8	19.0	34.2	18.1	16.0	7.1
12 2058	471.4	13891.1	0.2	0.2	0.4	7.2	22.2	20.2	22.6	19.8	7.6
13 0302	391.7	9590.0	0.1	0.1	0.2	6.0	21.0	23.4	21.1	19.1	9.5
13 0902	370.2	8567.1	0.2	0.2	0.3	3.3	10.5	28.4	21.5	24.2	11.8
13 2102	207.5	2690.8	0.2	0.3	0.3	1.0	11.1	26.1	16.4	17.0	28.1
14 0302	187.4	2194.2	0.1	0.1	0.3	1.2	12.7	18.2	36.5	16.2	15.2
14 0901	133.5	1113.2	0.1	1.0	1.2	4.5	22.3	13.8	23.5	19.9	14.2
14 2059	140.8	1239.3	0.2	1.6	23.3	11.4	12.8	28.6	12.8	6.0	3.7
15 0251	136.4	1162.4	0.2	0.6	18.4	26.4	13.9	7.1	6.5	4.0	23.3
15 0857	220.1	3027.9	0.3	0.2	3.0	9.5	7.4	3.9	1.5	37.6	37.1
16 0255	732.4	33523.8	0.3	0.3	0.4	2.5	23.3	41.5	17.4	9.7	4.9
16 0855	597.2	22293.1	0.2	0.2	0.9	5.4	26.7	28.0	18.9	13.3	7.0
16 1501	520.0	16897.0	2.1	1.1	0.7	1.9	5.9	38.8	27.3	13.8	8.8
16 2057	347.8	7559.9	0.1	0.1	0.5	1.6	11.4	31.2	30.6	15.9	9.0
17 0257	309.3	5981.0	0.1	0.1	0.3	2.0	8.0	34.4	40.0	10.1	5.5
17 0857	294.3	5414.7	0.1	0.1	0.3	1.8	13.6	32.9	35.3	12.1	4.1
17 1459	285.4	5091.9	0.6	0.5	0.5	1.6	20.1	36.4	20.8	13.6	6.4
17 2059	265.3	4400.3	0.2	0.2	0.2	1.4	15.8	34.0	23.1	16.8	8.9
18 0259	252.5	3984.2	0.1	0.2	0.3	1.1	6.7	38.3	28.9	16.4	8.5
18 1459	207.0	2677.9	0.2	0.7	0.3	0.7	2.6	26.7	30.8	26.5	11.9
18 2059	228.8	3270.8	0.7	2.9	0.7	0.9	1.9	15.1	44.7	21.6	11.8
19 0259	269.4	4537.2	0.2	10.5	4.5	0.4	1.7	8.9	34.3	26.2	13.9

Figure 10. North Monterey Bay buoy, December 1987, wave energy data. [Ref. 22]

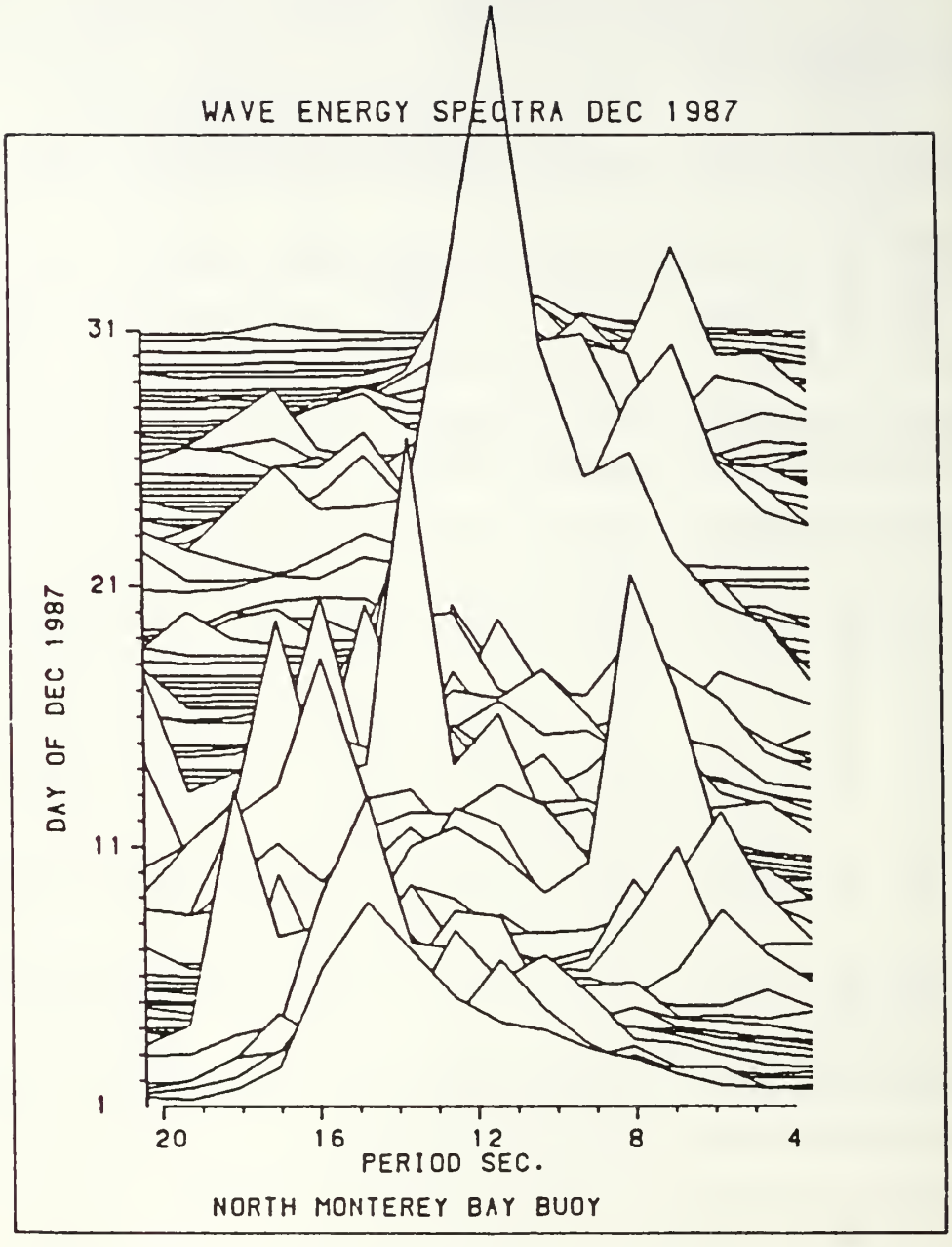

Figure 11. North Monterey Bay buoy, December 1987, wave energy spectra graph. [Ref. 22]

Based on a chart from the CDIP Annual Report [Ref. 23], the October through December 1987 period had the highest average wave height. There was a 58% seasonal probability that the significant wave height would exceed 2 m, 32% for 3 m and 13% for significant wave heights greater than 4 m. These conditions for December 1987 may not be representative of the ocean situation that will occur during the tomography experiment. The important point is that the CDIP report for December 1988 will be an excellent source of surface wave information, in corroboration with other experimental measurements, when the tomography data is analyzed for determining the surface wave spectrum.

H. INTERNAL WAVES AND CANYON CURRENTS

As defined by Clay and Medwin [Ref. 3], internal waves "... are volume gravity waves having their maximum vertical displacement amplitude at a plane where the density is changing most rapidly with depth or between two water masses of different densities." A number of studies [Refs. 12,21,24,25], have presented evidence that the Monterey Submarine Canyon commonly has internal waves of a semidiurnal nature. The results of a conductivity-temperature-depth (CTD) time series for five stations in the Monterey Canyon have indicated that these internal tides had heights of 50 m to 120 m [Ref. 24].

Along the bottom of the Monterey Canyon the currents are strong and fluctuating, with speeds up to 50 cm/s [Ref. 12]. These flows are generally in an upcanyon direction, but in truth they appear to have almost no connection with the canyon axis. Cross valley flows are a predominant feature along MSC [Ref. 21], but there has not been a determination as to the cause of this phenomenon. Tides and wind direction appear to have no relationship to the cross currents [Ref. 21].

Current-meter data (Table 1 on page 26) from MSC provide information on the internal tide up- and downcanyon reversal cycles. Estimated upcanyon advance rates for an internal wave in the Monterey Canyon is 25 cm/sec between 7.5 km and 8.5 km away from the canyon head (depth of 400-375 m), and 38 cm/sec from 7.5 km to 2 km up the canyon (375-150 m depth) [Ref. 25].

Based on small amplitude wave theory, a long wave will increase in height as it moves into shallow water, but its period will remain constant. As an internal wave advances up the canyon towards the head, where it is narrow and shallow, the wave energy may become focused and the wave height increase, taking on the appearance of an internal tidal bore. This bore "... is characterized by a rapid increase in temperature at

a fixed position, in which the advancing water forms an abrupt front." An internal bore at the MSC head has been indicated by thermistor data showing a 3.8°C/hr temperature change. [Ref. 24]

Table 1. UP- AND DOWN-CANYON REVERSAL CYCLE DATA FOR MONTEREY CANYON. [Ref. 21]

METER POSITION		AVERAGE CYCLE LENGTH (hrs)	DIRECTION OF NET FLOW	AVERAGE SPEED (cm/sec)		
DEPTH (m)	HEIGHT ABOVE FLOOR (m)			UP	DOWN	CROSS
155	3	7.2	down	9.2	10.3	4.0
155	30	4.4	up	8.5	6.7	3.7
357	3	8.8	down	13.8	11.4	5.2
384	3	8.0	up	12.1	13.1	5.6
1061	3	6.5	up	19.7	16.6	15.3
1061	30	6.5	up	20.3	26.0	9.8
1445	3	8.7	up	13.2	11.1	5.8
1445	30	10.0	up	13.6	10.0	4.2

Broenkow and Smethie [Ref. 12] conducted a 24 hr time series study at two stations near the head of the Monterey Submarine Canyon. They observed internal tidal oscillations with the same period as the surface tides, but approximately 180° out of phase. The wave height was 80 m at a depth of 130 m, while at 250 m deep the height of the wave was about 120 m.

The oscillating internal tide produces a volume convergence during ebb tide and divergence at flood tide. During volume convergence, the denser canyon water rises above the rim and settles on the shelf. When the internal tide reverses and goes downcanyon, the dense canyon water on the shelf starts flowing back into the canyon; however, as a result of mixing, surface heating and inertia, the edge of this dense water remains behind on the shelf. Figure 12 on page 27 illustrates volume convergence and divergence for 13 and 14 September 1979. A 20 m thick lens of 12°C water flowed out of the canyon as the internal tide rose, and remained on the north shelf when the rest of the dense water fell back into MSC at tidal reversal. This lens was estimated to affect an area of 26 km^2. Data indicate that the volume convergence is about $240x10^6 m^3$/8 hr, which would put the speed of water crossing the rim of MSC at about 13 cm/s. [Ref. 24]

Internal waves along Carmel Submarine Canyon appear to follow the axis, unlike the situation in Monterey Canyon. The currents at 3 and 30 m above the floor showed very similar characteristics. Current-meter data (Table 2 on page 27) is given for Carmel Canyon's up- and downcanyon reversal cycles for internal tides. Interestingly, almost all of the northern cross canyon flows occurred at ebb tide. [Ref. 21]

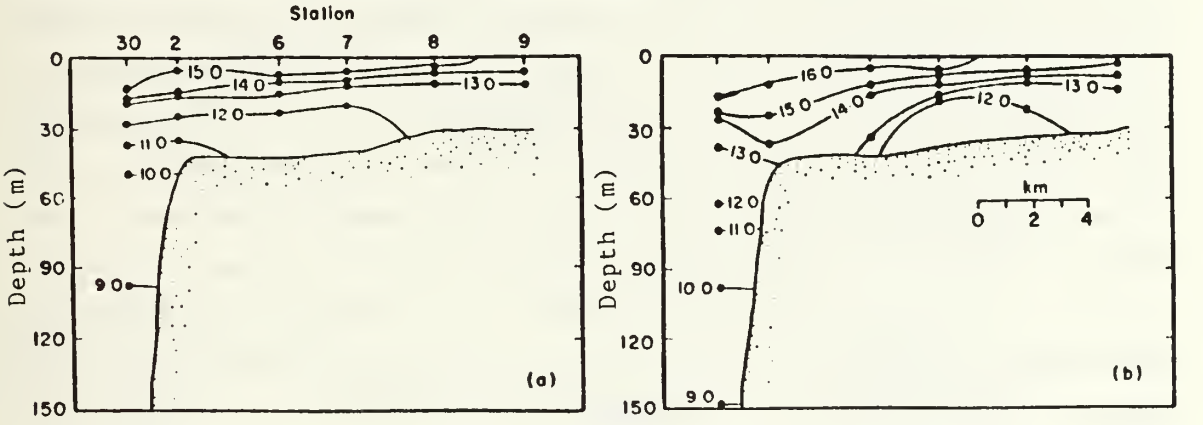

Figure 12. Temperature distribution (°C) at (a) high, and (b) low internal tide, Monterey Canyon axis, 13-14 September 1979. [Ref. 24]

Table 2. UP- AND DOWN-CANYON REVERSAL CYCLE DATA FOR CARMEL CANYON. [Ref. 21]

METER POSITION		AVERAGE CYCLE LENGTH (hrs)	DIRECTION OF NET FLOW	AVERAGE SPEED (cm/sec)		
DEPTH (m)	HEIGHT ABOVE FLOOR (m)			UP	DOWN	CROSS
156	3	3.6	down	5.0	7.6	4.0
205	3	4.1	down	12.4	14.5	4.3
348	3	5.1	down	15.8	19.5	7.9
1070	3	10.2	down	9.6	15.0	4.4
1445	3	11.7	down	11.3	10.3	5.2

IV. THE MULTIPLE PROFILE RAY-TRACING PROGRAM (MPP)

A. DESCRIPTION

The analysis tool that was the basis for the selection of receiver locations in Monterey Bay for the December 1988 tomography experiment is called the *Multiple Profile Ray-Tracing Program (MPP)*. Originally written as five separate programs by Ocean Data, Inc., for the Office of Naval Research [Ref. 26], the MPP program has evolved to its present form through extensive modification by John Spiesberger of the Woods Hole Oceanographic Institution. This program computes transmission loss and arrival structure for the eigenrays that it determines will arrive at a fixed receiver, from a source at a fixed depth. The ocean is modeled with a range-dependent sound speed profile (SSP), variable bottom depth and bottom reflectivity. Transmission loss is calculated under a variety of options, including

1. asymptotic treatment of caustics with rms or fully coherent addition of the two paths in the interference region of the airy functions;
2. surface-image interference at the source; and
3. source and or receiver vertical directivity patterns.

Output that is generated, based on a successful finding of eigenrays, is

1. all input data;
2. ray trajectories at arrivals;
3. sequential signature groups;
4. precise angle, time and intensity at a limited number of range points using quadratic interpolation;
5. transmission loss versus range;
6. plot of eigenray path from source to receiver; and
7. stick plot of transmission loss versus arrival time for the eigenrays.

B. PROGRAM FLOW

Figure 13 on page 29 is a block diagram of the program flow, with input files shown on the left side of each routine and output files on the right side of the routine block. The command file runart is called upon to execute the routines writefiles2art, mpp1, mpp2cout (1st pass), zofth, post63 and mpp2cout (2nd pass), after an input data file has

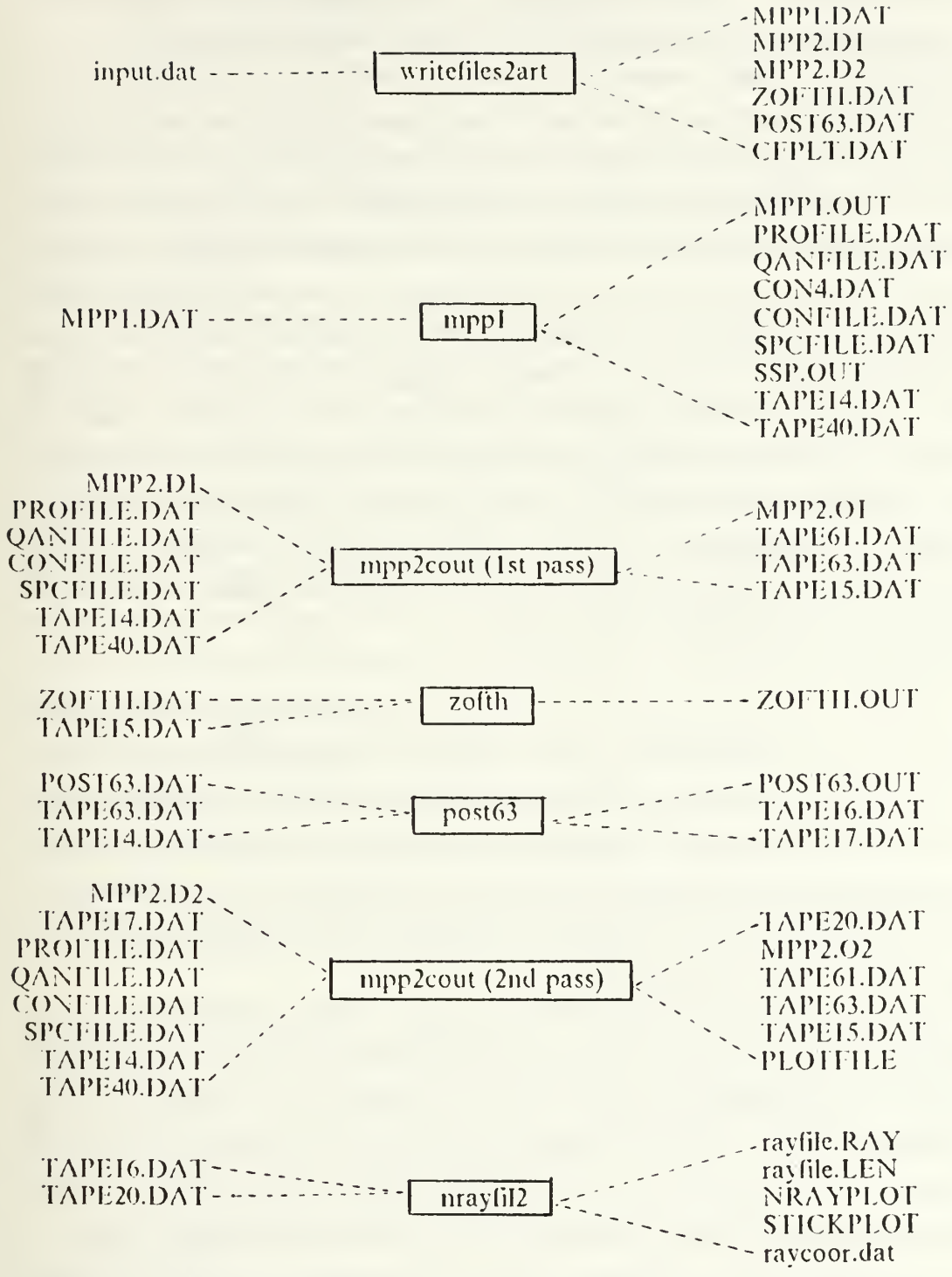

Figure 13. MPP block diagram with input and output files.

been created by the user. The routine nrayfil2 is used to generate the ray tracing and stick plot graphs from binary data in files TAPE16.DAT and TAPE20.DAT.

Writefiles2art is a small routine that separates and reformats the user-generated input data into six different files. These six files are accessed by the other programs that runart executes. Zofth is another short routine that plots initial angle versus the depth at which its ray path arrives at the receiver location (range). Most of these rays do not arrive at the receiver, i.e., they are beyond the the vertical miss allowance. For the simulation, a ray has to come within a vertical distance of 15 m from the receiver, either above or below. Since the receiver was placed 1 m above the floor, the simulated vertical miss is 15 m above and 1 m below the receiver. Post63 is the eigenray post-processor routine. It determines the eigenrays' arrival angle at the receiver, creates file TAPE16.DAT which is used by nrayfil2 to generate the ray trace graph, and produces a printout enumerating the eigenrays in three sorted lists, based on increasing travel time, decreasing initial angle and increasing transmission loss. The function and logical flow of the four main programs, used to determine and plot the eigenrays at a given receiver location, will be described in more detail.

1. MPP1

Mpp1 is the second routine called by the command file runart. Its purpose is to determine the sectors within the region between two range-stipulated input SSPs. These sector determinations are required for calculating ray paths in mpp2cout. Mpp1 also uses the input bottom data to assemble the bottom profile and tabulate the bottom loss as a function of grazing angle in each of the range domains. If a loss function is specified as "modified Rayleigh", the program tabulates it on a variable mesh to yield accurate values by linear interpolation.

Sectors can be either triangular or rectangular. Rectangular sectors ease the computational crunching of the ray path determination logic, and speeds up the computer time. Sector determination begins with a comparison of the sound speed at the very bottom of the first SSP (ssp1) versus the very bottom of the second SSP (ssp2). If ssp1 equals ssp2 at the bottom, then a horizontal line is attached between the two points, and the next higher profile values for ssp1 and ssp2 are compared. If the two values are not identical, then a triangular sector will be specified. Once one sector has been determined to be a triangle, the entire upper region will be triangularized, even though all shallower points of the two SSPs may match. The only way to have all rectangular sectors is to have completely identical SSPs.

2. MPP2COUT (1st pass)

Mpp2cout (1st pass) is the first half of the eigenray processing programs. The main program is very small, but it calls seven subroutines that in turn call other subroutines. The first subroutine, ctl1, inputs data and takes care of initialization. The program then loops through the rest of the subroutines, until it equals the number of passes that the user's input file stipulated as a maximum number of passes. The first subroutine in the loop, reset, locates the sound speed triangular section that encompasses the receiver.

The next subroutine, ctl2, is the longest and accomplishes the most. After initialization, it determines the initial velocity sector for the ray and the direction that the ray will go. As the ray travels toward the receiver, ctl2 computes the ray intersections with sector boundaries (top, bottom and sides), stores parameters and checks for bottom reflections. Next, it calculates the spreading factors and performs a check for caustics. If there is a caustic, it locates the caustic for both curved and straight rays. Continuing, this subroutine updates the intensity derivatives for bottom reflection, surface reflection, sector crossings and region crossings, and the transmission loss is then updated. After arrival information is stored, then the ray is checked to see if it should be cut. The following are reasons to cut a ray:

1. ray has reached maximum range (ray range > target range);
2. ray angle too steep (ray has reflected at an angle > $\pm 85°$);
3. max bottom reflections exceeded (as stipulated by the user); and
4. max turning events exceeded (the total number of bottom reflections, bottom horizontals, surface reflections and surface horizontals have exceeded the maximum number of turning points as stipulated by the user).

The rays that were not cut are now sorted in increasing angle order by the subroutine sort61. The second biggest subroutine, iterat, then determines the relationship of the uncut rays with the receiver at the target range. It also extrapolates new rays and checks the angle loss tolerance for these new extrapolated rays. All of the uncut rays have one of the following ray/target relationships:

1. good bracketted source depth (IDENT = 2), where a pair of rays vertically surround the receiver;
2. good diffraction field (IDENT = 3), where a pair of rays do not bracket the source but they appear to be within the receiver's focus or convergence region;
3. badly bracketted source depth (IDENT = 4), where a pair of rays fail the criteria for the above relationships;

4. bad diffraction field (IDENT = 5), where the ray pair appear to be within the receiver's focus, but they are outside of the time tolerance;
5. good bracketted source, two eigenrays (IDENT = 6);
6. badly bracketted source, two eigenrays (IDENT = 7); and
7. bad signature pair of rays (IDENT = 8), which is the most common ray/target relationship, resulting from the ray pair being too close to each other.

Mpp2cout concludes by calling subroutines clean, which removes the deletable angles from file TAPE61, and dump63, which prints out the ray status for all uncut rays. The program then increments the pass number counter and starts all over again.

3. MPP2COUT (2nd pass)

The second pass of mpp2cout is the eigenray plotting run and is logically very similar to the first pass of mpp2cout. It is executed after post63. This run begins with the "good bracketted source" and "good diffraction field" rays that were first identified in mpp2cout (1st pass) and post-processed in post63. A trace for each of these rays is produced. The following information is provided in the trace at every surface reflection, bottom reflection, refraction and caustic along each ray's path:

1. range (km),
2. depth (m),
3. angle (deg),
4. time (sec),
5. loss (dB),
6. number of caustics,
7. arrival number,
8. number of surface horizontals (refractions),
9. number of surface reflections,
10. number of bottom horizontals (refractions),
11. number of bottom reflections, and
12. total number of turning points.

Another main difference between the two passes is that this second pass generates the file TAPE20.DAT, used by nrayfil2 to graph the ray plots and stick plots. For each coordinate on the ray trace, not just the turning points, TAPE20.DAT stores the range (km), depth (km), angle (radians) and sound speed (km/sec). In the beginning of this pass, angle values are read in from file TAPE17.DAT. Otherwise, mpp2cout (2nd

pass) goes through the same logical flow as mpp2cout (1st pass), and is the final eigenray processing program executed by the command file runart.

4. NRAYFIL2

The routine nrayfil2 is called by the user after the command file runart has executed all of the eigenray-determining programs and eigenrays have been identified. Since nrayfil2 is used to generate the ray tracing and stick plot graphs, there is no reason to execute this routine if there are not any eigenrays. This routine should be run immediately after the programs executed by runart determine one or more successful eigenray(s), or else rename TAPE16.DAT and TAPE20.DAT files so that they can be accessed later by nrayfil2.

There are six options that can be accessed in this program: 1. make, 2. inspect, 3. rayplot, 4. stick, 5. add, and 6. delete. "Make" has to be the first option specified since it generates two files of ray data that is used by the other options. It requires as input the files TAPE16.DAT and TAPE20.DAT that were generated for the last executed MPP run. The output file name has to be all capitalized and end in .RAY. If, for example, the user specifies the ray file name as RCVR2.RAY, this "make" option creates a file with that name and another file with the name RCVR2.LEN. Both are needed for the other options.

"Inspect" allows the user to inspect the rays and to store all of the ray coordinates in the file RAYCOOR.DAT. These ray coordinates are used to graph the ray trace, and include the values of range, depth, angle and sound speed for every specified point on the ray trace graph. "Add" allows a new ray to be added to an existing ray file, while "delete" removes an unwanted ray from the ray file.

The last two options plot graphs. "Rayplot" will plot the ray trace of one or more rays, based on the inputted ray file name. For the first ray file stipulated, a list of all the initial ray angles are displayed on the screen, after the user has specified the graph dimensions and titles. The user indicates the ray angle that is to be plotted, and has the option of plotting more rays on the same graph or stopping. Another ray file can be accessed, and those angles can be added to the graph with the first ray file angles. The graph data is placed in the NRAYPLOT file, which is then plotted. The ray traces in Appendix B were produced with this option. "Stickplot" graphs the transmission loss for all the rays that are contained in the user-specified ray file. The only input options are graph dimensions, graph title and ray file name.

V. MPP INPUT/OUTPUT

The focus of this thesis is to recommend the locations for six receiver hydrophones that will be used in the December 1988 tomography experiment, and to provide eigenray and travel time information related to each site. The recommendations will be based on the results from two-dimensional, range and bathymetry dependent, ray tracing computer simulations for various locations in and around the bay, as well as a preliminary assessment of the oceanographic and geo-acoustic environment of the region. This chapter will identify the possible receiver locations that were addressed, the input parameters used in the MPP computer program, and the results from the simulations.

A. SIMULATED RECEIVER LOCATIONS

Seventeen locations for possible receiver hydrophone placement were tested using the MPP program. These points are on the continental shelf surrounding the Monterey Canyon, from southwest of Santa Cruz to Pacific Grove, excluding the Monterey-Seaside nearshore area where a direct ray from the Point Sur seamount (source location) could not reach. All of these sites are shallower than 300 ft (100 m), and the hydrophones in the simulation were placed 1 m above the sea floor.

All of these locations were selected for specific reasons. Figure 14 on page 35 delineates the position of these receiver locations in the area of Monterey Bay, while Table 3 on page 36 provides the specific position. Any eigenrays arriving at receiver numbers 6 and 7 will have traveled through Carmel Canyon and the trough of Monterey Canyon. Sites 4, 8 and 15 are in the general area of the Monterey Canyon head, where internal waves are at their highest amplitudes. Receiver 5 is located on the edge of the south wall of Monterey Canyon, and was selected for comparison between rays going through the narrow part of MSC and those that do not. Any eigenrays that receiver 14 would pick up have traveled right down the Monterey Canyon in the granite wall formation. Locations 3, 9, 10, 12 and 13 surround the Soquel Canyon. Finally, receiver positions 1, 2, 16 and 17 are out of Monterey Bay and would have eigenrays that traveled through the trough of Monterey Canyon, where the floor is wider.

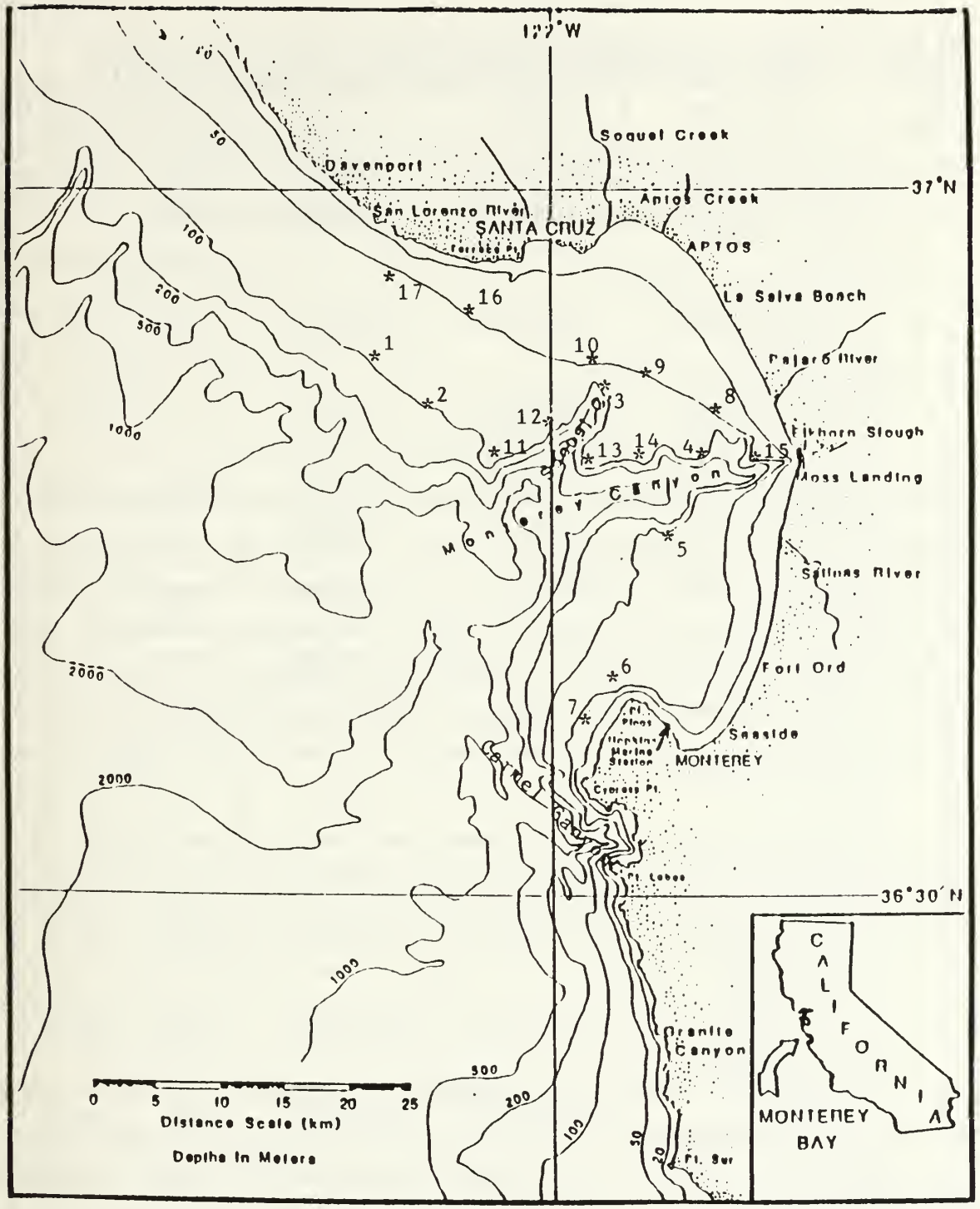

Figure 14. Possible receiver hydrophone locations for tomography experiment.

Table 3. SIMULATION RECEIVER POSITIONS, RANGE AND DEPTH.

RCV NO	LOCATION	LONGI-TUDE	LATITUDE	RANGE (km)	DEPTH (m)
1	SW of Santa Cruz	122°09.60′W	36°53.10′N	59.35	97.76
2	SSW of Santa Cruz	122°05.00′W	36°51.20′N	57.99	90.44
3	Head of Soquel Canyon	121°57.35′W	36°51.75′N	63.87	90.44
4	W of Moss Landing, Monterey Canyon north wall	121°52.20′W	36°48.65′N	63.49	90.44
5	W of Salinas River mouth, Monterey Canyon south wall	121°54.10′W	36°45.00′N	56.51	90.44
6	NW of Point Piños	121°58.35′W	36°39.25′N	44.43	90.44
7	WSW of Point Piños	121°59.25′W	36°37.60′N	42.02	50.21
8	W of Pajaro River mouth	121°51.00′W	36°50.00′N	67.49	54.00
9	ENE of Soquel Canyon head	121°54.90′W	36°57.00′N	67.15	48.38
10	N of Soquel Canyon head	121°57.40′W	36°52.75′N	68.39	44.72
11	North wall, west of Soquel Canyon juncture	122°01.55′W	36°48.80′N	56.04	90.44
12	North wall, Soquel Canyon	121°59.65′W	36°50.25′N	59.72	90.44
13	East side, Soquel Canyon juncture	121°57.90′W	36°48.65′N	58.53	90.44
14	North wall of Monterey Canyon, prior to Soquel Canyon juncture	121°55.00′W	36°48.25′N	60.36	90.44
15	Near head of Monterey Canyon	121°50.20′W	36°47.90′N	64.36	90.44
16	SW of Santa Cruz, nearshore	122°03.50′W	36°54.50′N	66.20	45.00
17	W of Santa Cruz, nearshore	122°08.17′W	36°56.50′N	67.47	48.93

B. INPUT

For each receiver location of interest, an input file was created that provided the MPP routines with the following information:

1. range and depth of source;
2. range and depth of receiver;
3. minimum and maximum angle range for the eigenray search;
4. number of initial rays;
5. number of turning points and bottom reflections;
6. sound speed profile (SSP) data;
7. bathymetry data from source location to beyond the receiver location; and
8. bottom reflectivity values, i.e., loss for a given angle.

MPP sets limits on some of the input variables. For instance, the maximum number of initial rays is 80, the maximum number of points in the SSP is 100, the maximum number of bottom loss domains is five and the maximum number of bathymetry points is 62. The source and receiver were placed 1 m above the floor; otherwise, negative initial rays would have been deleted immediately. All of the individual input files contained exactly the same information on the source position, SSP, initial rays, turning points and bottom reflection data. The source and receiver were always placed 1 m above the sea floor.

A 15 December 1987 sound speed profile (Figure 15 on page 39), generated by a computer system called ICAPS [Ref. 27], was used for both SSP curves in each individual file. The ICAPS-generated sound speed profiles for an approximate source position (36°21′N, 122°18′W) and a general receiver position in the bay (36°50′N, 121°51′W) were identical down to a depth of 360 m, which was the cutoff for the receiver area SSP. The MPP computer routines triangularize all sectors between two inputted sound speed profiles if the SSPs do not begin at the same maximum depth, which complicates the ray tracing calculations and requires much longer processing time. Since it was advantageous to have rectangular sectors for the SSP region, the deeper ICAPS SSP (source location) was specified for both the source location and for a spot about 2 km beyond the receiver location. This did put the profile through the sea and shelf floor in all areas. The exact values used for the sound speed profile in the MPP computer simulation are specified in Table 4 on page 40.

Each receiver location's input file contained the following parameters with associated values:

1. source depth = 831.1 m and source range = 0.0 km;
2. minimum and maximum angles allowed in eigenray search = -15.0 to -10.0, -10.0 to -5.0, -5.0 to 0.0, 0.0 to 5.0, 5.0 to 10.0 and 10.0 to 15.0 degrees (six separate computer runs);
3. number of rays shot out from source on first pass of search = 31;
4. maximum number of passes allowed for ray search = 100;
5. total number of turning points or reflections allowed = 350;
6. maximum number of bottom reflections = 100;
7. number of loss domains = 1; and
8. bottom loss at angles of 0 and 90 degrees = 0.0 dB.

This data facilitated a "best case" simulation in which there was no bottom loss when rays bounced off the sea floor and canyon walls (total reflectivity), while allowing for a large number of surface and bottom reflections.

The range value for each receiver was determined by a computer program that used the longitude and latitude of both source and receiver positions to determine the range and bearing from source to receiver. This program included a correction for earth curvature. Table 3 on page 36 gives the range and depth for all 17 locations.

Bathymetry values along a straight line from source to receiver were manually extracted from a NOAA ocean bottom contours chart [Ref. 28]. The selected depths were generally contour rings of some multiple of 100 fathoms. Every once in a while a significant reading (based on the author's subjectivity) that wasn't a contour ring was included in the bathymetry data to provide a more relevant and accurate bottom profile. The maximum number of bathymetric points that could be entered per input file was 62, but none of the files contained more than 50 points. The distance of each bathymetic point from the source location was calculated by using linear interpolation between source and receiver positions. All points beyond the receiver were considered to be at the same depth as the receiver location for this simulation. The program appeared to prefer this little idiosyncracy, but the eigenray results were not affected. The bathymetric data for all 17 receiver hydrophone sites are provided in Appendix A.

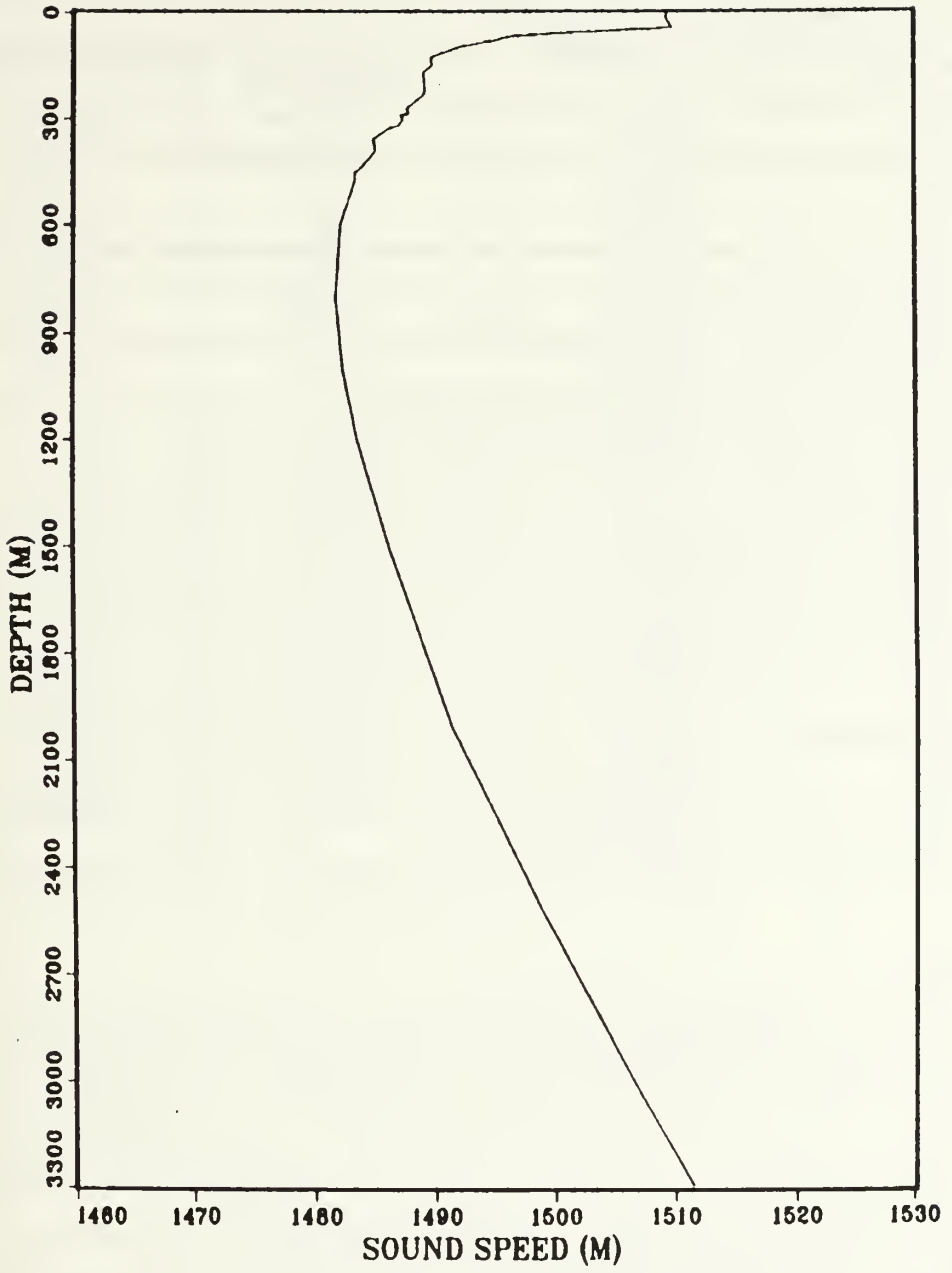

Figure 15. Typical December sound speed profile for Monterey Bay.

Table 4. DECEMBER SOUND SPEED PROFILE VALUES FOR MONTEREY BAY REGION.

DEPTH (m)	SOUND SPEED (m/s)		DEPTH (m)	SOUND SPEED (m/s)
0.	1509.46		321.	1487.08
16.	1509.40		327.	1486.41
43.	1509.85		357.	1485.00
58.	1500.48		390.	1485.18
65.	1497.58		438.	1484.04
68.	1496.60		451.	1483.47
82.	1494.82		475.	1483.49
95.	1492.64		600.	1482.32
116.	1490.60		800.	1481.89
128.	1489.78		1000.	1482.54
150.	1489.91		1200.	1483.73
169.	1489.18		1500.	1486.26
230.	1489.26		2000.	1491.44
273.	1487.77		2500.	1498.67
287.	1488.01		3000.	1506.65
291.	1487.32		3290.	1511.51
303.	1487.53			

C. OUTPUT.

More that 100 computer runs were performed to determine possible eigenrays with associated travel time and transmission loss for the December tomography experiment. In a majority of these runs, no eigenrays were identified. This Monterey Bay experimental region is a particularly tough area to conduct a tomography experiment due to the wide fluctuations in the sea floor. The MPP program would drop a ray if it ever exceeded a $\pm 85°$ angle anywhere along its path. Most of the time when a ray hit one of the steep canyon walls, the ray would bounce off at greater than 85°. A few of the rays exceeded the maximum number of turning points or reflections that was stipulated in the input file, and thus were dropped along the way of the ray search.

The MPP program identified rays that either bracketted the receiver or were within the diffraction field. The bracketting rays were shown to arrive at the receiver, and will

be considered eigenrays. The diffraction field rays passed through the receiver's focus or convergence zone, but did not necessarily arrive at the receiver. For this simulation, the maximum vertical distance that a ray could miss the receiver was stipulated at ±15 m. Of the 58 rays that the program identified, 17 diffraction field rays were outside of the vertical miss tolerance. These 17 rays are not considered eigenrays and have been eliminated from post-program analysis. Twenty-six of the remaining 41 rays arrived at location 17.

Nine locations had no rays arriving at the receiver. These were sites 3, 6, 9, 10, 11, 12, 14, 15 and 16. Five of these positions are in the area of Soquel Canyon, one was near the head of Monterey Canyon, another (receiver 14) was at a position selected for its difficult ray path due to the winding canyon, the seventh was off of Point Piños in a shallow area, and the last was in the shallow nearshore area of Santa Cruz. The results for the other eight receiver spots will be outlined and a table of all eigenrays with initial angle, arrival angle, travel time and transmission loss will follow the output discussion.

An interesting result occurred for receiver location 16 when the source was positioned down the slope in front of the seamount at the 913.0 m depth (which changed the range to 64.0 km), instead of on the top of the seamount where the source was placed for all of the other simulations. Four eigenrays in the 0° to -5° range now arrived at receiver 16 when before all rays were lost. On top of the seamount these initial rays bounced off of the seamount immediately and were driven upward, eventually to be lost by exceeding the 85° angle. However, on the side of the seamount they continued a downward trace until they refracted up (did not hit the bottom). Table 5 on page 42 provides data on these four eigenrays. For the simulation, the source was placed on the top of the mount because the author felt that in the actual experiment, it would be easier to moor the source on the top rather than at some particular point on the slope of the seamount. This is just one indication that the eigenray arrivals are very sensitive to both source and receiver placement.

Because a 16 Hz bandwidth pseudo-random phase-encoded signal of 1.9375 s duration is planned to be used in the December experiment, a separation of ray arrivals by 1/16 Hz = 62.5 ms is necessary for resolving those arrivals [Ref. 29]. Also, the entire bundle of eigenrays must arrive at the receiver with a total separation time of under 1.9375 s. The description of the output is based on this requirement.

Table 5. EIGENRAY INFORMATION FOR SITE 16 BASED ON CHANGE OF SOURCE PLACEMENT.

TRAVEL TIME (sec)	INITIAL ANGLE (degrees)	ARRIVAL ANGLE (degrees)	TRANSMISSION LOSS (dB)
47.0753	-2.8463	-32.0741	93.6
47.4651	-2.9378	-54.3062	94.1
47.4652	-4.6413	-54.3904	94.2
47.4872	-2.9774	55.7486	94.1

1. Receiver Location 1.

Receiver 1 was placed southwest of Santa Cruz on the continental slope not far from the canyon edge. Eigenrays would have to travel along a path that brings them over the deepest but widest part of Monterey Canyon in this experimental area. Two eigenrays at initial angles of 2.0837° and -3.9048° were identified (Table 6 on page 49). These two rays have a fairly clean ray path. After leaving the seamount with one possible bounce, the rays travel along the sound channel axis track until they hit the north wall of the Monterey Canyon trough at around 31 and 39 km downrange. They then bounce up and have a turning point refraction before again bouncing off of the now gentler slope at around the 52.0 km mark. Either three or four bottom reflections occur before each ray arrives at the receiver. These rays experience very few bottom bounces that could absorb some of the sound or change the direction of the rays.

The separation time between the 2.0837 and -3.9048 ray is not good at 43 ms. This spacing is below the experiment's separation minimum for identifying the individual rays. The transmission loss values for both rays are in the upper 90 dB. The ray trace and the transmission loss profile graphs for these rays can be found in Appendix B.

2. Receiver Location 2.

East-southeast of receiver 1 is the site for receiver 2. The simulated hydrophone is placed on a gentle slope a little north of the main Monterey Canyon wall. Rays arriving at this receiver would travel across a wide and deep portion of the canyon, similar to the receiver 1 rays. The north wall rises until at about 39 km downrange of the source, there is a drop of the sea floor for about 6 km before rising steeply again up to the continental shelf.

One eigenray was identified by the simulation with a 96 dB transmission loss. The -14.8056 angle ray initially bounces off of the seamount and refracts before striking the north wall close to 28 km away from the seamount. It then reflects off the surface and bounces in the dropped floor of the north wall before surface reflecting and bouncing its way on the shelf, prior to arriving at the receiver. It bounces off of the continental shelf six times. Information on this ray is found in Table 6 on page 49, and the graphs for the ray trace and transmission loss are located in Appendix B.

3. Receiver Location 4.

Receiver 4 is due west of Moss Landing, situated on the Monterey Canyon north wall edge. Rays arriving at this location will pass over Carmel Canyon and the continental shelf before crossing Monterey Canyon. This position is above the narrower and shallower portion of Monterey Canyon, so it may be a good location for an internal waves study.

Three eigenrays were identified, having transmission losses between 83.5 dB and 95.6 dB, and with good arrival separation between the first two rays (Table 6 on page 49). A graphical depiction of the ray paths can be found in Appendix B, along with the transmission loss graph. The arrival time separation between the last two rays (-5.9567 and -5.9841) of 0.8 ms is too short for the conditions of the experiment. The ray with the initial angle of -9.5632° arrives first and is followed in 134 ms by ray -5.9567.

The three eigenrays have the same general ray path. Ray -9.5632 has one refractive turning point, while the other two rays display one cycle of refraction (two turning points). All of the rays have a multitude of surface and bottom bounces as they proceed along the shelf, and they bounce twice in Monterey Canyon with one refraction between the bounces. Ray -9.5632 has three surface reflections at the end of its path, and the other two rays have two surface bounces. All of the rays have paths that could be used in both the internal wave and surface wave studies.

4. Receiver Location 5.

Situated on the south edge of the Monterey Canyon, due west of the Salinas River mouth, is the location for receiver 5. It was selected to give the tomography experiment a means by which to possibly recognize the effects that traveling through the Monterey Canyon head would have on an eigenray, such as internal waves or internal bores. The unfortunate aspect of this location is that the rays have to travel over 16 km of shallow shelf, which manifests itself in possibly a hundred or more surface and bottom reflections. The ray trace graph in Appendix B illustrates this oscillation. Transmission

loss plot follows the ray trace. Table 6 on page 49 contains tabularized data on the two eigenrays.

Ray 6.4800 refracts once on either side of reflecting off the bottom, then hits high on the side of the Carmel Canyon east wall, before oscillating its way along the continental shelf. The shelf is sandy, so there will be some absorption and not the total reflectivity that was simulated. Simulated transmission loss for the ray is 97.7 dB, but parameters for bottom loss were not included in the computer input because of the great variation in the sediment and geology along any one path. It should be expected that the real world case would have a larger dB loss.

5. Receiver Location 7.

The shallow nearshore region just off of Asilomar Beach in Pacific Grove is the location for receiver 7. This is the closest position to the source-moored seamount in this simulation. The rays pass perpendicularly over the Carmel Canyon axis and the wider Monterey Canyon trough, but a straight path from source to receiver stays clear of the narrower portion of the winding canyon. Since the receiver site is situated on the shelf at approximately 3 km from the edge of the Carmel Canyon, most of the rays oscillate between the surface and shelf bottom before completing the trek to the receiver.

Four eigenrays were identified by the simulation process. Specific values for these rays are given in Table 6 on page 49. Ray trace and transmission loss graphs are found in Appendix B. Rays 1.5429 and 1.7497 appear to travel together because their paths are almost identical and there is only a 0.1 ms timespan between them. These two rays refract prior to bouncing off the trough wall just before the 31 km range. They then reflect off the surface and hit the Carmel Canyon wall twice before oscillating on the continental shelf.

The first eigenray to arrive at 28.6596 s is the 3.6113° initial angle ray. It first refracts before reflecting off the sea floor, hitting the wall above the Carmel Canyon, and oscillating along the shelf. It was a slightly weaker signal at 92 dB loss than the 2-ray pair. Arriving 57.7 ms later but a full ½ second before the ray pair is initial ray 1.7916°. This ray refracts once before bouncing off of the trough wall, reflecting off the surface, reflecting off Carmel Canyon west wall, and then refracting and bottom reflecting along the shelf. Of all the eigenrays identified in this simulation, ray 1.7916 was the strongest with only a 79 dB loss.

6. **Receiver Location 8.**

Receiver 8 is positioned due west of the mouth of the Pajaro River. Rays traveling from the source location to this receiver would follow nearly the same horizontal path as do the eigenrays to receiver 4, except that site 8 is situated a little further behind location 4 on the continental shelf. Eigenrays have to pass over Carmel Canyon, not far from the Monterey Canyon junction, and over the continental shelf before crossing Monterey Canyon just a little downslope from its head.

The MPP program determined that three eigenrays would be picked up by receiver 8; however, two of these rays are almost identical. These two rays (initial angle of 6.4969°) will be treated as though they were just one ray for the rest of the discussion. A comparison of the eigenrays may be found in Table 6 on page 49 while graphs of the ray trace and transmission loss are located in Appendix B. Ray 6.4825 makes two refracted-bottom reflected (RBR) cycles, with bounces at 22.0 nm and 40.5 nm, prior to oscillating on the continental shelf between the surface and shelf floor. This oscillating portion of the ray path covers 15.5 nm in about 14.2 s. At Monterey Canyon it bounces off the wall twice, with one refraction within the canyon, before making 13 surface/bottom reflection cycles just prior to arriving at the hydrophone. The other ray (6.4969) follows an almost identical path to ray 6.4825, with its first two bounces at the same location, one refraction within Monterey Canyon, and the same number of surface and bottom reflections at the end of its path.

Even though the paths of these two eigenrays are very similar, there is a good arrival time separation of 124.0 ms between them. Transmission losses range between 105.7 dB for the slower ray and 106.0 dB for the faster ray. These rays bounce in an area of Monterey Canyon that should exhibit internal wave effects, plus they have a considerable number of surface reflections. This location is very promising.

7. **Receiver Location 13.**

The juncture of the Soquel Canyon east wall and the Monterey Canyon north wall is the location of receiver 13. The straight-line path from source to receiver is over the section of the Monterey Canyon that has many winding and meandering turns, and includes the point where Carmel Canyon joins Monterey Canyon. It is not a good prospect for finding any eignerays, but fortunately one lone ray, which happened to stay in the deep sound channel for a long distance after its initial seamount bounce, was identified by the MPP simulation.

The first time that this ray bounces off any canyon walls is at the 54.79 km mark, not far from the edge of the continental shelf. After hitting the wall, the ray surface refracts and shelf bounces seven times before it is picked up by receiver 13. It should be a fairly strong signal at only an 84 dB transmission loss which is received in 39.6526 s at an angle of -33.2°. The eigenray data is given in Table 6 on page 49 while the ray trace and dB loss graphs are in Appendix B.

8. Receiver Location 17.

This last receiver position is located slightly south of due west of Santa Cruz in the open nearshore shelf area. It was one of the first sites to be simulated, but the resulting large number of identified eigenrays oscillating along the continental shelf made a change in receiver depth a necessity. The rest of the locations were selected based on their proximity to the canyon edge. The rays which arrive at location 17 travel about the same course as they would if going to receiver 1, except that they have a longer trek along the shelf.

The ray tracing simulation and eigenray identification at this receiver location can be best described as a complete mess. Twenty-six eigenrays were identified by the MPP program and almost all of them have a tremendous number of surface reflections and continental shelf bounces before arriving at the receiver. Needless to say, this would be an extremely complicated experimental site and probably not a good one for a first-time tomography experiment in these waters.

The ray trace graph in Appendix B for location 17 only contains a few representative rays, since graphing all of the rays would annihilate any possible distinguishing individual lines. All of the stick plots (dB losses) are on the transmission loss graph following the ray trace graph. Travel time, transmission loss and arrival angle for each ray are listed in Table 7 on page 50.

The entire package of rays can be categorized in just a few groups. Eight rays follow an almost identical path of two refractions before bouncing off of the steep slope above the Monterey Canyon, from a downward approach at a depth of 780 m and a range of around 44.6 km from the source. They continue bouncing up the slope and onto the shelf with one or two refractions and the rest surface reflections. These rays start at angles -1.6163, -2.0828, -3.0111, -3.0509, -3.1028, -3.1411, -3.1431 and -3.2418. Rays of -3.6277 and -5.3708 are very similar to the first eight with the exceptions that they bounce off the slope at just a slightly longer range and a few meters more shallow, and the -5.3708 ray hits at an upward angle. An 11th ray at -4.5475 refracts three times

before hitting the slope at about the same spot of the first group of eight, following the path of the above 10 rays up the slope with the exception that this ray has three more refractions.

Another set of seven rays (1.6711, 1.7248, 2.1406, -6.3534, -6.3988, -6.4516 and -6.4559) are very similar to the first group of eight, with two refractions before bouncing up the slope. The three main differences are that this second set reflect off the wall at a spot with a slightly shorter range and lower depth (41.3 km and 950 m), the rays are heading upward just before their first wall bounce, and that they have many more oscillations on the shelf than does the first group. With the abundance of reflections, it is understandable why this group as a whole has the slowest arrival times to the receiver.

Ray -3.9658 has two refractions before striking the sloping wall at a depth of 860 m and a range of 42.9 km. It then bounces up the slope with three refractions and 14 surface reflections. The last three individual and one group of four rays are different from the preceding 19 rays.

The rays -8.6415, -8.7093, -8.7180 and 4.0027 are grouped together due to their parallel paths and they arrive as a group in a span of 0.6 ms. These rays make one refractive turn before colliding with a lower north canyon wall point at a depth of 1410 m and a range of 32.85 km from the source on the seamount. They next hit the upper slope at the 53.8 km mark and 300 m depth after one refraction. One more refractive turn remains for this group prior to 17 surface and bottom oscillations along the shelf.

The last three rays are individuals. The fastest eigenray originates at an angle of -1.1110°, reaches receiver 17 in 45.4324 s, but has the largest transmission loss at 110.6 dB. This ray has two refractive turns before striking the slope at 45.67 km downrange and 734 m deep. It refracts and then bounces off the shelf area (178 m deep) at a distance of 56.64 km from the source. It makes three more refracted-bottom reflected (RBR) cycles and one surface reflection before arriving at its destination. Ray 0.3232 arrives 18.4 ms later and has a somewhat similar path. It has three refractions prior to colliding with the wall 44.48 km away at a depth of 788 m. The second bounce occurs at the 59.4 km mark on the shelf in 124 m of water. Seven RBR cycles and one surface reflection complete this ray's path. It takes another 114.8 ms of time before the third fastest ray (-3.0111) arrives on the scene.

The very last ray to be described should be easily identified in an experimental situation. Arriving at the 46.3275 s time mark, ray -12.5001 follows the next faster ray by 233.6 ms and is followed by another ray 669.8 ms later. This is the best separation

for the entire 26-ray package. Another interesting fact is that this ray strikes the Monterey Canyon on its south wall and refracts once in the canyon before one more refraction and a bounce at 50.48 km range and 460 m depth. It then oscillates along the shallow shelf with one more refraction but a multitude of surface and bottom reflections.

Looking at the results in Table 7 on page 50, one can begin to understand why this location would be a bit of a problem in a tomography experiment. The dB loss ranges from 89.5 dB for ray -8.7093 to 110.6 dB for the first arriving ray (-1.1110). There is not enough arrival time separation for most of these rays, based on 16 Hz bandwidth, except for the following:

1. 114.8 ms between ray 0.3232, arriving at 45.4508 s, and ray -3.0111;
2. 289.5 ms between ray -2.0828, arriving at 45.7567 s, and ray 2.1406;
3. 233.6 ms between ray -3.6277, arriving at 46.0939 s, and ray -12.5001;
4. 669.8 ms between ray -12.5001, arriving at 46.3275 s, and ray -6.4559;
5. 425.3 ms between ray -6.4516, arriving at 47.0019 s, and ray 1.6711; and
6. 191.7 ms between ray -6.3988, arriving at 47.4270 s, and ray -6.3534.

Six adequate arrival time separations with 26 arriving rays does not put this receiver location on the top of the list for best spots. The condition that eliminates this location as a recommended receiver site is that the arrival separation between the first and last eigenray is 2.1863 s. The acoustic signal from the source is of 1.9375 s duration, which is the maximum separation time that will be experimentally allowed for all of the rays arriving at one location.

Table 6. EIGENRAY INFORMATION FOR SITES 1, 2, 4, 5, 7, 8 AND 13.

RCVR	TRAVEL TIME (sec)	RAY SEPARATION (sec)	INITIAL ANGLE (degrees)	ARRIVAL ANGLE (degrees)	TRANSMISSION LOSS (dB)
1	40.0920	40.0920	2.0837	20.1333	98.1
	40.1353	0.0433	-3.9048	23.5287	95.9
2	39.3994	39.3994	-14.8056	-17.1602	95.9
4	45.7964	45.7964	-9.5632	-51.3754	95.6
	45.9304	0.1340	-5.9567	-28.2386	84.8
	45.9312	0.0008	-5.9841	40.3657	83.5
5	43.4764	43.4764	6.4800	56.6509	97.7
7	28.6596	28.6596	3.6113	41.5440	92.1
	28.7173	0.0577	1.7916	6.2005	79.0
	29.2176	0.5003	1.7497	55.4856	89.6
	29.2177	0.0001	1.5429	55.1058	90.5
8	49.7370	49.7370	6.4825	-34.7151	106.0
	49.8610	0.1240	6.4969	-39.4762	105.7
	49.8610	0.0000	6.4969	-39.5973	105.7
13	39.6526	39.6526	-13.6680	-33.1896	83.7

Table 7. EIGENRAY INFORMATION FOR SITE 17.

TRAVEL TIME (sec)	RAY SEPARATION (sec)	INITIAL ANGLE (degrees)	ARRIVAL ANGLE (degrees)	TRANSMISSION LOSS (dB)
45.4324	45.4324	-1.1110	5.4710	110.6
45.4508	0.0184	0.3232	-4.6675	100.9
45.5656	0.1148	-3.0111	-19.9961	104.4
45.5825	0.0169	-4.5475	-19.6807	97.7
45.6019	0.0194	-3.9658	-20.3254	91.1
45.6364	0.0345	-3.2418	-23.1483	93.2
45.6641	0.0277	-8.6415	-23.5988	90.5
45.6641	0.0000	-8.7093	-23.5525	89.5
45.6645	0.0004	4.0027	24.7201	91.1
45.6647	0.0002	-8.7180	24.7281	90.3
45.6656	0.0009	-3.1411	-24.1419	99.6
45.6656	0.0000	-1.6163	-24.1725	99.4
45.6656	0.0000	-3.1431	-24.5613	99.8
45.6938	0.0282	-3.1028	-25.6257	100.8
45.6960	0.0022	-5.3708	-25.7395	100.6
45.7237	0.0277	-3.0509	27.8458	98.4
45.7567	0.0330	-2.0828	-28.2343	93.8
46.0462	0.2895	2.1406	39.3321	96.5
46.0939	0.0477	-3.6277	-39.6695	97.0
46.3275	0.2336	-12.5001	-44.7474	93.8
46.9973	0.6698	-6.4559	-60.2335	99.5
47.0004	0.0031	1.7248	-60.4129	99.8
47.0019	0.0015	-6.4516	61.2411	99.6
47.4270	0.4251	-6.3988	69.1542	100.2
47.4272	0.0002	1.6711	69.1952	100.4
47.6187	0.1915	-6.3534	72.1043	101.5

VI. CONCLUSIONS

The purpose of this thesis is to determine the optimal placement of the receiver hydrophones for the December 1988 experiment, to indicate probable eigenray characteristics at the recommended sites, to provide oceanic environmental information that would most likely affect the experiment, and to suggest or warn of possible pitfalls between the simulation results versus the real world situation. Before concluding the thesis with a recommendation of receiver locations, it is best to restate the conditions of the tomography experiment, and to indicate some simplifications of the simulation that will influence the comparison between predicted eigenrays and the experimental results.

A. TOMOGRAPHY EXPERIMENT REQUIREMENTS

The week of 12-16 December 1988 is the scheduled date for the Monterey Bay tomography experiment. An acoustic source, capable of continuously transmitting a pseudo-random phase-encoded signal of 1.9375 s duration, 224 Hz center frequency and source level of 183 dB re 1 μPa, is to be moored 1 m above the top of a seamount that is due west of Point Sur. The source location will be in the general area of latitude 36°22'N and longitude 122°19'W at a depth of approximately 840 m. Up to 11 AN/SSQ-57A sonobuoys (modified) will be stationed 1 m above the continental shelf at various locations around Monterey Bay. The boat crew will attempt to place the receivers at approximately the 100 m depth. These sonobuoys will transmit the received acoustic signals to a shore-based van. A frequency spectra buoy and ARGOS RC/WASID drifting buoys will be providing measurements during the experiment.

The purpose of this experiment is to test a low-cost tomographic system that can be used to analyze surface waves and internal waves. Locations will be selected, partially on the basis of simulated eigenray determination, that appear to receive eigenrays which are distinguishable and subject to surface and/or internal wave interference. Nearshore locations with congested commercial fishing traffic will not be considered good sonobuoy sites.

B. SIMULATION VS REAL WORLD

It is sometimes difficult to simulate the real world, especially when the conditions of the real world at a particular point in time are not known in advance. The environmental conditions for the December experiment can be forecasted, based on previous

years' trends, but the prediction may not be accurate. The sound speed profile used in the simulation was taken from 15 December 1987 data. The entire month of December 1987 was stormy. A difference in the weather and/or current patterns from last year's situation would definitely affect the sound speed profile. This in turn would have a considerable effect on the eigenray characteristics. For this reason, the simulation will have to be rerun after the December experiment with sound speed data taken during the experiment.

The simulation input is greatly simplified from the real world situation. MPP is a two-dimensional program which does not consider sideways reflection off of the canyon walls. The facets of the canyon wall may throw a ray away from its intended receiver location, and thus the ray would miss its destination. The bathymetry profile has been reduced to just a limited number of points, due to the program's input constraints. The canyon axis was depicted as being wider and shallower than it truly is. Bottom loss for each reflection was stipulated at 0 dB, which is complete reflectivity, because the bottom loss coefficients cannot be specified per range. The sediment, which the eigenrays pass over and bounce on, varies considerably. Ray bounces on mud or clay would result in a higher bottom loss than reflections off of rock. An unsuccessful attempt was made to obtain shallow water bottom loss data in order to show the relationship between the grazing angle and bottom loss for various sediment types within the experimental region.

How accurate is the simulation? It is hard to tell. The program logic is based on Snell's Law and appears to be very thorough in determining eigenrays and developing the ray traces. The problem lies with the input constraints. MPP simulation can be a predictor of trends, such as Soquel Canyon being a difficult place to receive eigenrays. The fact that the number of initial rays from the source is limited in the simulation to 80, rather than the almost unlimited number of rays that would travel from a source, keeps some true eigenrays from being identified. In its defense, MPP is considered the state-of-the-art with respect to available eigenray simulation tools for deep water tomography. It was not designed for shallow water tomography when there are excessive reflections along the eigenray's path. The predictions from this simulation will give the members of the tomography experiment some basis to focus in on the results, rather than just shooting in the dark.

C. RECEIVER LOCATION RECOMMENDATIONS

Figure 16 on page 54 graphically indicates the locations that are being recommended for receiver sonobuoy placement during the December tomography experiment. These sites were selected from the 17 positions simulated. They are:

1. Station 2, south-southwest of Santa Cruz, latitude 36°51.20′N, longitude 122°05.00′W;
2. Station 4, west of Moss Landing on the north rim of Monterey Canyon, latitude 36°48.65′N, longitude 121°52.20′W;
3. Station 5, west of Salinas River mouth on the south rim of Monterey Canyon, latitude 36°45.00′N, longitude 121°54.10′W;
4. Station 8, west of Pajaro River mouth on the continental shelf; latitude 36°50.00′N, longitude 121°51.00′W; and
5. Station 13, juncture of Soquel Canyon east rim and Monterey Canyon north rim, latitude 36°48.65′N, longitude 121°57.90′W.

Station 2 has one ray arrival with two bounces in the canyon, before having a small number of surface and bottom reflections on the shelf. The bottom loss value should be small. Probably the best location for the experiment is receiver location 4. The eigenrays refract in the canyon, bounce along the continental shelf when the canyon meanders away, and then refract in the narrower portion of Monterey Canyon where internal waves would be more noticeable. Two eigenrays will be identifiable with strong signals. This appears to be an excellent location for the study of both surface and internal waves. Location 5 has one eigenray that oscillates on the continental shelf. This location was selected in order to contrast results where eigenrays are affected by the internal waves in the narrower and shallower portion of Monterey Canyon. Station 8 would give corroboration to the results from received signals at position 4, since the rays travel very nearly over the same path. Two weak eigenrays with good separation should be acquired. Station 13 looks very promising since it has only one bottom reflection in Monterey Canyon, thereby reducing the possibility of the ray being lost to a sideways reflection off the wall.

Most of the simulated locations were eliminated as recommended sites since the simulation failed to predict any eigenrays for them. Location 17 had the largest number of eigenrays, but the arrival time separations were not good and the separation between first and last eigenrays were outside of the constraints of the experiment. Also, there would be just too many eigenrays to handle. Site 1 was closer to the canyon, but the separation between the two eigenrays was below the experimental criteria. With extra

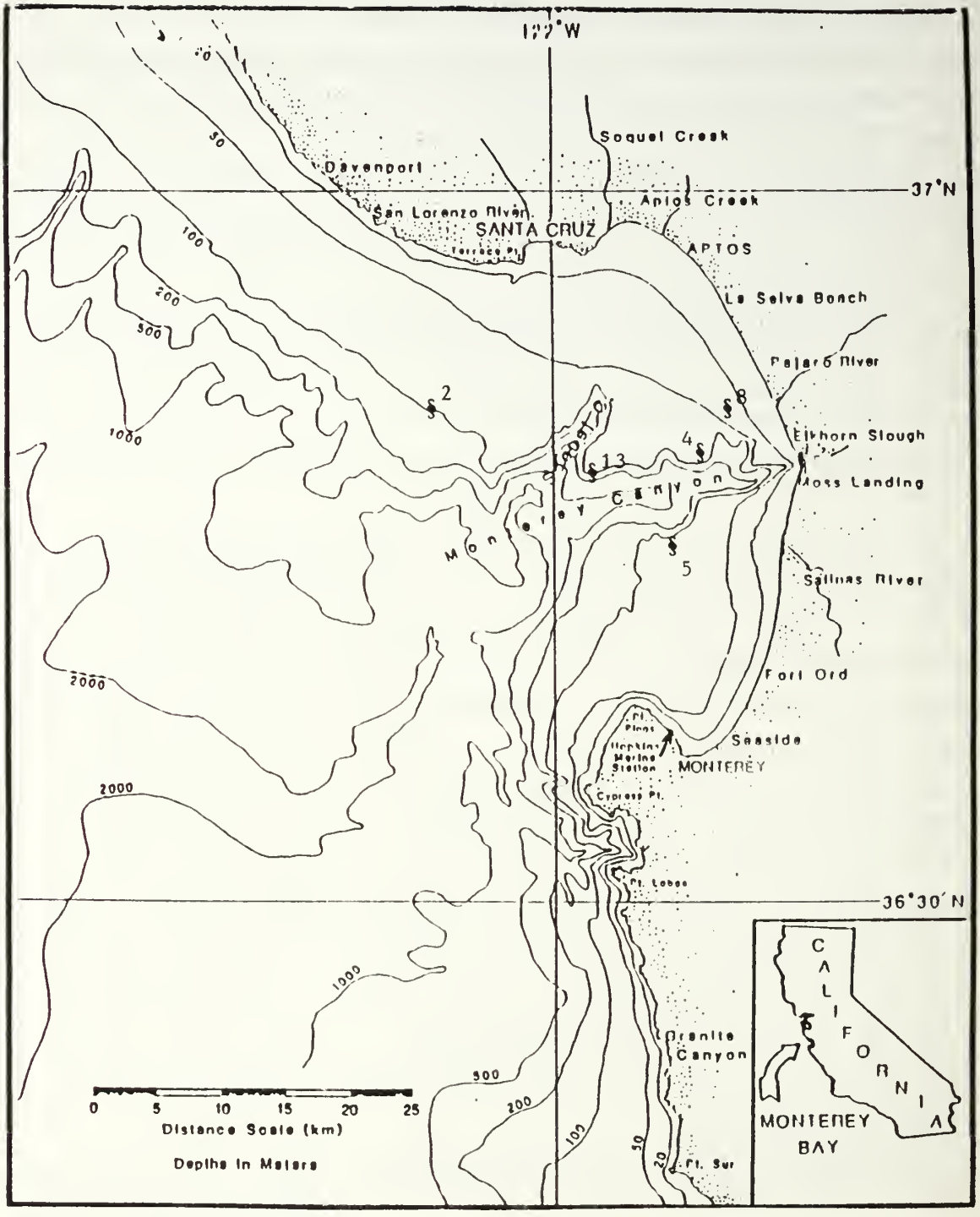

Figure 16. Recommended receiver positions.

buoys for the experiment, this position could be selected for a spare buoy. Receiver 7, off of the Monterey Peninsula, received four eigenrays. Two of these would definitely be identifiable, while the third is just below the minimum required arrival separation but may be heard since it is a very strong signal, the strongest of all the eigenrays identified in the simulation. This is a good alternate location, even though it was not a recommended position due to its lack of travel time along the Monterey Canyon and basically short eigenray total travel time.

Rather than stating that the receivers have to be placed exactly as recommended, it is fitting to describe the pros and cons of sonobuoy placement in more general locations. Any place on the shelf, away from the canyon rim, will indubitably result in eigenray paths with tremendous surface and bottom reflection. For the surface wave study, it would be nice to have these reflections; however, a very large number of bottom bounces will lead to a large transmission loss. The signal make not be picked out of the ambient noise. High ambient noise locations will be found in areas of the bay where there is heavy commercial fishing. Moss Landing is a prime example. For purposes of the study, the Moss Landing area would be an ideal receiver location for eigenrays to intercept internal tidal bores and denser shelf water resulting from volume divergence. Unfortunately, the heavy commercial boat traffic would interfere in the managing of the experiment, as well as contributing to the high ambient noise level.

The simulation had a particularly difficult time with finding eigenrays when the receiver was placed around Soquel Canyon. The only eigenray identified, out of six locations around Soquel Canyon, has a few reflections near the receiver only, with a refracted path through most of the canyon. The straight-line path from source to a Soquel Canyon receiver has to pass over the portion of Monterey Canyon that bends around quite a bit, resulting in a large variance in the sea floor depth. It may be difficult to receive any signals in this general area when the source is on the seamount, as simulated.

Receiver sites outside of Monterey Bay, southwest of Santa Cruz, should pick up more eigenrays, but there might be too many eigenrays to distinguish. Also, the internal wave study would probably not benefit by placing the receivers in this area since the waves would not be as noticeable in the wider Monterey Canyon trough. The most productive locations for placement of the sonobuoys may be along the north wall of Monterey Canyon, between Soquel Canyon and the head near Moss Landing, and along the east wall of Carmel Canyon, just before the juncture with Monterey Canyon.

APPENDIX A. BATHYMETRY DATA FOR RECEIVER LOCATIONS

Table 8. BATHYMETRY DATA FOR RECEIVER LOCATIONS 1, 2 AND 3.

RECEIVER LOCATION 1		RECEIVER LOCATION 2		RECEIVER LOCATION 3	
Range (km)	Depth (m)	Range (km)	Depth (m)	Range (km)	Depth (m)
0.0	832.10	0.0	832.10	0.0	832.10
3.26	826.62	1.09	914.40	0.76	914.40
4.07	914.40	3.75	914.40	4.07	1097.28
7.06	1463.04	6.16	1280.16	5.75	1280.16
17.37	1463.04	6.74	1463.04	6.64	1463.04
18.57	1645.92	9.96	1463.04	7.32	1463.04
21.53	2560.32	12.71	1280.16	12.14	1280.16
21.89	2560.32	14.67	1280.16	15.54	1280.16
23.07	2377.44	17.17	1463.04	18.80	1463.04
24.61	2194.56	19.56	1828.80	20.39	1828.80
25.65	2011.68	21.01	2194.56	22.36	1828.80
27.25	1828.80	21.51	2377.44	23.80	2011.68
27.69	1645.92	23.85	2377.44	27.65	2011.68
30.07	1463.04	25.75	1828.80	29.46	2194.56
35.29	1280.16	26.51	1645.92	30.54	2011.68
37.51	1097.28	29.74	1463.04	32.71	1828.80
40.31	914.40	33.32	1280.16	35.02	2011.68
44.11	731.52	36.07	1097.28	39.31	1828.80
46.68	548.64	37.30	1047.90	39.96	1645.92
51.84	365.76	38.03	1097.28	41.53	1463.04
55.55	182.88	39.60	958.29	42.47	1645.92
59.35	98.76	40.47	1097.28	43.10	1828.80
70.50	98.76	41.01	1280.16	43.43	1828.80
		45.41	1280.16	44.10	1463.04
		45.99	1325.88	45.65	1097.28
		46.45	1280.16	46.95	731.52
		47.42	1097.28	48.52	731.52
		48.53	731.52	49.52	1097.28
		50.34	365.76	50.29	1097.28
		51.72	182.88	50.96	914.40
		54.87	106.07	51.78	806.50
		57.99	91.44	53.00	914.40
		70.50	91.44	53.40	1005.84
				54.35	914.40
				55.30	731.52
				57.06	548.64
				61.26	365.76
				62.89	182.88
				63.87	91.44
				70.50	91.44

Table 9. BATHYMETRY DATA FOR RECEIVER LOCATIONS 4, 5 AND 6.

RECEIVER LOCATION 4		RECEIVER LOCATION 5		RECEIVER LOCATION 6	
Range (km)	Depth (m)	Range (km)	Depth (m)	Range (km)	Depth (m)
0.0	832.10	0.0	832.10	0.0	832.10
0.54	914.40	0.60	914.40	0.60	914.40
3.30	1097.28	2.89	1097.28	2.35	1097.28
5.19	1280.16	4.76	1280.16	4.33	1280.16
6.38	1351.48	6.60	1351.48	6.76	1351.48
10.33	1280.16	10.01	1280.16	9.52	1280.16
14.25	1252.73	15.83	1280.16	11.85	1126.54
16.05	1280.16	16.73	1463.04	16.34	1280.16
17.04	1463.04	19.16	1463.04	17.14	1463.04
23.54	1463.04	20.57	1280.16	17.68	1556.31
24.67	1645.92	23.06	1280.16	18.40	1463.04
25.61	1828.80	25.98	1828.80	19.54	1280.16
26.24	1828.80	26.74	1828.80	24.41	1280.16
27.78	1463.04	29.28	1280.16	25.80	1645.92
28.73	1280.16	29.91	1097.28	26.65	1645.92
32.33	1280.16	31.83	1097.28	28.50	1463.04
33.73	1097.28	32.48	914.40	29.66	1280.16
35.22	1097.28	34.28	914.40	30.17	1280.16
35.71	1280.16	34.75	1097.28	31.39	914.40
36.79	1280.16	36.67	1097.28	33.77	914.40
38.24	731.52	38.65	365.76	34.31	1097.28
39.68	548.64	39.62	182.88	34.58	1097.28
40.26	365.76	44.79	107.90	35.45	731.52
43.56	182.88	54.78	91.44	37.23	548.64
46.89	118.87	70.50	91.44	38.06	182.88
52.70	104.24			41.40	91.44
56.33	182.88			70.50	91.44
57.46	365.76				
58.33	548.64				
58.80	548.64				
61.63	365.76				
62.63	182.88				
63.49	91.44				
70.50	91.44				

Table 10. BATHYMETRY DATA FOR RECEIVER LOCATIONS 7, 8 AND 9.

RECEIVER LOCATION 7		RECEIVER LOCATION 8		RECEIVER LOCATION 9	
Range (km)	Depth (m)	Range (km)	Depth (m)	Range (km)	Depth (m)
0.0	824.79	0.0	825.	0.0	824.79
1.21	1097.28	0.37	915.	1.61	1097.28
14.24	1097.28	1.73	1097.	2.26	1280.16
18.97	1280.16	6.35	1251.	17.30	1280.16
21.55	1097.28	7.75	1280.	20.04	1645.92
24.72	1097.28	8.18	1280.	21.22	1645.92
26.38	1280.16	13.56	1127.	22.62	1463.04
27.67	1645.92	17.65	1280.	24.28	1463.04
29.34	1463.04	18.46	1463.	26.00	1828.80
31.11	914.40	18.90	1556.	27.29	1828.80
32.72	731.52	20.26	1463.	28.63	1463.04
33.26	731.52	21.27	1280.	30.08	1463.04
34.01	914.40	24.68	1280.	30.73	1645.92
34.39	914.40	25.55	1463.	32.39	1645.92
35.79	548.64	26.44	1646.	36.21	1463.04
37.13	365.76	27.32	1829.	37.07	1280.16
37.99	182.88	27.91	1829.	37.82	1280.16
39.12	91.44	28.57	1646.	39.22	1645.92
39.98	73.15	29.05	1562.	40.45	1645.92
40.84	73.15	29.39	1463.	41.79	1097.28
41.91	54.86	30.35	1280.	43.62	1097.28
42.02	51.21	31.31	1097.	45.18	1645.92
45.0	51.21	32.19	1097.	45.80	1645.92
		33.82	1097.	47.11	1097.28
		35.00	915.	48.17	1097.28
		35.82	940.	49.15	1280.16
		36.18	1097.	50.07	1280.16
		36.60	1280.	52.29	731.52
		37.91	1280.	55.01	731.52
		38.57	1097.	57.96	182.88
		38.95	915.	59.41	91.44
		39.28	732.	64.57	73.15
		41.06	366.	66.72	54.86
		42.17	229.	67.15	49.38
		44.56	183.	70.15	49.38
		48.07	119.		
		53.61	104.		
		56.41	99.		
		56.98	183.		
		57.90	366.		
		59.08	549.		
		59.67	549.		
		62.40	366.		
		63.06	183.		
		63.63	91.		
		64.48	75.		
		67.33	73.		
		67.49	55.		

Table 11. BATHYMETRY DATA FOR RECEIVER LOCATIONS 10, 11 AND 12.

RECEIVER LOCATION 10		RECEIVER LOCATION 11		RECEIVER LOCATION 12	
Range (km)	Depth (m)	Range (km)	Depth (m)	Range (km)	Depth (m)
0.0	824.79	0.0	832.10	0.0	832.10
1.84	1097.28	0.81	914.40	0.81	914.40
2.43	1280.16	2.81	914.40	2.81	914.40
18.20	1280.16	5.95	1280.16	5.85	1280.16
21.01	1463.04	6.60	1463.04	6.60	1463.04
22.43	1828.80	7.17	1463.04	7.17	1463.04
24.05	1645.92	12.31	1280.16	12.31	1280.16
24.88	1645.92	15.01	1280.16	15.26	1280.16
26.25	2011.68	17.96	1463.04	18.22	1463.04
26.61	2011.68	20.83	2011.68	20.89	2011.68
27.47	1828.80	22.50	2011.68	23.22	2011.68
29.84	1828.80	23.31	2194.56	24.36	2194.56
30.67	2011.68	23.94	2194.56	35.18	2194.56
32.43	2011.68	24.48	2377.44	36.05	2011.68
33.59	1828.80	26.07	2377.44	39.84	2011.68
41.64	1828.80	31.37	2194.56	41.00	1828.80
42.84	1645.92	33.08	2194.56	41.86	1775.76
44.73	1645.92	33.75	2011.68	42.35	1828.80
45.34	1828.80	34.75	1828.80	42.97	1828.80
45.72	1828.80	39.22	1828.80	44.11	1463.04
46.47	1463.04	39.76	2011.68	46.14	1097.28
48.15	1097.28	40.57	2011.68	46.44	914.40
49.42	731.52	41.16	1828.80	47.22	731.52
51.11	731.52	42.84	1828.80	49.31	731.52
52.23	1097.28	44.63	1463.04	50.77	1097.28
52.95	1097.28	45.26	1463.04	51.74	1097.28
53.83	914.40	46.30	1097.28	52.86	914.40
56.26	914.40	47.92	731.52	53.91	731.52
57.64	548.64	49.22	731.52	54.85	548.64
60.56	548.64	50.36	548.64	56.02	365.76
61.50	365.76	53.37	548.64	57.19	182.88
62.16	182.88	54.81	365.76	59.72	91.44
66.63	91.44	55.28	182.88	70.50	91.44
67.18	73.15	56.04	91.44		
67.84	54.86	70.50	91.44		
68.39	45.72				
71.39	45.72				

Table 12. BATHYMETRY DATA FOR RECEIVER LOCATIONS 13, 14 AND 15.

RECEIVER LOCATION 13		RECEIVER LOCATION 14		RECEIVER LOCATION 15	
Range (km)	Depth (m)	Range (km)	Depth (m)	Range (km)	Depth (m)
0.0	832.10	0.0	832.10	0.0	832.10
0.87	914.40	0.59	914.40	0.54	914.40
3.90	1097.28	3.25	1097.28	2.29	1097.28
5.69	1280.16	5.30	1280.16	4.43	1280.16
6.68	1463.04	6.36	1351.48	6.48	1351.48
7.32	1463.04	10.60	1280.16	9.90	1280.16
11.60	1280.16	13.93	1252.73	11.82	1126.54
16.15	1280.16	16.05	1280.16	15.79	1280.16
19.10	1463.04	17.67	1463.04	16.87	1463.04
19.87	1645.92	18.80	1645.92	18.90	1463.04
20.32	1828.80	19.83	1645.92	19.87	1280.16
20.77	1828.80	21.15	1463.04	23.49	1280.16
21.89	1645.92	21.91	1431.95	25.27	1645.92
23.03	1645.92	23.04	1463.04	27.75	1645.92
23.71	1828.80	24.99	1828.80	28.98	1463.04
24.39	2011.68	26.14	1828.80	29.80	1280.16
24.66	2011.68	27.26	1463.04	30.18	1097.28
25.36	1828.80	28.23	1404.52	31.75	914.40
26.66	1645.92	29.48	1463.04	32.88	731.52
27.31	1645.92	32.05	1463.04	33.20	691.29
28.51	1828.80	34.26	1280.16	33.65	731.52
29.13	2011.68	34.94	1097.28	34.61	1097.28
30.08	2011.68	35.88	1097.28	34.96	1097.28
30.35	1828.80	36.29	1463.04	36.77	914.40
32.25	1645.92	37.00	1463.04	38.51	365.76
38.80	1645.92	37.64	1280.16	39.20	182.88
39.13	1728.22	39.30	1097.28	42.06	102.41
39.62	1645.92	40.13	731.52	53.51	91.44
39.89	1463.04	42.05	548.64	61.87	91.44
40.92	1280.16	42.73	429.77	62.99	182.88
42.14	1280.16	43.45	548.64	63.82	182.88
43.63	1828.80	44.71	731.52	64.36	91.44
43.84	1907.44	47.73	731.52	70.50	91.44
44.03	1828.80	48.52	548.64		
44.87	1280.16	49.87	365.76		
46.34	914.40	52.03	182.88		
46.79	914.40	53.98	182.88		
48.23	1097.28	55.53	365.76		
49.05	1280.16	56.66	548.64		
49.32	1280.16	58.47	548.64		
51.43	731.52	59.55	182.88		
53.19	731.52	60.36	91.44		
53.47	914.40	70.50	91.44		
54.47	548.64				
56.63	182.88				
58.53	91.44				
70.50	91.44				

Table 13. BATHYMETRY DATA FOR RECEIVER LOCATIONS 16 AND 17.

RECEIVER LOCATION 16		RECEIVER LOCATION 17	
Range (km)	Depth (m)	Range (km)	Depth (m)
0.0	825.	0.0	824.79
8.4	1463.	6.60	1097.28
9.0	1463.	8.00	1280.16
14.1	1280.	8.59	1463.04
16.6	1280.	11.65	1463.04
24.2	2378.	14.63	1280.16
25.8	2378.	16.37	1280.16
41.2	958.	19.05	1463.04
42.4	1280.	20.13	1645.92
47.8	1280.	20.93	1828.80
53.5	139.	21.58	2011.68
66.2	46.	22.22	2194.56
70.0	46.	22.87	2377.44
		24.90	2377.44
		25.76	2194.56
		27.80	2011.68
		28.82	1828.80
		29.68	1645.92
		31.40	1463.04
		36.39	1280.16
		39.24	1097.28
		41.71	914.40
		45.73	731.52
		48.68	548.64
		52.39	365.76
		56.41	182.88
		61.14	91.44
		64.14	73.15
		66.99	54.86
		67.47	49.93
		70.47	49.93

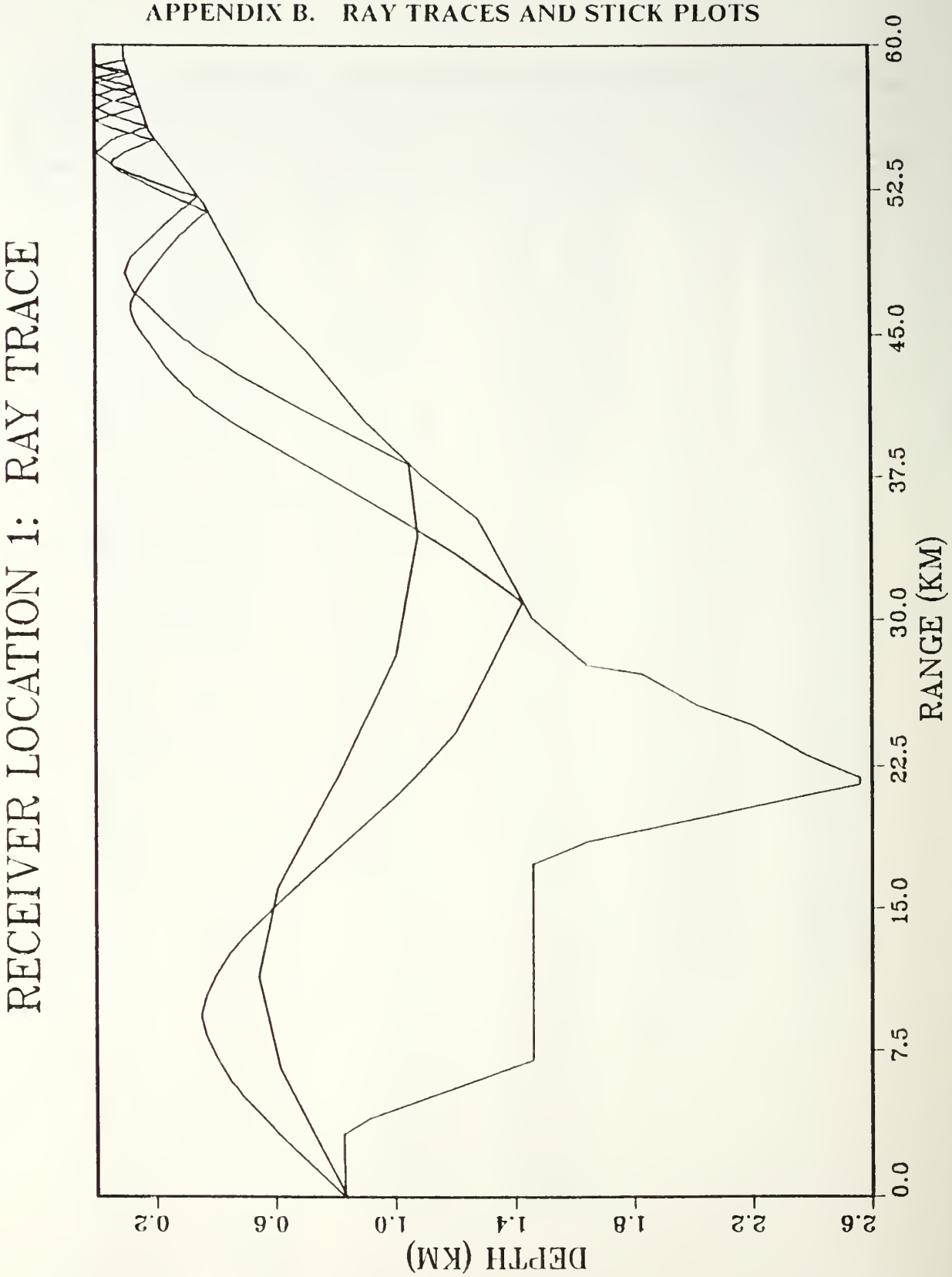
RECEIVER LOCATION 1: RAY TRACE
DEPTH (KM)
0.2
0.6
1.0
1.4
1.8
2.2
2.6
RANGE (KM)
0.0
7.5
15.0
22.5
30.0
37.5
45.0
52.5
60.0

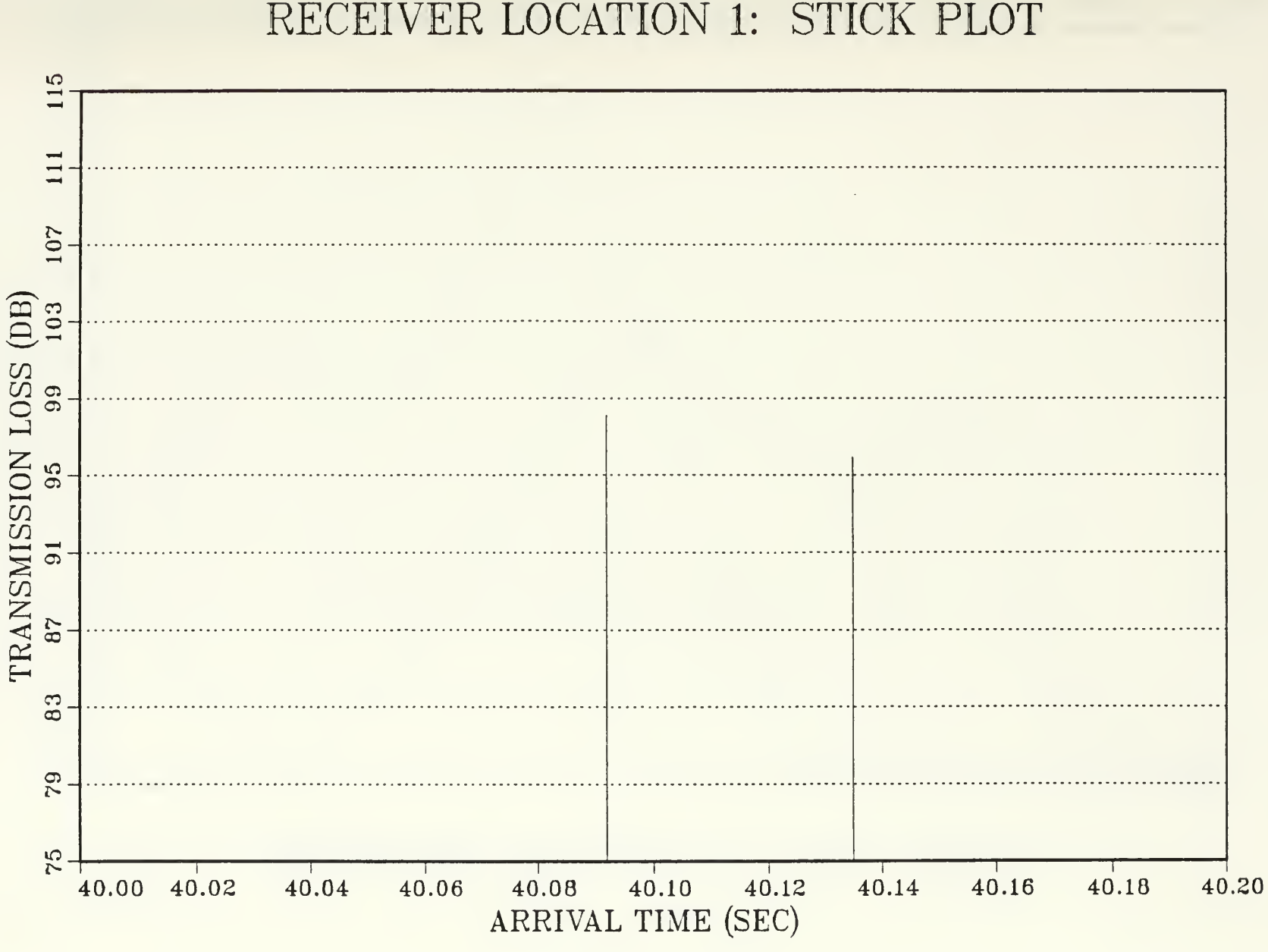
RECEIVER LOCATION 1: STICK PLOT
TRANSMISSION LOSS (DB)
115
111
107
103
99
95
91
87
83
79
75
40.00
40.02
40.04
40.06
40.08
40.10
40.12
40.14
40.16
40.18
40.20
ARRIVAL TIME (SEC)

RECEIVER LOCATION 2: RAY TRACE

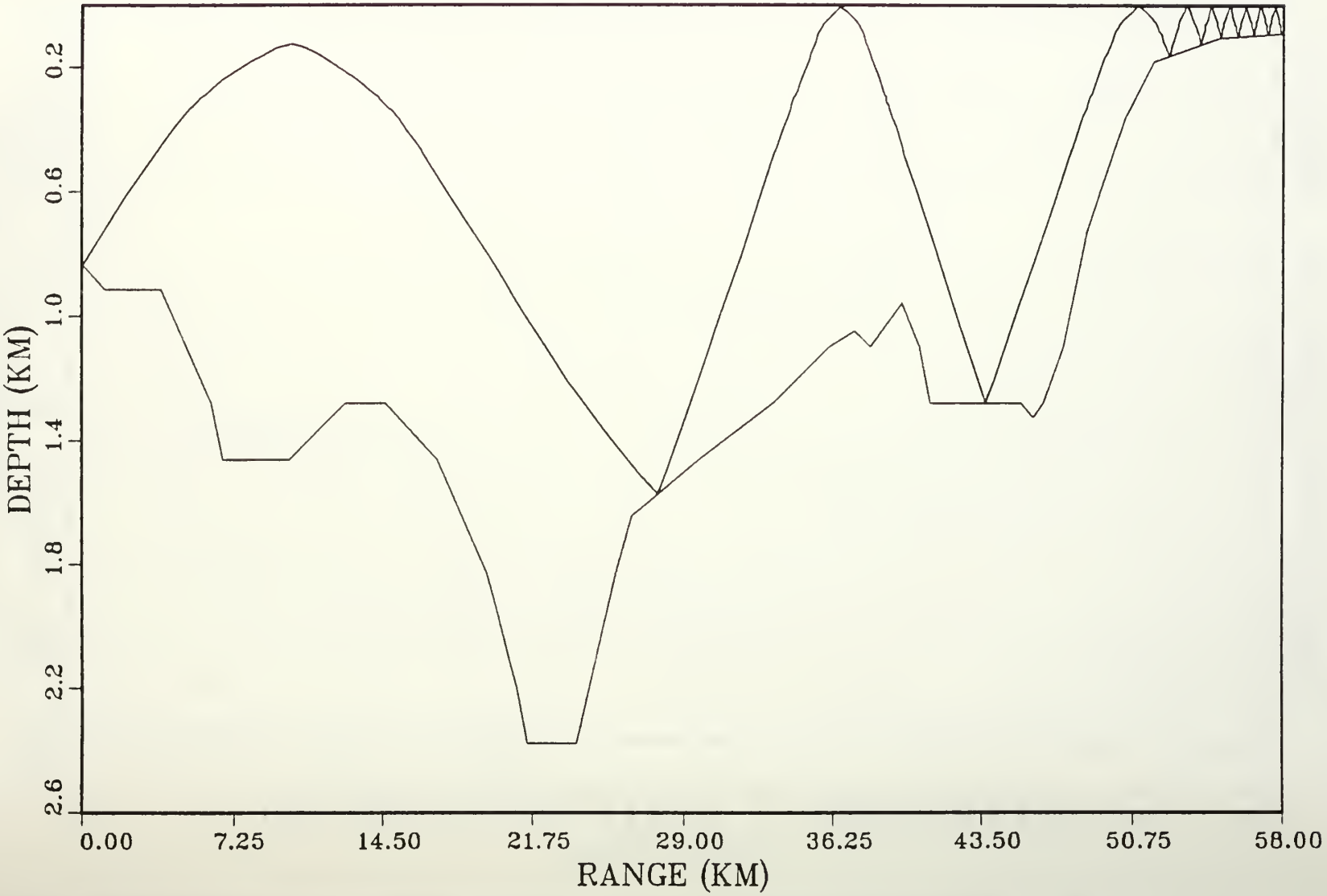

RECEIVER LOCATION 2: STICK PLOT

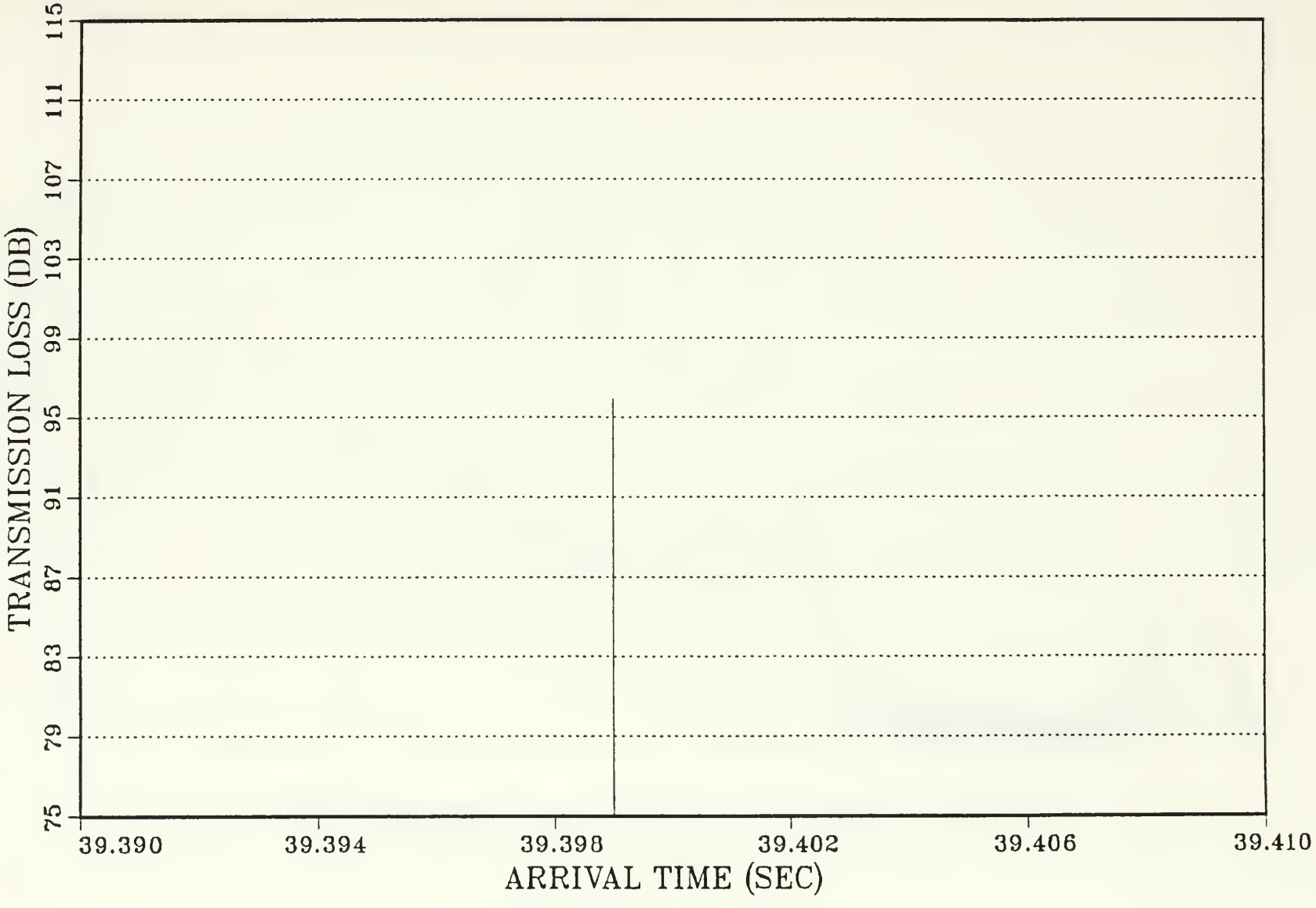

RECEIVER LOCATION 4: RAY TRACE

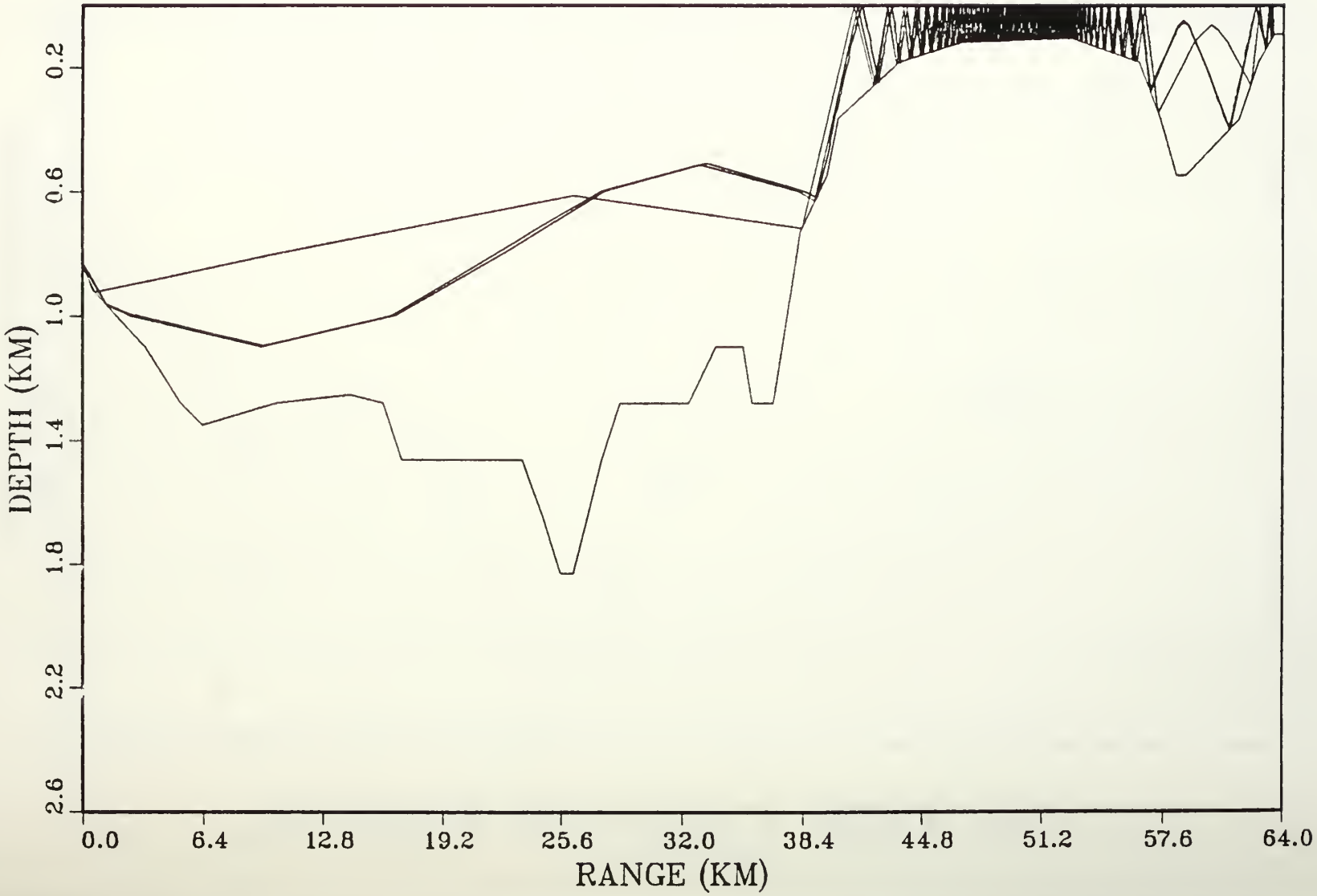

RECEIVER LOCATION 4: STICK PLOT

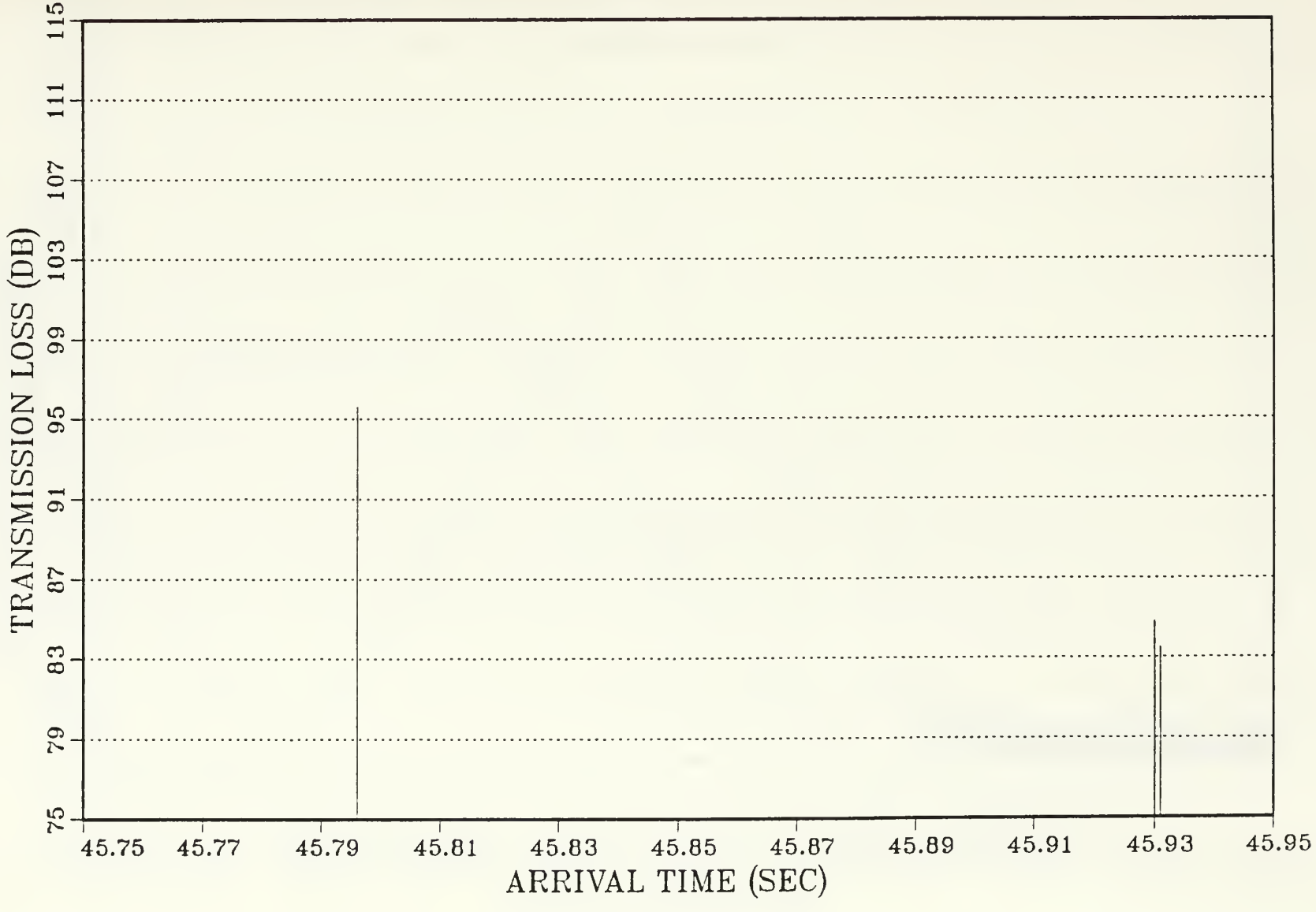

RECEIVER LOCATION 5: RAY TRACE

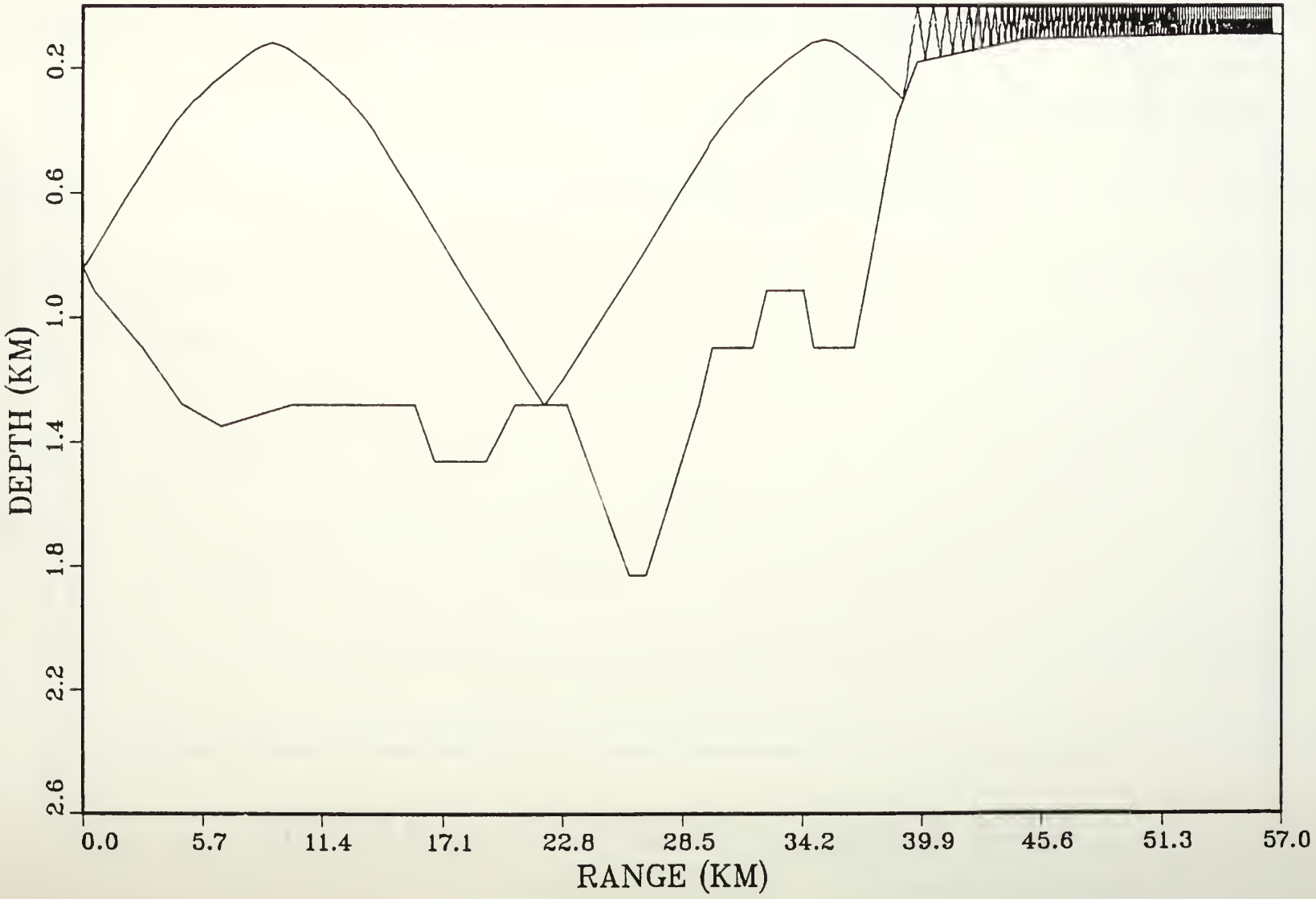

RECEIVER LOCATION 5: STICK PLOT

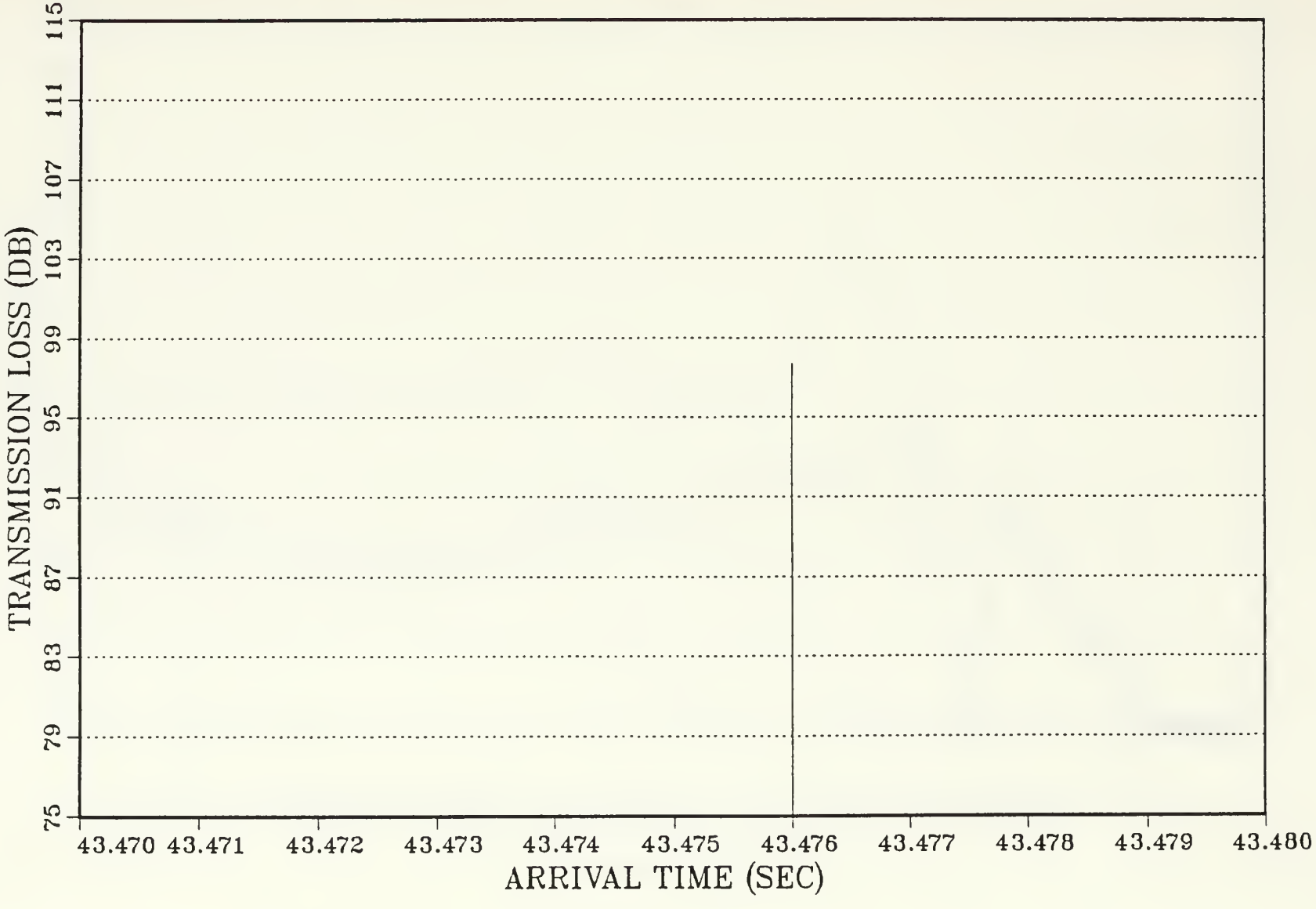

RECEIVER LOCATION 7: RAY TRACE

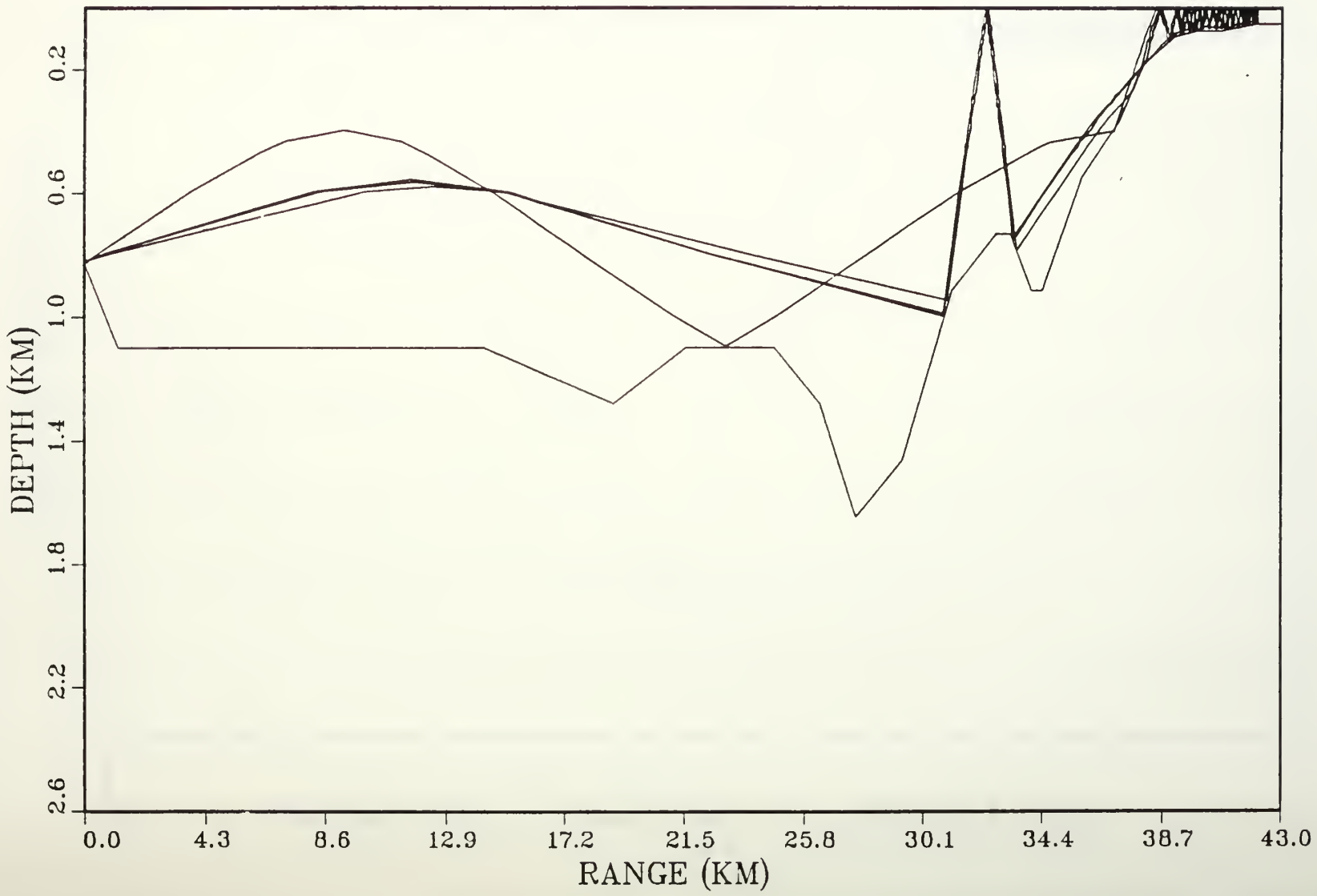

RECEIVER LOCATION 7: STICK PLOT

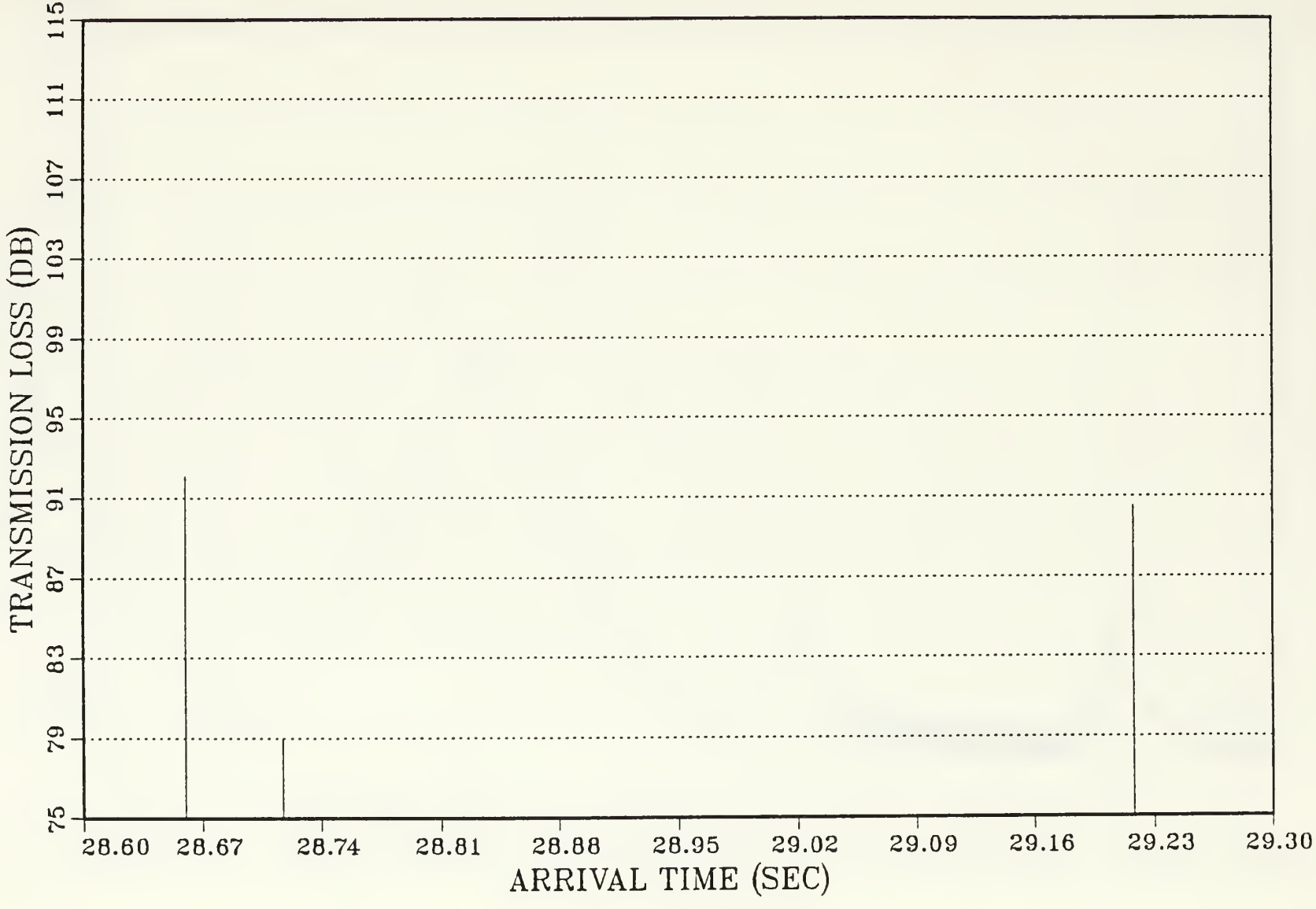

RECEIVER LOCATION 8: RAY TRACE

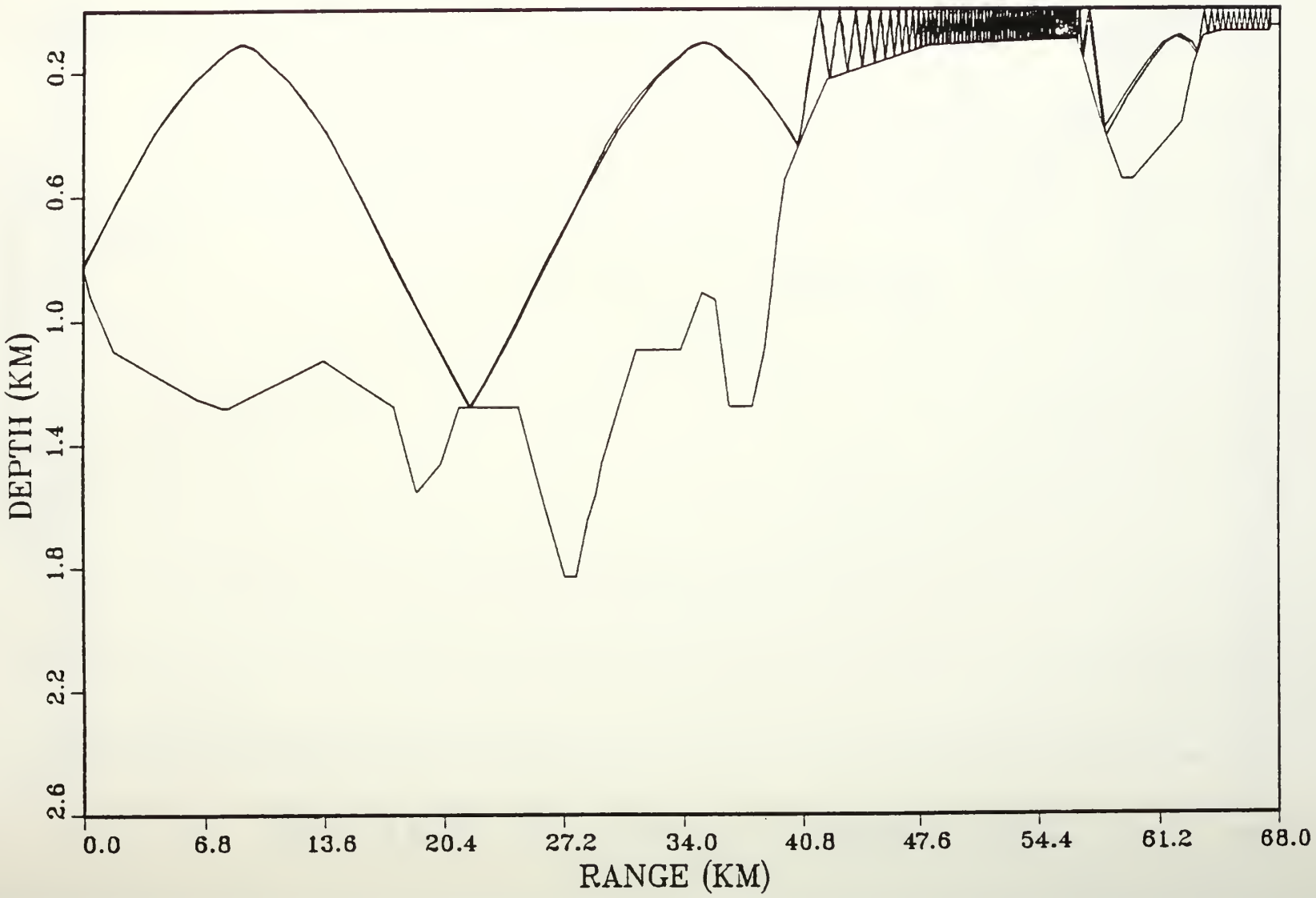

RECEIVER LOCATION 8: STICK PLOT

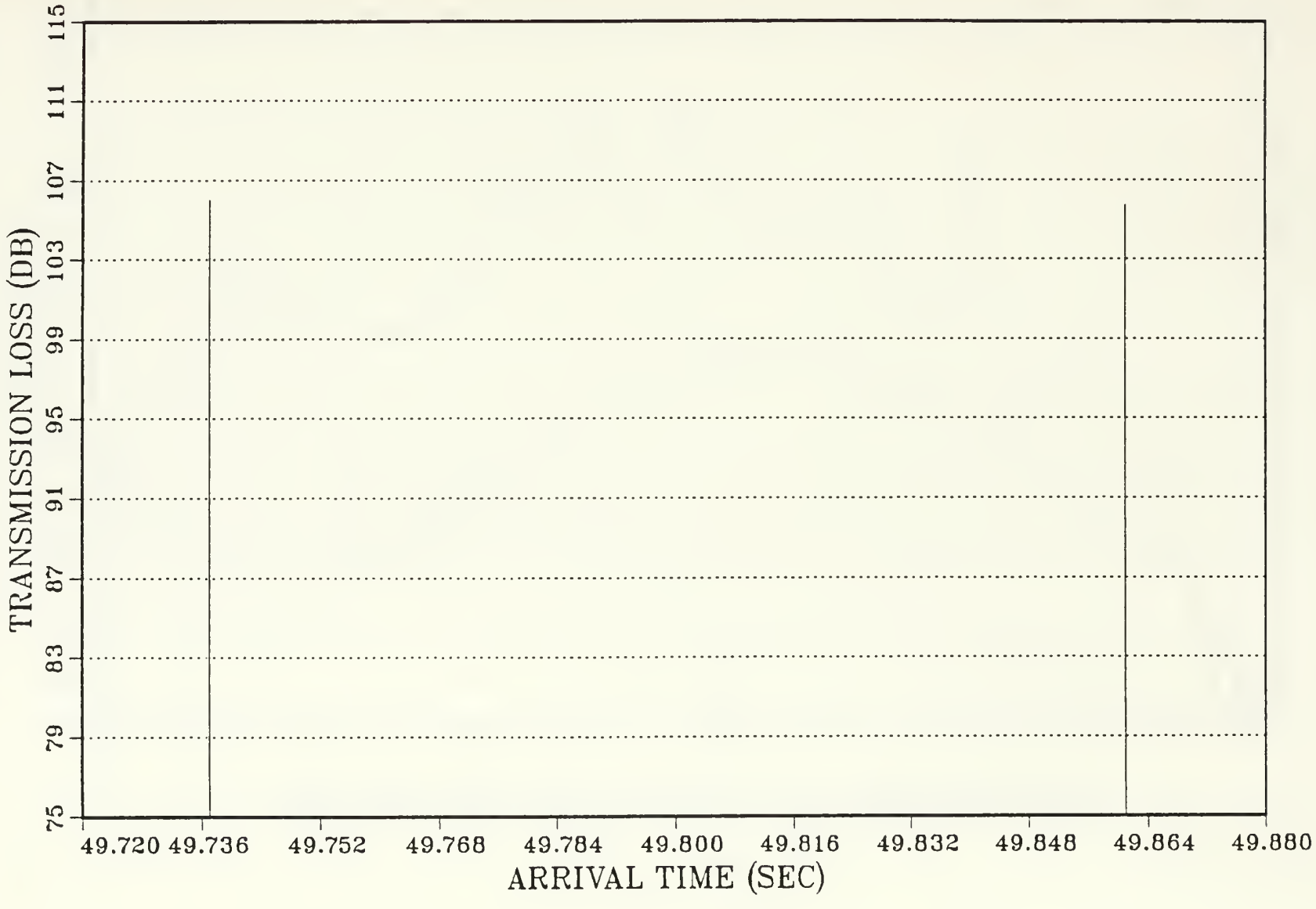

RECEIVER LOCATION 13: RAY TRACE

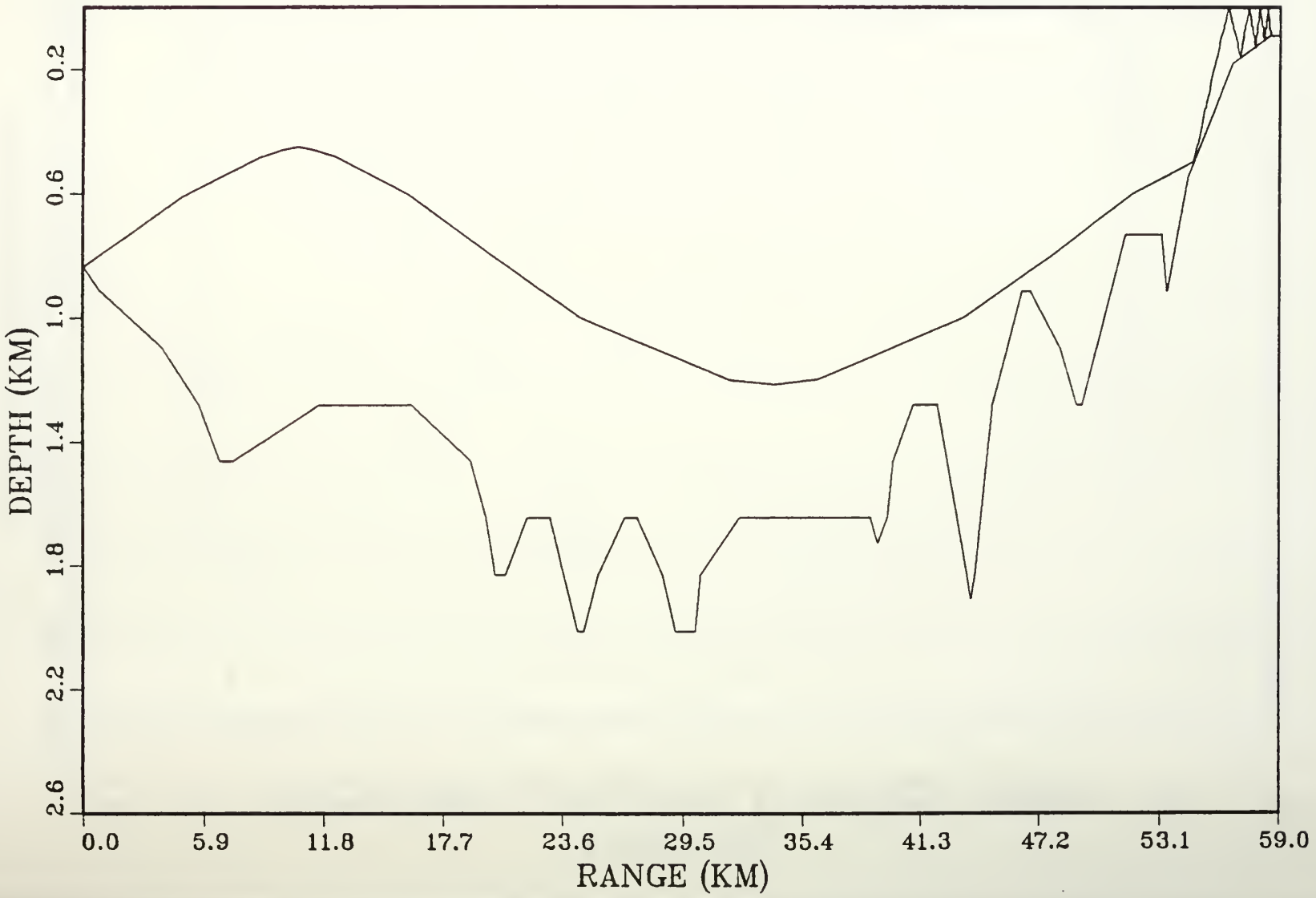

RECEIVER LOCATION 13: STICK PLOT

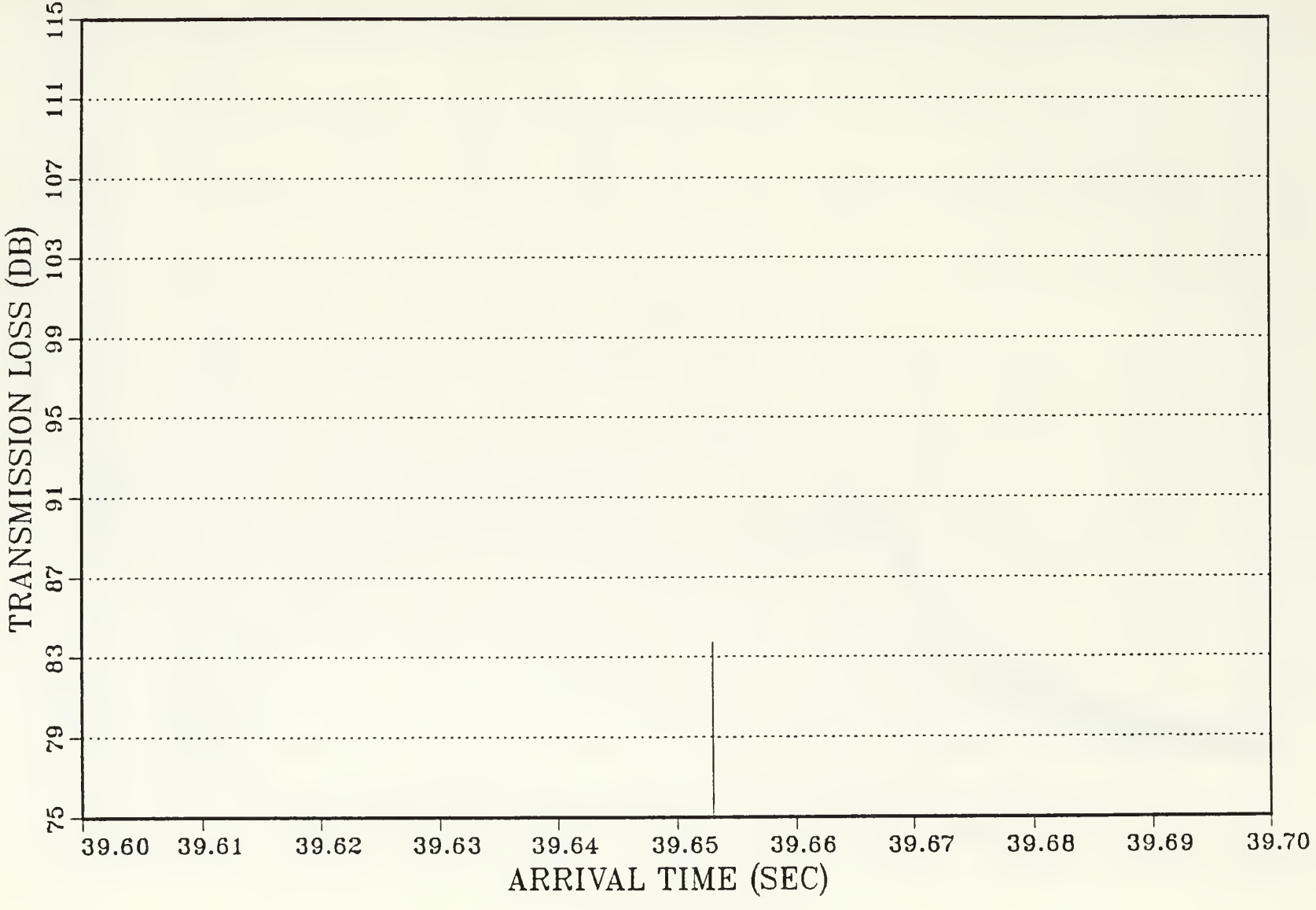

RECEIVER LOCATION 17: RAY TRACE

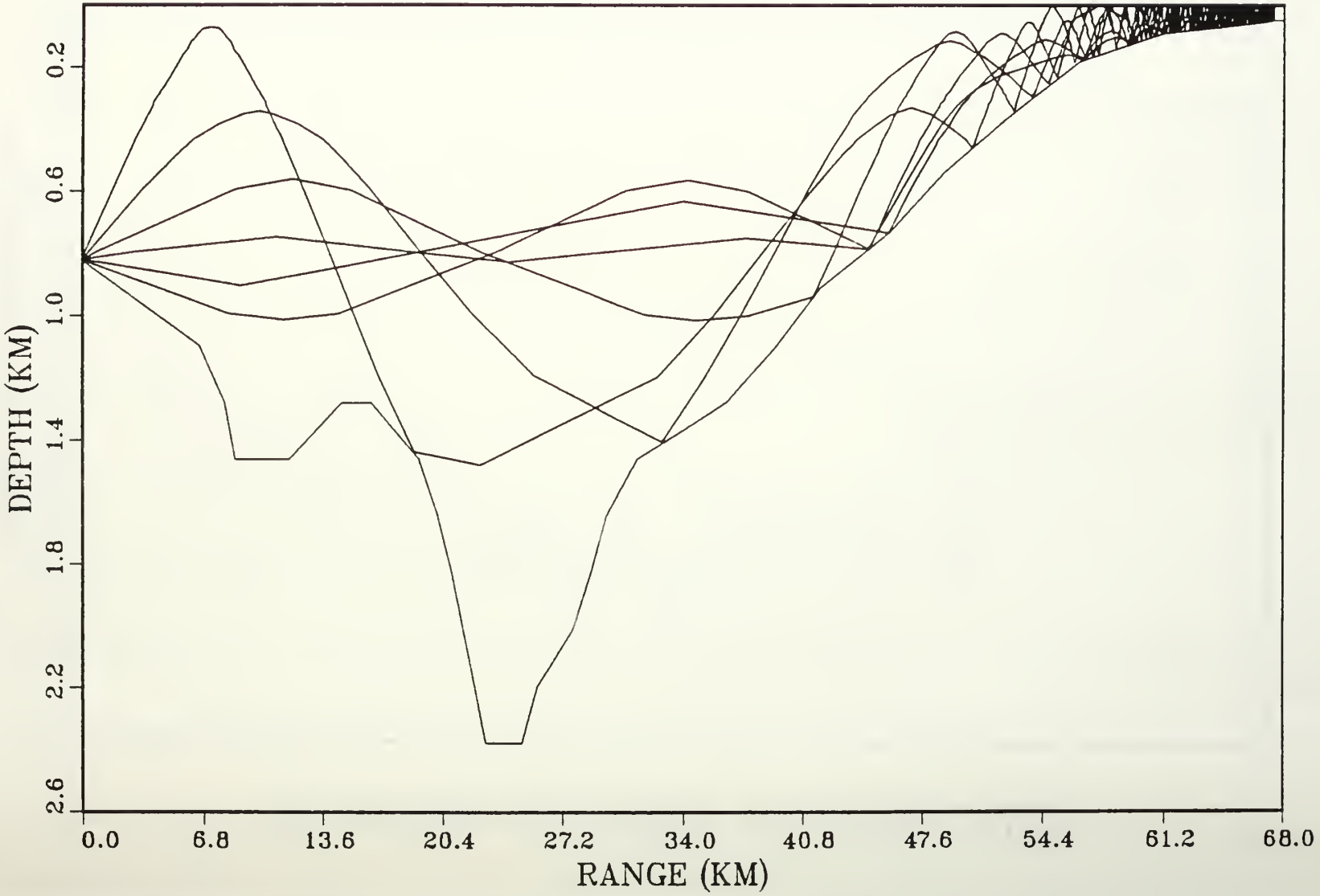

RECEIVER LOCATION 17: STICK PLOT

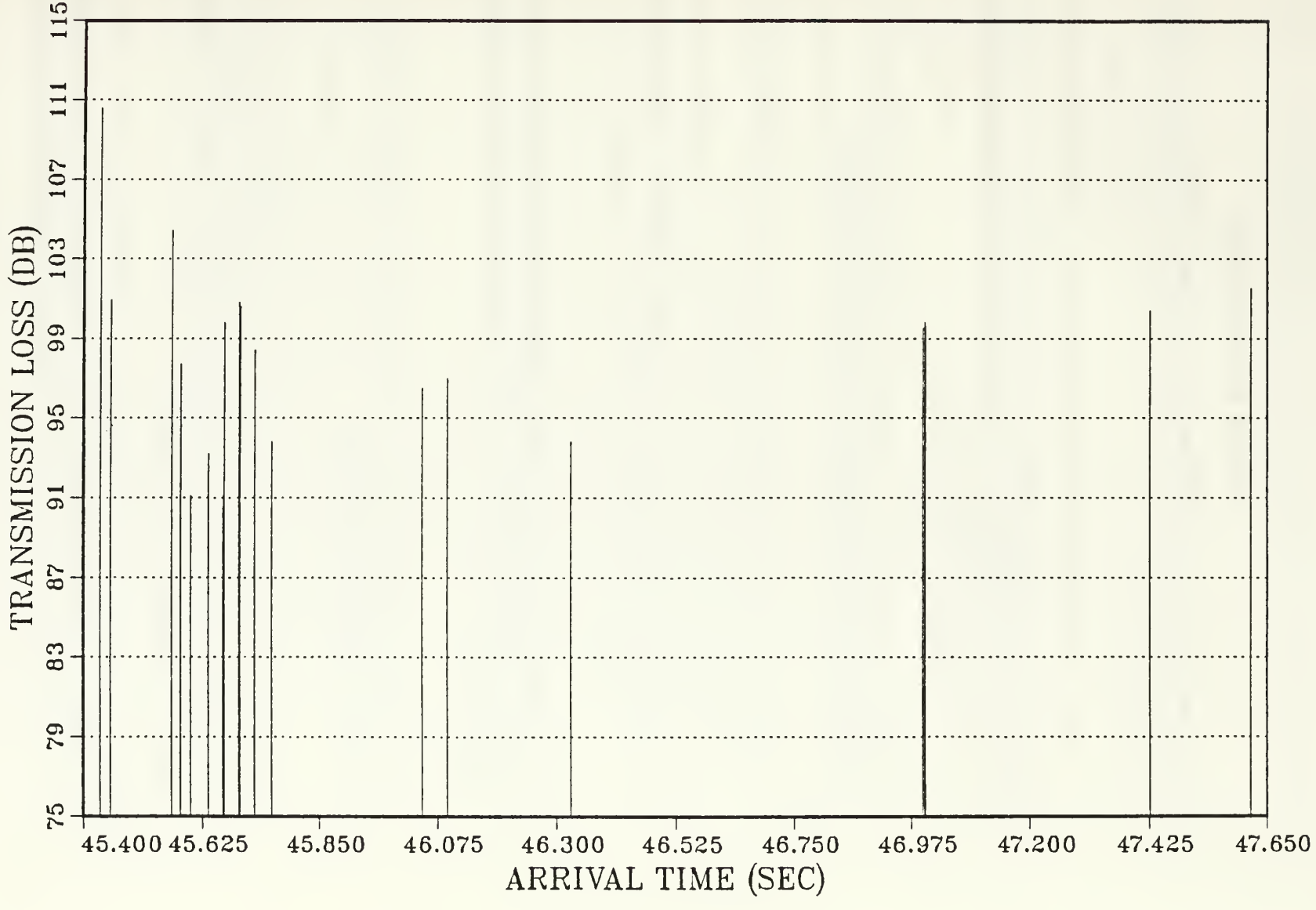

LIST OF REFERENCES

1. Kinsler, L.E., and others, *Fundamentals of Acoustics*, 3rd ed., p. 112, John Wiley & Sons, 1982.

2. Urick, R.J., *Principles of Underwater Sound*, 3d ed., p. 122, McGraw-Hill, 1983.

3. Clay, C.S. and Medwin, H., *Acoustical Oceanography: Principles and Applications*, pp. 78-89, John Wiley & Sons, 1977.

4. Munk, W. and Wunsch, C., "Ocean acoustic tomography: a scheme for large scale monitoring," *Deep-Sea Research*, v. 26A, pp. 123-161, 1979.

5. Wunsch, C., "Acoustic Tomography and Other Answers," unpublished paper based on talk given at La Jolla, CA, 19 October 1982.

6. Spindel, R.C., "Ocean Acoustic Tomography: a Review," *Current Practices and New Technology in Ocean Engineering*, v. 11, pp. 7-13, 1986.

7. Conversations between J.H. Miller, Electrical Engineering professor, Naval Postgraduate School, Monterey, CA, and the author, from 1 December 1987 to 5 September 1988.

8. The Ocean Tomography Group, "Ocean acoustic tomography: a demonstration," *Nature*, v. 299, pp. 121-125, 1982.

9. Lynch, J.F., and others, "Results From the 1984 Marginal Ice Zone Experiment Preliminary Tomography Transmissions: Implications for Marginal Ice Zone, Arctic, and Surface Wave Tomography," *Journal of Geophysical Research*, v. 92(C7), pp. 6869-6885, 30 June 1987.

10. Miller, J.H., *Estimation of Sea Surface Wave Spectra Using Acoustic Tomography*, Sc.D. Dissertation, Woods Hole Oceanographic Institution and Massachusetts In-

stitute of Technology Joint Program, Woods Hole and Cambridge, MA, September 1987.

11. Moss Landing Marine Laboratories Technical Publication 73-01, *Some Aspects of the Temperature, Oxygen and Nutrient Distributions in Monterey Bay, California*, by W.M. Smethie, Jr., 1973.

12. Broenkow, W.W. and Smethie, W.M., Jr., " Surface Circulation and Replacement of Water in Monterey Bay," *Estuarine and Coastal Marine Science*, v. 6, pp. 583-603, 1978.

13. Lasley, S.R., *Hydrographic Changes in Monterey Bay Surface Waters in Relation to Nearshore Circulation*, M.A. Thesis, San Jose State University, San Jose, CA, May 1977.

14. Engineering-Science, Inc., *Monterey Peninsula Water Pollution Control Agency Interim Report No. 4, Draft Oceanographic Predesign Report Volume 1*, pp. II-21 - II-53, October 1976.

15. Shepard, F.P. and Emery, K.O., *Submarine Topography off the California Coast: Canyons and Tectonic Interpretation*, pp. 72-79, Geological Society of America, 1941.

16. Scholl, D.W., and others, "The Structure and Origin of the Large Submarine Canyons of the Bering Sea," *Marine Geology*, v. 8(3/4), pp. 187-210, 1970.

17. Shepard, F.P. and Dill, R.F., *Submarine Canyons and Other Sea Valleys*, pp. 81-90, 223-231, 343-345, Rand McNally & Company, 1966.

18. Normark, W.R., "Growth Patterns of Deep-Sea Fans," *American Association of Petroleum Geologists Bulletin*, v. 54(11), pp. 2187-2192, 1970.

19. Combellick, R.A. and Osborne, R.H., "Sources and Petrology of Beach Sand From Southern Monterev Bay, California," *Journal of Sedimentary Petrology*, V. 47(2), pp. 891-907, 1977.

20. Welday, E.E. and Williams, J.W., *Offshore Surficial Geologic Map of California, Map Sheet 26*, 1975.

21. Shepard, F.P., and others, *Currents in Submarine Canyons and Other Seavalleys*, pp. 14-51, 78-95, The American Association of Petroleum Geologists, 1979.

22. U.S. Army Corps of Engineers and the California Department of Boating and Waterways, *Coastal Data Information Program, Monthly Summary Report #143 (December 1987)*, 6 January 1988.

23. U.S. Army Corps of Engineers and the California Department of Boating and Waterways, *Coastal Data Information Program, Twelfth Annual Report, January 1987 Through December 1987*, by R.J. Seymour, D. Castel, and J.O. Thomas, 19 May 1988.

24. Shea, R.E. and Broenkow, W.W., "The Role of Internal Tides in the Nutrient Enrichment of Monterey Bay, California," *Estuarine, Coastal and Shelf Science*, v. 15, pp. 56-66, 1982.

25. Shepard, F.P., "Progress of Internal Waves Along Submarine Canyons," *Marine Geology*, v. 19, pp. 131-138, 1975.

26. Ocean Data Systems, Inc., *Multiple Profile Restructuring and Supplemental Plot Programs*, by G. Jacobs, 30 June 1974.

27. U.S. Naval Oceanographic Office, *Integrated Command ASW Prediction System (ICAPS)*, NSTL, Bay St. Louis, MS.

28. National Oceanic and Atmospheric Administration. *Nautical Chart of Point Sur to San Francisco*, 24th ed., DMA Stock No 18ACO18680, 21 February 1987.

29. Spindel, R.C., "Signal processing in ocean tomography", *Adaptive Methods in Underwater Acoustics*, pp. 687-710, 1985.

INITIAL DISTRIBUTION LIST

		No. Copies
1.	Defense Technical Information Center Cameron Station Alexandria, VA 22304-6145	2
2.	Library, Code 0142 Naval Postgraduate School Monterey, CA 93943-5002	2
3.	Dr. Ching-Sang Chiu Institute for Naval Oceanography NSTL, MS 39529-5005	1
4.	Dr. James F. Lynch Woods Hole Oceanographic Institution Woods Hole, MA 02543	1
5.	Mr. Arthur Newhall Woods Hole Oceanographic Institution Woods Hole, MA 02543	1
6.	Dr. Leonard Healy, Code 742 Naval Training Systems Center 12350 Research Parkway Orlando, FL 32826	1
7.	Mr. Frank Jamison, Code 742 Naval Training Systems Center 12350 Research Parkway Orlando, FL 32826	1
8.	Dr. Richard Barber Monterey Bay Aquarium Research Institute 160 Central Ave. Pacific Grove, CA 93950	1
9.	Prof. James H. Miller, Code 62Mr Dept. of Electrical and Computer Engineering Naval Postgraduate School Monterey, CA 93943-5000	11
10.	Prof. Lawrence J. Ziomek, Code 62Zm Dept. of Electrical and Computer Engineering Naval Postgraduate School Monterey, CA 93943-5000	1

11. Prof. Timothy P. Stanton, Code 68St — 1
Dept. of Oceanography
Naval Postgraduate School
Monterey, CA 93943-5000

12. Prof. Edward B. Thornton, Code 68Tm — 1
Dept. of Oceanography
Naval Postgraduate School
Monterey, CA 93943-5000

13. Prof. Calvin R. Dunlap, Code 68Du — 1
Dept. of Oceanography
Naval Postgraduate School
Monterey, CA 93943-5000

14. Mrs. Theresa Rowan, Code 742 — 4
Naval Training Systems Center
12350 Research Parkway
Orlando, FL 32826

Thesis
R8143 Rowan
c.1 Monterey Bay acoustics
tomography.

Thesis
R8143 Rowan
c.1 Monterey Bay acoustics
tomography.

DEMCO

thesR8143
Monterey Bay acoustics tomography :
3 2768 000 84379 1
DUDLEY KNOX LIBRARY